A systems biology approach to cellular homeostasis, volume changes and regulation of metabolism

by

Gunhild Fjeld

Thesis submitted in fulfillment of
the requirements for the degree of

PHILOSOPHIAE DOCTOR
(PhD)

University of
Stavanger

Faculty of Science and Technology
Department of Chemistry, Bioscience and Environmental Engineering
2020

Preface

This thesis is submitted as partial fulfillment of the requirements for the degree of *Philosophiae Doctor* at the University of Stavanger, Norway. The research has been carried out at the Centre for Organelle Research (CORE), at the University of Stavanger.

The research has resulted in three articles, one of which have been published and two submitted for publishing. To fully grasp the process and progress throughout my work, I present the background and results in a chronological manner. The first paper is the most theoretical, with focus on control theoretic properties of negative feedback structures with different enzyme kinetics; the second paper uses a bottom up modeling approach to describe glucose uptake in growing cancer cells; and finally, the last paper is an experimental study on cancer metabolism. The chapters of this thesis are written so that the reader can understand the work and the results without having to carefully read each of the individual articles. The full articles are nevertheless, for completeness, included at the end of the thesis.

Gunhild Fjeld, February 2020

Abstract

Cells need to respond to a vast range of different disturbances and changes over small and large time scales. This can be disturbances in the form of molecules used to fight infectious states, changes in growth patterns, disturbances in the external environment, or even just normal maintenance processes that require compensatory actions. Throughout all of these processes, the cell always needs to maintain its inner environment relatively constant. This phenomenon is called homeostasis and happens through interactions between genes, proteins and metabolites that form complex regulatory networks.

The regulatory function of these networks is achieved through a combination of control mechanisms, such as negative feedback, feedforward, integral control and proportional control, although often in a bit disguised form as the networks typically contains imperfections such as leakage, saturation and other nonlinearities. This thesis is a systems biology approach, inspired by concepts from control engineering and control theory, to examine properties and functions of regulatory networks.

The first part of this thesis aims to explore how regulatory networks in the form of two-component negative feedback controller motifs respond to various types of disturbances or perturbations. The controller motifs have been introduced in previous work and have a structure that combines negative feedback and integral control, consequently giving them homeostatic functions. However, as we show in this work, their ability to compensate for time-dependent perturbations that increase linearly, exponentially, and hyperbolically, is different dependent the kinetics of the reactions in the motif.

The second and third parts of this thesis is a study of cancer metabolism, with emphasis on how cancer cells can regulate and maintain a high sustained glucose uptake during growth. Cell growth cause dilution effects and is an example of a perturbation that increase over time. The coupling between glucose metabolism and glutamine metabolism is also explored, and how this may be linked to growth and advantages for cancer cells.

This last part is done through experimental measurements of metabolic fluxes using a Seahorse XFp analyzer. Inhibitors of key enzymes are used sequentially in customized protocols through the experiments and enables the isolation of individual pathways and the evaluation of these fluxes. The use of the two new inhibitors is novel and so is the comparison between three pathways originating from glutamine.

Acknowledgements

x

List of papers

The main part of this dissertation is made up of the following scientific papers:

- **Paper 1**

  The Performance of Homeostatic Controller Motifs Dealing with Perturbations of Rapid Growth and Depletion
  G. Fjeld, K. Thorsen, T. Drengstig, P. Ruoff
  J Phys Chem B., vol. 121, no. 25, pp. 6097-6107, June. 2017.

- **Paper 2**

  Exploring Mechanisms of Glucose Uptake Regulation and Dilution Resistance in Growing Cancer Cells
  D. Tveit, **G. Fjeld**, K. Thorsen, P. Ruoff, T. Drengstig
  Submitted, January 2020 - Biophysical Journal

- **Paper 3**

  Using UK5099 and galloflavin to examine glutamine metabolism through sequential inhibition in a real time setting
  G. Fjeld, O. Nordgaard, K. Thorsen
  Submitted, January 2020 - Cancer and Metabolism BMC

List of other imparts

Results from the dissertation have in addition to the papers been communicated to the scientific community at:

(i) **Different Implementations of Integral Control Affect Controller Performances During Time-Dependent Perturbations**
G. Fjeld, T. Drengstig, K. Thorsen and P. Ruoff, *Poster presentation.* CSHL. , New York, USA, April 2017.

(ii) **How different implementations of integral control affect the homeostatic performances of negative feedback regulators during time-dependent perturbations.**
G. Fjeld *Talk.* BioCat annual conference, Oslo, Norway. June 2017

(iii) **Combining real time experimental data with a mathematical model to understand cancer cell metabolism**
G. Fjeld *Talk.* ISGSB, Sommarøy, Norway. September 2018

(iv) **Modeling the Redirection of Metabolic Flux in Cancer Cells**
G. Fjeld, K. Thorsen and O. Nordgård, *Poster presentation* Cell Symposium, Seattle, USA, December 2018.

Funding application:

A funding application was granted in September 2018 to support the experimental work on cancer cells.

(v) **Funding from Validè, Plogen grant à 50 000 NOK**
G. Fjeld, *Funding* Granted in September 2018.

Contents

Chapter 1

Introduction

Cells are constantly exposed to an ever-changing environment caused by e.g., infections, changes in growth pattern, alteration of nutrient availability or normal maintenance functions [23, 85]. In order to keep a relatively stable inner environment, the cells perform compensatory actions to counteract the impact of disturbances. This phenomenon is called *homeostasis*, and is achieved through regulatory networks consisting of nonlinear interactions between genes, proteins and metabolites [31, 52]. The term homeostasis was first coined by Walter Cannon in 1929, essentially as a term describing how physiological variables are kept within narrow limits [28]. In recent years, the notion of homeostasis has been extended to include cellular growth [19, 90, 150], the circadian clock [20, 111], and even oscillatory homeostasis [18, 82, 144], in addition to the regulation of temperature, pH, energy expenditure and other classical examples discussed in Cannon's own book [29]. Further examples of work related to homeostasis include studies on calcium homeostasis [18, 54], iron homeostasis [1, 7], sleep homeostasis [48], potassium homeostasis [110, 143] and nitrogen homeostasis [114], to mention a few. As *feedback* mechanisms are often involved in homeostatically regulated processes, we will in the following section look into different aspects of this structurally important property.

1.1   Feedback mechanisms

In control engineering in general, and also in biological systems, feedback can be classified as either positive or negative. Positive feedback loops are often referred to as *autocatalytic* if a compound in some way activates its own formation [59]. One of the most basic example of such structures is shown in figure 1.1. The overall effect of positive feedback is a self-increasing system [120].
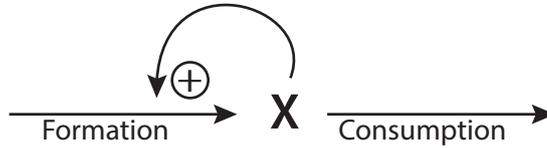
Figure 1.1: Positive feedback loop where x activates its own formation rate.

On the other hand, negative feedback loops are often referred to as *autoinhibitory* if the product inhibits its own formation [117, 120]. Again, one of the most basic example of such structures is shown in figure 1.2 .
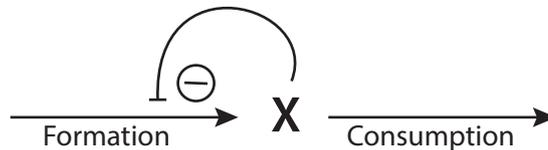
Figure 1.2: Negative feedback loop where x inhibits its own formation rate.

Negative feedback is a basic structure used in control engineering as it compensates for the effect of disturbances in the output of the regulated system [9, 130, 135]. The concept of negative feedback is also common in biological systems, where e.g., a signal or effector, or even a conformational change of an enzyme, causes a compensatory response when a biological system is subjected to a disturbance [10, 15, 38, 149].

Although there are examples of pure autoinhibitors, most regulation occurs through more elaborate network structures. Our research group has previously focused on networks with two interacting components that are able to demonstrate negative feedback functionality and which also can show perfect adaptation[1] [50, 51, 142, 145, 146]. Hence, in the work presented in this thesis, we have continued along this path and investigated other properties of these two-component motifs.

---

[1]Perfect adaptation is the ability to regulate a system back to its preperturbed value after the system has been exposed to a sustained perturbation. This is explained further in section 1.4.

1.2 Two-component negative feedback motifs

In our two-component negative feedback systems, one of the components will function as the *controlled variable* (i.e. the regulated variable), whereas the other will function as the *manipulated variable* (i.e. the controller). We term the regulated variable as component A, and the controller as component E. Hence, A can for instance represent calcium, iron, or some other ion or molecule tightly regulated in the cell, and E can represent a transporter or enzyme that degrades or forms A, and thus E contributes to reduce or increase the concentration of A.

One example of a so-called *controller motif* is shown in figure 1.3, where A activates the degradation of E, and E activates the synthesis of A. In the presence of an increased outflow perturbation in A (upward arrow), the level of A will decrease. This decreased level will, in turn, decrease the degradation of E, resulting in an increased level of E. This increased level will then increase the flux termed *Controller-regulated synthesis of A*, and hence increase the concentration of A back towards the preperturbed level. Based on the controller action, this controller is termed an *inflow controller*.
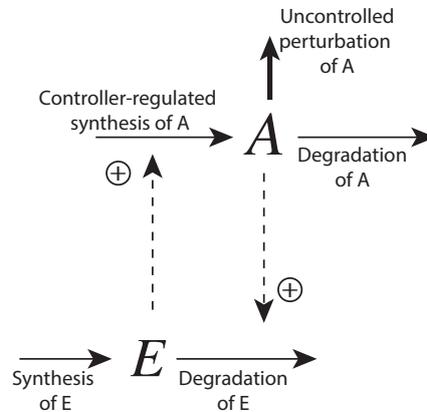
Figure 1.3: An example of a two-component negative feedback structure where the compound E functions as a controller by adding A, in the presence of an outflow disturbance in A.

Taking into account that A and E can either activate or inhibit each other's synthesis and/or degradation, there are in total 16 different two-component feedback structures. These were first presented by the chemist

U.F. Franck in 1980 [59]. Eight of these are negative feedback structures (see figure 1.4), whereas the other eight are positive feedback structures (not shown). We will in this thesis focus on the eight negative feedback structures which are further divided into four inflow controllers (motifs 1-4) and four outflow controllers (motifs 5-8). As briefly mentioned above, an inflow controller compensates by adding A to the system, whereas an outflow controller compensates by removing A from the system [50].
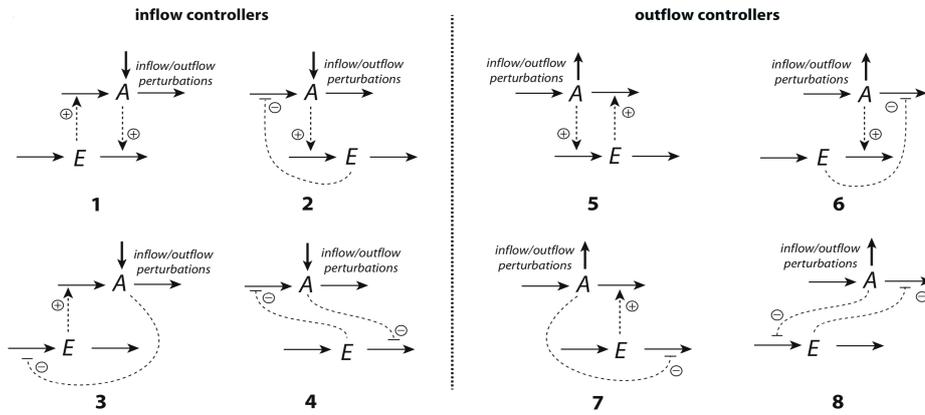
Figure 1.4: The complete set of stable two-component homeostatic controller motifs. The motifs fall into two operational classes termed inflow and outflow controllers where controller motifs 1-4 are the inflow controllers and controller motifs 5-8 are the outflow controllers (for definition, see main text). Figure from [50].

In order to determine whether the feedback is positive or negative for a given structure, we consider i) activation to be positive, ii) inhibition to be negative, iii) synthesis to be positive and finally, iv) degradation to be negative. Then, based on the product of all signs in the loop, we are able to determine the overall feedback sign. This procedure is illustrated in figure 1.5 for the outflow 5 controller. As we see, the overall sign is negative (the minus sign in black).
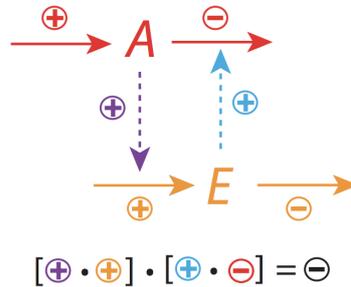
Figure 1.5: Procedure for determining the overall sign of a feeedback loop. Figure from [50].

1.3 Zero-order, first-order and second-order kinetics

Before we present the control theoretic properties of the controller motifs, we will first give an overview of the different types of kinetics we apply in our models.

The reaction order of a chemical or biological reaction describes how the reaction rate depends on the substrate concentration, and this can be graphically illustrated as in figure 1.6. The reaction rate of a zero-order reaction is independent of the substrate concentration, whereas the reaction rate of a first-order reaction depends linearly on the substrate concentration. Finally, the reaction rate of a second-order reaction depends on the square of the substrate concentration, or the product of the concentrations if there are two substrates [36].
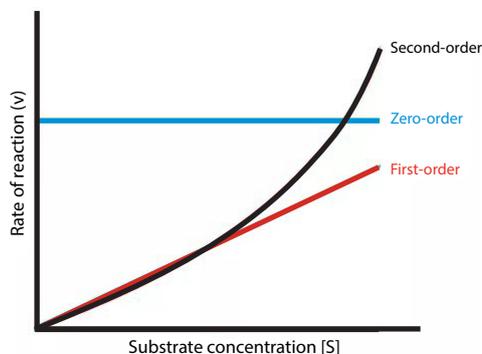
Figure 1.6: Rate of reaction versus concentration plot for zero-order reactions (blue), first-order reactions (red) and second-order reactions (black). A zero-order reaction rate is independent of substrate concentration, whereas a first-order reaction rate is linearly dependent on substrate concentration and a second-order reaction rate depends quadratically on substrate concentration.

For enzymatic reactions, the overall reaction rate is best described using saturation kinetics, as the amount of enzyme is often low compared to the amount of substrate. Thus, the enzyme is quicky saturated. One simple model that represent the kinetic properties of enzymes was developed by Michaelis and Menten in 1913 [81]. Together they formulated the famous Michaelis Menten equation, which describes how an enzyme becomes saturated as the concentration of substrate S increases [16]. This relationship is shown in the equation below,

$$v = \frac{V_{max}[S]}{K_M + [S]} \tag{1.1}$$

where V_{max} is the product of the catalytic rate constant (k_{cat}) and the total concentration of the enzyme (E_{tot}), and K_M is the Michaelis constant corresponding to the substrate concentration where $v = \frac{V_{max}}{2}$ [36]. As illustrated in figure 1.7, Michaelis Menten kinetics can be approximated to a first-order reaction for low substrate concentrations $S \ll K_M$, and to a zero-order reaction for high substrate concentrations $S \gg K_M$.
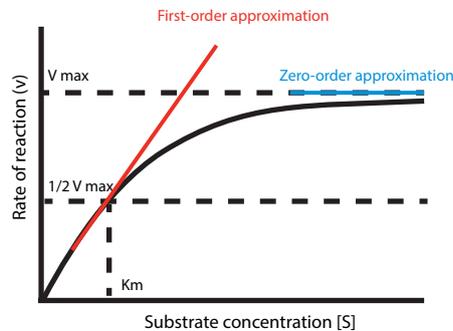
Figure 1.7: Michaelis Menten kinetics. The reaction rate v approaches V_{max} as the substrate concentration increases. The Michaelis constant, K_M, is the substrate concentration at $v = \frac{V_{max}}{2}$. The reaction rate is approximated to a first-order reaction at low substrate concentrations (red) and to a zero-order reaction at high substrate concentrations (blue).

To summarize, we use in our models, to a certain extent, all of the above described kinetics.

1.4   Perfect adaptation by integral control

If the output variable of a system being exposed to an external perturbation, is regulated back to its preperturbed value, we call it *perfect adaptation* [56]. This term is widely used when describing homeostatic regulation of biochemical and physiological systems, and corresponds to the *disturbance rejection* properties of an industrial control system [130, 159]. Perfect adaptation to step-type perturbations can be achieved if the controller motif exhibit so-called *integral action* in the controller species E, which means that the controller operates as an integrator [9, 109, 169]. In order to achieve integral control in the controller motifs in figure 1.4, there are some kinetic properties in the degradation of E that needs to be fulfilled. This, together with the derivation of the set-point, is the topic of this section.

To illustrate the concepts, we continue using the motif in figure 1.3 and specify rate constants and parameters, see figure 1.8.
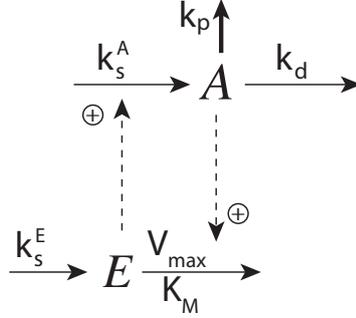
Figure 1.8: Inflow controller motif 1 from figure 1.3 depicted with rate constants and parameters used in the mathematical model. k_p is the outflow perturbation in A, k_s^A and k_s^E are the synthesis rate constants for A and E, respectively. k_d is the degradation rate constant of A, and K_M is the Michaelis constant which together with V_{max}, determines the rate of removal of E.

Based on figure 1.8, the rate equations of A and E forms two coupled first-order ordinary differential equations (ODEs), see equations 1.2 and 1.3.

$$\frac{dA}{dt} = k_s^A \cdot E - k_p \cdot A - k_d \cdot A \tag{1.2}$$

$$\frac{dE}{dt} = k_s^E - \frac{V_{max} \cdot E}{K_M + E} \cdot A \tag{1.3}$$

Note that the degradation of E is modeled using Michaelis Menten kinetics.

In order for E to behave as an integrator, the degradation process of E should be independent on the level of E [8, 109]. Thus, we need to assume that $K_M \ll E$, i.e., the degradation process is saturated. The rate equation of E is then simplified to:

$$\frac{dE}{dt} = k_s^E - V_{max} \cdot A \tag{1.4}$$

In order to identify the expression for the set-point of A, i.e., A_{set}, we calculate the steady state value of A, based on equation 1.4, as:

$$A_{set} = \frac{k_s^E}{V_{max}} \tag{1.5}$$

As we see, the steady state value of A is independent of the perturbation term k_p. In order to show that equation 1.4 corresponds to an integral

controller, we consider first the integral control law from control engineering [155, 159], i.e.,

$$u(t) = K_i \int_0^t e(\tau)d\tau \qquad (1.6)$$

where $u(t)$ is the control signal, K_i is the integral gain and $e(t)$ is the control error between the set-point $y_{set}(t)$ and the measurement $y(t)$, i.e.,

$$e(t) = y_{set}(t) - y(t) \qquad (1.7)$$

By differentiating equation 1.6, we find:

$$\begin{aligned} \frac{du}{dt} &= K_i \cdot e(t) \\ &= K_i \cdot (y_{set}(t) - y(t)) \end{aligned} \qquad (1.8)$$

Using equation 1.5, we can rewrite equation 1.4 as,

$$\begin{aligned} \frac{dE}{dt} &= V_{max}\left(\frac{k_s^E}{V_{max}} - A\right) \\ &= V_{max}(A_{set} - A) \\ &= K_i(A_{set} - A) \end{aligned} \qquad (1.9)$$

where we identify V_{max} to be the integral gain K_i. To summarize, we have now shown that the controller species E corresponds to an integral controller with a set-point of A_{set} if the degradation process of E is saturated.

There are many examples of integral control in biological systems. One example is bacterial chemotaxis, where the receptor activity, measured as the methylation level of the CheA-receptor, perfectly adapts when subjected to a step-wise perturbation in the chemoattractant [11, 169]. Furthermore, it has been shown that calcium homeostasis in mammals rely on a hormonal integral feedback system [54]. Integral control has also been studied in yeast cells, where it has been suggested that yeast cells regulate their intracellular osmolarity through an integral feedback loop that involves the mitogen-activated protein kinase Hog1, known to trigger the synthesis of glycerol [107].

It can be shown that all of the eight controller motifs in figure 1.4 can act as integral controllers, where each of them will have different expressions for the set-points of A [50]. According to the internal model principle (IMP), a control system will asymptotically adapt its output $y(t)$ in the presence

of a disturbance if the controller is capable of creating the same class of signals as the disturbance [58, 78]. In terms of biological control systems, the IMP implies that in order to achieve perfect adapation, the kinetic properties of the controller must be in accordance with the nature of the perturbation [137]. Taking the controller in figure 1.8 as an example, the zero-order degradation in E will limit the controller's ability to counteract complex perturbation profiles.

As we will see in the next chapters, we found that increased complexity in the synthesis and degradation of E resulted in increased controller performance when exposed to complex time-dependent perturbations. We also found that the reaction rate of the synthesis and degradation of E need to be of the same order with respect to E.

For the inflow controller motif 1 shown in figure 1.8, an example of such increased complexity in the dynamics of E is,

$$
\begin{aligned}
\frac{dE}{dt} &= k_s^E E - k_d^E EA \\
&= k_d^E E \left(\frac{k_s^E}{k_d^E} - A \right)
\end{aligned}
\tag{1.10}
$$

where k_d^E is the degradation rate constant of E. Solving for the steady state solution of equation 1.10, gives the set-point $A_{set} = \frac{k_s^E}{k_d^E}$.

1.5 Overflow metabolism and volume changes

Cellular metabolism can be described and modeled using enzyme kinetics. Each conversion step through a metabolic pathway is driven, or catalyzed, by specific enzymes where the reaction rate depends on the concentration of the substrates and on the kinetics of the particular enzymes [140].

Because a cell has a finite size and a cytosol that requires a balance for osmolarity, toxicity, and space, it must balance its uptake and secretion of metabolites [90]. A cell cannot continously increase the uptake rate of a metabolite, without increasing the consumption of downstream metabolites of that particular pathway. If the consumption or secretion is not increased accordingly, there will be a buildup and congestion of molecules inside the cell, which will have adverse consequences [154].

Overflow metabolism, or the Crabtree effect, is a metabolic mode used by yeast cells when exposed to nutrient abundance [44]. In overflow metabolism, a higher growth rate and a higher secretion rate is coupled with higher uptake rates [43]. This seemingly wasteful metabolic mode, or metabolic phenotype, resembles that of aerobic glycolysis, often referred to as the Warburg effect [93, 125, 156, 157]. Aerobic glycolysis is a common metabolic phenotype used by cancer cells to maximize growth rates. Cells that use aerobic glycolysis take up much more glucose and secrete much more lactate than normal cells [152]. A higher uptake rate followed by a higher secretion rate to overcome the buildup of molecules inside the cell is illustrated in figures 1.9A and B. The buildup of molecules inside the cell can cause so-called *macromolecular crowding*. Macromolecular crowding occurs when higher concentrations of macromolecules build up to reduce the volume of solvent available for other molecules in the solution [5, 154]. A cell may also increase its volume as a result of increased uptake rate as illustrated in figure 1.9C.

Volume changes are becoming more commonly explored when modeling metabolism, and has been considered in many metabolic models [4, 55, 94]. To account for a changing volume when modeling metabolic reactions, we must consider effects that deal with dilution of the concentration of metabolites. The mass, or equivalently the number of molecules, of a certain chemical species x can be described by the following equation,

$$n_x = c_x \cdot V \qquad (1.11)$$

where n_x is the amount of x [moles], c_x is the concentration of x [moles/L], and V is the volume [L]. The change in n_x, denoted by $\dot{n}_x$, is found by the product rule for derivatives as:

$$\dot{n}_x = \dot{c}_x \cdot V + c_x \cdot \dot{V} \qquad (1.12)$$

Reordering this we can express the change in concentration caused by a relative volume change as:

$$\dot{c}_x = \frac{\dot{n}_x}{V} - c_x \cdot \frac{\dot{V}}{V} \qquad (1.13)$$

We can relate equation 1.13 to the description above and figure 1.9 in the following way. A high concentration of x (left part of figures 1.9B and C) can be reduced ($\dot{c}_x < 0$) either by exporting x out of the cell ($\dot{n}_x < 0$) while leaving the volume constant (figure 1.9B), or by increasing the volume of the cell ($\dot{V} > 0$) while leaving the amount of x constant (figure 1.9C), or by a combination of the two.
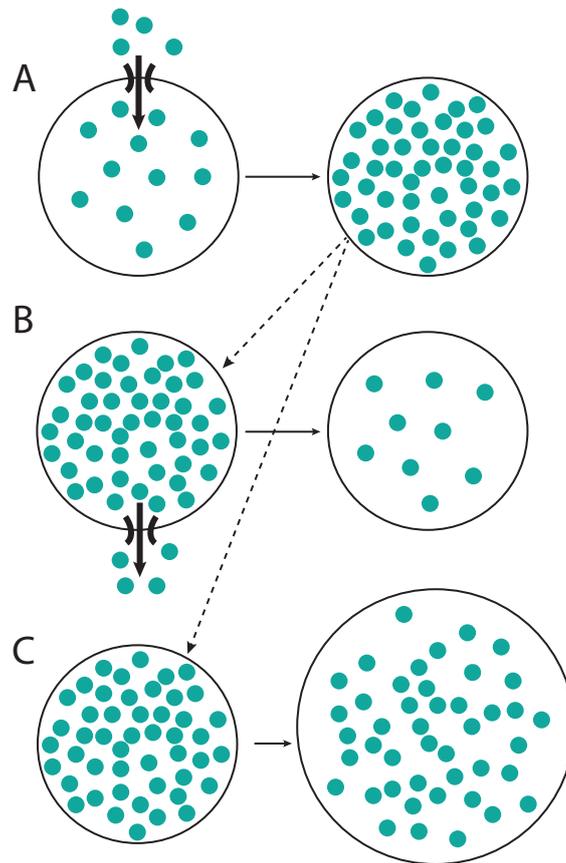
Figure 1.9: Compensating for a higher uptake rate with either a higher secretion rate or a volume increase. **A**. A high uptake rate causes more molecules inside the cell. As the amount of molecules build up it becomes difficult for the cell to maintain a high uptake rate. **B**. The problem of buildup can be dealt with by increasing the secretion rate of other metabolites or waste products. **C**. Alternatively, the cell can increase its volume to compensate for the high uptake rate. This leads to a dilution of molecules inside the cell. Most likely, a higher uptake rate can be supported by a combination of higher secretion rates and volume increases.

1.6 Redirection of metabolic flux in cancer cells

The rewiring of glycolytic enzymes and transporters often observed in cancer cells allows for a much higher uptake of glucose. To avoid overflow metabolism or macromolecular crowding (see fig. 1.9) cancer cells often secrete much more lactate than normal cells [93]. This is a common metabolic phenotype, also observed in fast growing cells [152]. Normally, nearly all of the pyruvate from glycolysis would enter the mitochondria to undergo oxidative phosphorylation in the tricarboxylic acid (TCA) cycle. Glycolysis and the TCA cycle together produce roughly 30 ATP molecules per glucose molecule [17]. If the glucose-derived pyruvate is converted to lactate instead, only 2 ATP molecules are produced. This lactate production also has an effect on the redox balance through the cofactors NADH and NAD^+. The simplified scenario of pyruvate undergoing oxidative phosphorylation or lactate secretion, is shown in figure 1.10. The *redirection* of metabolic flux in cancer cells represents a shift in flux where more pyruvate is metabolized to lactate, instead of predominantly being oxidized in the mitochondria.

Although a high uptake rate of glucose followed by a high secretion rate of lactate may seem wasteful, it is a common metabolic phenotype that supports growth. The increased glucose uptake allows for more glycolytic intermediates, which can lead to more biomass production [79, 152]. Glycolysis branches off into the pentose phosphate pathway (PPP) after the first glycolytic intermediate, glucose-6-phosphate (G6P). The PPP generates NADPH, which is used for de novo lipid synthesis [174]. The PPP also produces ribose-5-phosphate, required for nucleotide synthesis [152]. Even though aerobic glycolysis and lactic fermentation produce less ATP per glucose molecule, the total production rate of ATP is comparable to normal cells [134]. This is because it takes 10-100 times longer time to completely oxidize glucose in the mitochondria, than to secrete it as lactate [93].

One way to study the redirection of metabolic flux is to build a computational model that incorporates the supply and demand put on the cell according to its uptake and secretion rates. In modeling metabolism, the main energy supply, ATP, and the main cofactors used to carry electrons in redox reactions, NADH and NAD^+ (reduced and oxidized form, respectively), can be used to drive the supply and demand of reactions [32]. This is because some reactions require energy, like ATP, and others produce it. The same is true for NADH and NAD^+. Since these molecules are used in
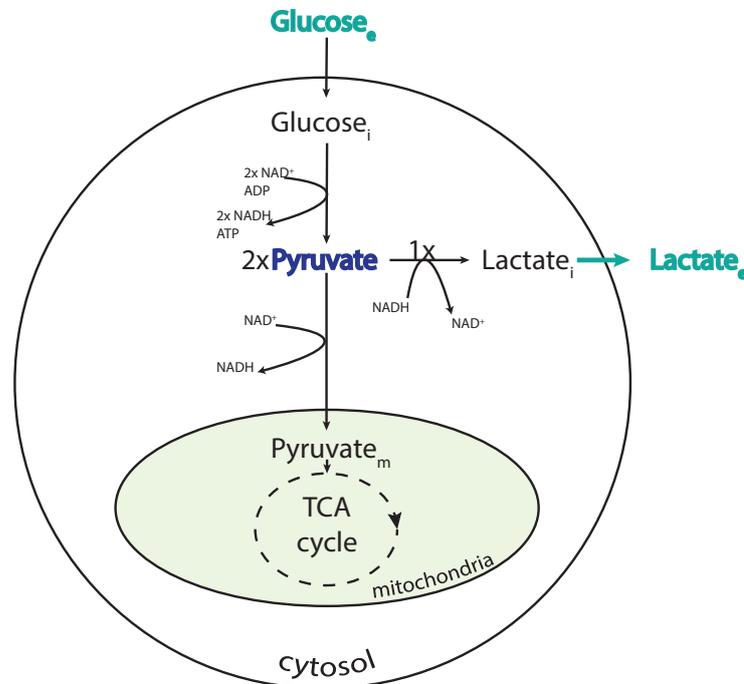
Figure 1.10: A higher glucose uptake coupled to a higher lactate secretion rate is a common metabolic phenotype observed for cancer cells. The end-product of glycolysis is pyruvate, and pyruvate can be converted to lactate or be transported into the mitochondria to undergo oxidative phosphorylation in the tricarboxylic acid (TCA) cycle. The cofactors NAD^+ and NADH are coupled to key reactions in these pathways, and so is the cell's energy supply, through the use and production of ATP.

so many metabolic reactions, they ultimately become decisive for which reactions can or will occur within the cell [104].

By looking at the simple model in figure 1.10, the conversion of one glucose molecule into two pyruvate molecules, produces a total of two NADH molecules. These two NADH molecules are again consumed when two pyruvate molecules are converted into two lactate molecules. One of the simplified explanations of the high lactate secretion rate, is that it balances out the redox potential in the cytosol [40, 61]. Along with the biosynthetic precursors produced from the PPP at the top of the glycolytic chain, this can support a high growth rate, despite wastage of lactate. The high secretion rate of lactate can be directly coupled to the overflow to

limit macromolecular crowding, as seen in figure 1.9B. Most likely, there is a connection between the higher secretion rate of lactate (fig. 1.9B) and the volume changes and accompanied growth (fig. 1.9C).

1.7 Rewiring of glycolysis in cancer cells

The Warburg effect is a shift from oxidative phosphorylation to aerobic glycolysis and lactate fermentation even in presence of oxygen [93, 156, 157]. Over the past decade, numerous studies and reviews have supported the hypothesis that the Warburg effect can be explained by alterations in multiple signaling pathways resulting from mutations in oncogenes and tumor suppressor genes [13, 39, 88]. Specifically, the Warburg effect is linked to a higher uptake rate of glucose. To support higher glucose uptake and faster utilization by glycolysis, many cancer cells show an upregulation of specific glycolytic transporters and enzymes [152]. The uptake starts with glucose being transported into the cell by a glucose transporter, and in cancer cells the most predominant glucose transporter is GLUT1 [27, 64, 165]. GLUT1 content at the cell surface is regulated in response to the intracellular level of glucose and the glycolytic intermediate glucose-6-phosphate (G6P) [68, 98, 138, 139]. In fact, comparisons of mammary tumors and normal mammary tissue in mice have shown that increased GLUT1 levels correlates with decreased intracellular glucose levels and increased glycolytic activity [170]. It may seem counterintuitive that a high level of GLUT1 is related to lower intracellular levels of glucose; the drive for this observation is that increased consumption leads to lower intracellular levels of glucose and G6P, which again is related to higher expression of GLUT1 [46].

One way in which intracellular glucose affects GLUT1 expression is via AMP-activated protein kinase (AMPK) [80]. AMPK is the main energy sensor of the cell, and its normal function is to ensure that the cell always has enough nutrients [67]. AMPK is comprised of one catalytic α-subunit, and two regulatory subunits, β and γ [42, 98]. If the cell has enough glucose-supply, AMPK becomes deactivated through a few different ways (see fig. 1.11): When glucose is abundant, it will quickly be phosphorylated to G6P, by the first glycolytic enzyme, hexokinase (HK). HK2 is the isoform of hexokinases most often upregulated in cancer cells [112]. G6P is used to supply glycolysis, lowering the AMP/ATP and ADP/ATP ratios which keeps AMPK from being activated by the binding of AMP and ADP

[80]. High glucose levels and increased biomass generation also reduce the $NAD^+/NADH$ ratio, which indirectly inhibits AMPK through the silent information regulator T1 (SIRT1) and serine-threonine liver kinase B1 (LKB1) [69, 80, 124, 153].
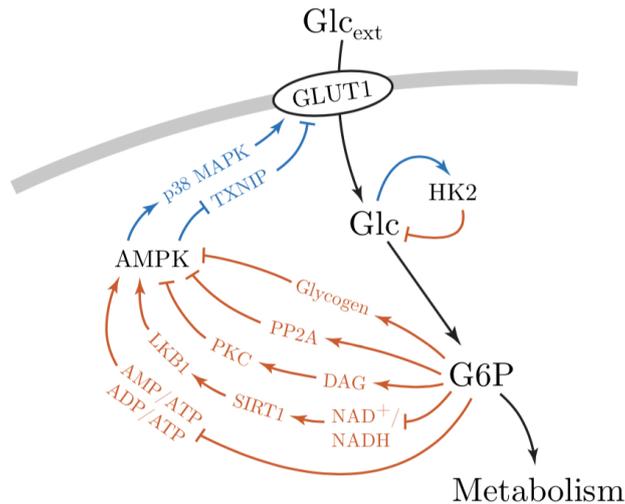
Figure 1.11: Summary of the AMPK related control mechanisms of glucose uptake in cancer reported in the literature. Line marker-ends indicate the effect one compound has on another, arrowhead for positive and flat head for negative. Colored pathways indicate the overall effect of that pathway, blue for positive and red for negative. Black lines represent the flow of glucose metabolism.

Downstream of G6P, the accumulation of diacylglycerol (DAG) and glycogen both lead to inhibition of AMPK. DAG inhibits AMPK by activating protein kinase C (PKC), which in turn induces the inhibitory phosphorylation of the AMPK α-subunit, while glycogen inhibits AMPK by binding to the β-subunit [80]. In addition, activation of protein phosphatase 2A (PP2A), as a result of high glucose levels, inhibits AMPK [60, 80, 84]. If AMPK becomes activated, it results in compensatory actions to increase the glycolytic flux, and AMPK has been shown to affect GLUT1 expression on the cell surface [12]. One mechanism by which this happens is by increasing the degradation of thioredoxin interacting protein (TXNIP). TXNIP can bind directly to GLUT1 and induce internalization, as well as reduce GLUT1 mRNA level [80, 163]. TXNIP is also regulated by G6P by MondoA [138, 139]. Another suggested mechanism is that downstream of

AMPK, p38 mitogen-activated protein kinase (MAPK) activation leads to enhancement of GLUT1 mediated glucose transport [164].

AMPK is furthermore known in normal cells to maintain so-called metabolic homeostasis [89, 115]. This also comes into play, when AMPK is deactivated by the mechanims in figure 1.11, because a higher G6P level would lower the amount of GLUT1, thereby stabilizing the level of G6P. The suggested AMPK related control mechanisms for sustained high glucose uptake in cancer cells forms the same feedback structure as in controller motif 3 (see section 3.2 and paper II).

1.8   Glutamine metabolism in cancer cells

Although glucose is often considered the main energy and carbon source of cancer cells, there is an increasing interest for understanding how cancer cells utilize glutamine as an alternative fuel, and why some cancer cells even seem to be addicted to glutamine in order to proliferate [160].

Glutamine is the most abundant free amino acid in muscles and plasma, and it is also one of the most metabolically flexible ones, serving many different functions [83]. Metabolism of glutamine starts with glutamine being transported in to the cell. Glutamine can then enter the mitochondria, where it in the inner membrane is converted to glutamate by glutaminase [101, 129], see figure 1.12. Glutamate in turn, can be converted to the TCA cycle intermediate α-ketoglutarate (α-KG) by glutamate dehydrogenase (GDH). Continuing along the TCA cycle, glutamine-derived α-KG is converted to succinate and then to fumarate to produce malate. From malate there are three possible pathways, each with a different outcome, i.e.,

(i) continuation along the TCA cycle (path 6 in fig. 1.12)

(ii) conversion of malate into cytosolic pyruvate by cytosolic malic enzyme (ME1) (path 7a in fig. 1.12)

(iii) conversion of malate into mitochondrial pyruvate by mitochondrial malic enzyme (ME2) (path 7b in fig. 1.12)
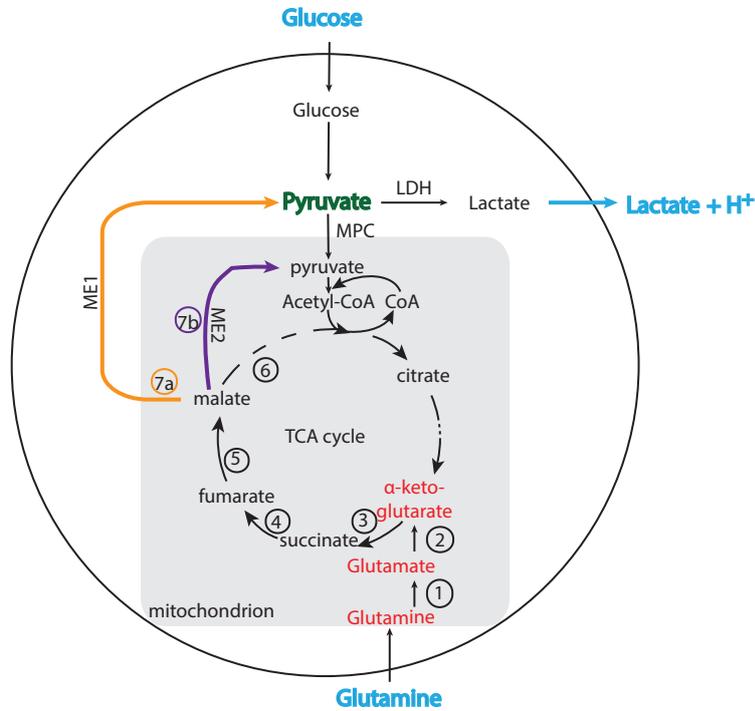
Figure 1.12: Glutamine metabolism. Glutamine is catabolized by glutaminase (1) into glutamate which again is turned into α-ketoglutarate, an intermediate of the TCA cycle, by glutamate dehydrogenase (2). Glutamine-derived α-ketoglutarate can either follow the whole TCA cycle (3-6), or break off from malate to be turned into pyruvate. The conversion of malate to pyruvate can happen either through transport of malate to the cytosol and conversion to cytosolic pyruvate by the cytosolic malic enzyme (ME1), through path 7a; or through the mitochondrial malic enzyme (ME2) to produce mitochondrial pyruvate, through path 7b.

These three different metabolic pathways have different implications for the cell. Path 6 is used to anaplerotically supply the TCA cycle with a carbon source. Cytosolic pyruvate from path 7a can be used in the mitochondria if it re-enters via the mitochondrial pyruvate carrier (MPC), or it can be fermented to lactate by lactate dehydrogenase (LDH). The latter is more common in cancer cells [106, 158]. Mitochondrial pyruvate from path 7b can be brought back into the TCA cycle through intramitochondrial recycling, making 7b a pathway that generates acetyl-CoA from glutamine-derived pyruvate. This again makes it possible for a cell to keep the TCA cycle going without the need for glycolytic pyruvate. The two different

malic enzyme paths leading from the TCA cycle intermediate malate (7a and 7b) have not been extensively compared, despite indicating differences in metabolic requirements. Path 7a, using ME1, leads to the formation of NAD(P)H in the cytosol, which is important for redox balance and lipid synthesis, as well as the PPP, in the cytosol [108]. Path 7b, using ME2, leads to the formation of NAD(P)H in the mitochondria, which affects the mitochondrial redox balance and enables more production of ATP [119, 126]. The ME2 pathway also helps removing reactive oxygen species in the mitochondria [30].

Since both glutamine and glucose can be converted to pyruvate, they both serve as important carbon sources to fuel metabolism and an increased uptake of any or both of them can lead to an increase in lactate secretion rates or oxidative phosphorylation. In simple terms, the former produces more biomass precursors and the latter more energy. Differences between tumors in this metabolic setting may reflect the growth properties and invasiveness of the cancer cell type, as a connection between high glutamine and/or glucose uptake and lactate secretion has been linked to poor prognosis [24, 161, 171].

1.9 Motivation and aim

This thesis deals with a systems biology approach to cellular homeostasis and metabolism. The work included in this thesis covers both theoretical and experimental approaches, which are used to gain a better understanding of the complex interplay between cellular components. The motivation and aim of each study is in the following presented by their respective papers.

1.9.1 Paper I

Most biological systems are exposed to various kind of perturbations, e.g., step-type or different time-dependent profiles, where the step-type is one of the most used test signal for control theoretic analysis. However, the perturbation strength by e.g., invasive agents increases (sometimes rapidly) with time, and examples of such include the exponential growth of pathogenic bacteria [14, 166] and the hyperbolic/hypercyclic growth of viruses [35, 53]. Hence, our motivation was to investigate how each of the eight controller motifs would cope when subjected to such time-dependent perturbations. We therefore applied *i*) linearly, *ii*) exponentially

and *iii*) hyperbolically increasing perturbations to the controller motifs implemented with either *i*) zero-, *ii*) first-, or *iii*) second-order kinetics in the synthesis (autocatalytic) and degradation of the controller species E. Our aim was to identify whether there are structural relationships between the perturbation type, the motif type (inflow/outflow and activating/inhibiting signaling kinetics), and the kinetics of the controller species E.

1.9.2 Paper II

Most cancer cells rely on aerobic glycolysis and increased glucose uptake for the production of biosynthetic precursors needed to support rapid proliferation [93, 152]. Aside from biomass formation for the purpose of growth, a high glycolytic metabolism also affects cell volume by osmotic swelling [90]. Thus, cell growth and shrinkage are other examples of perturbations that vary in time, since volume changes in general affects important cellular functions by dilution or upconcentration of cellular compounds [33, 90].

In paper II we therefore look into homeostatic mechanisms regulating glucose uptake in rapidly growing cancer cells and through simulations of a mathematical model we examine how these mechanisms are able to maintain a high metabolism of glucose in the presence of dilution (cell growth). Our aim was to investigate *i*) how the level of glycolytic intermediates and metabolic enzymes can be controlled, and *ii*) how a high glycolytic flux can be maintained when the volume increases.

Our model of glucose uptake is based on the reported rewiring of glycolysis in cancer, and includes dilution of both metabolites and enzymes. Key components are identified using differential gene expression data from the Expression Atlas database. With basis in the literature and expression data, we added control mechanisms to the model in a stepwise manner and investigated the role served by each regulatory mechanism.

1.9.3 Paper III

The motivation behind this study was to look closer into glutamine metabolism in cancer cells. Glutamine is the most abundant free amino acid in muscles and plasma, and is known to be important for growth of cancer cells [83, 168]. As described in section 1.8, glutamine can undergo oxidative metabolism in the mitochondria, or it can after having been converted to malate be transferred to the cytosol. In the cytosol, glutamine-derived

malate can be turned into pyruvate, which can then be fermented to lactate. We specifically wanted to examine how cancer cells use these pathways for glutamine metabolism and whether the same kind of redirection and shift towards fermentation and overflow metabolism that has been observed for glucose, i.e., the Warburg effect (see sections 1.5 - 1.8), can also be observed for glutamine.

Our aim was to investigate whether two different cancer cell lines utilized glutamine differently. Our approach included real-time measurements of oxygen consumption and extracellular acidification by a Seahorse XFp analyzer, to investigate the metabolic flux in the different branches of glutaminolysis.

1.10 Main contributions and thesis outline

The main contributions of this thesis are summarized in the following three points, each covered in separate papers (I-III):

- In paper I we altered the synthesize and degradational kinetics of E for all of the eight controller motifs of figure 1.4. For each variant, we investigated the disturbance rejection properties with respect to different time-dependent perturbations.

- In paper II we investigated regulatory mechanisms that enable a sustained high glucose uptake during growth in cancer cells, and created a model of glucose uptake and the first steps of glycolysis. We added feedback regulation to the model, by using controller motifs, and investigated how it coped with a time-dependent volume increase and step perturbations in external glucose.

- Paper III is an experimental study of glutamine metabolism on two different cancer cell lines (HCT116 and Caco2). By introducing two new inhibitors and developing two new protocols to an already preestablished metabolic flux analyzer method, we were able to investigate how the two cancer cell lines differ in their metabolism of glutamine.

This thesis is organized as follows; Chapter 2 encompasses the data material and methods used in the different studies. Chapter 3 summarizes the main results and contributions of each paper. Chapter 4 gives a

summary of the thesis and each paper is discussed separately. We also discuss a possible mechanism for regulation of glutamine uptake in cancer cells and end by giving an overall perspective on our approach.

Chapter 2

Materials and methods

This chapter is organized as follows. Section 2.1 presents the computational modeling approach of paper I, including details concerning i) the three different types of controller kinetics of E, and ii) the expressions for the three different time-dependent perturbations (as described in section 1.9.1). Thereafter, in section 2.2, the collection and analysis of differential gene expression data from studies comparing cancer and non-cancerous cells from paper II is covered. This section also describes the computational methods used in paper II. Finally, the experimental setup and the materials and methods used in paper III are described in section 2.3, with a focus on the Seahorse XFp analyzer and the new inhibitors used to block a specific enzyme or transporter in the metabolic pathways of glutamine.

2.1 Paper I

Paper I is a systematic study on how three kinetically different implementations of the controller action of species E perform during different time-dependent perturbations. The study includes all of the eight controller motifs from figure 1.4, and each controller motif is implemented with zero-, first-, or second-order kinetics in both the synthesis and degradation of the controller species E.

2.1.1 Time-dependent perturbations

As we in this study investigated both inflow and outflow controllers, we used separate notation for the perturbation rate constant (i.e. k_p in equation 1.2). Hence, this rate constant is termed k_1 for an inflow controller, and k_2 for an outflow controller. The expressions for the three different time-dependent perturbations, i.e., i) linear, ii) exponential and iii) hyperbolic increase, are given as follows:

i) Linear increase in perturbation,

$$k_1 \text{ or } k_2 = \begin{cases} 1.0 & \text{for } t < 2.0 \\ 1.0 + 20 \cdot (t - 2.0) & \text{for } t \geq 2.0 \end{cases} \tag{2.1}$$

ii) Exponential increase in perturbation,

$$k_1 \text{ or } k_2 = \begin{cases} 1.0 & \text{for } t < 2.0 \\ 1.0 + 2 \cdot (e^{0.5(t-2.0)} - 1) & \text{for } t \geq 2.0 \end{cases} \tag{2.2}$$

iii) Hyperbolic increase in perturbation[1],

$$k_1 \text{ or } k_2 = \begin{cases} 1.0 & \text{for } t < 2.0 \\ \frac{8.0 \cdot 40.5}{\frac{40.5}{1.0} - (t - 2.0)} & \text{for } t \geq 2.0 \end{cases} \tag{2.3}$$

The parameter values in all of these perturbation expressions are chosen arbitrarily.

2.1.2 Controller kinetics

As a mean to present the mathematical expressions behind the three different kinetic implementations used in paper I, we include here only the details of controller motifs 1 and 4. The reason for this is that motif 1 is solely based on activating kinetics in the control loop (see figure 2.1), whereas motif 4 is solely based on inhibiting kinetics (see figure 2.2). Thus, the three different expressions for the dynamics of E for these two motifs are good candidates to illustrate the variety of expressions used in paper I. For more details, confer the paper and the supporting information which includes the full analysis of all eight controller motifs.

---

[1] Note that some of the simulations in paper I using the hyperbolic time-dependencies apply the step at t=1.0 instead of t=2.0. Note also that the hyperbolic perturbation will go to infinity when t reaches 41.5 for the step at t=1.0, or 42.5 for the step at t=2.0.
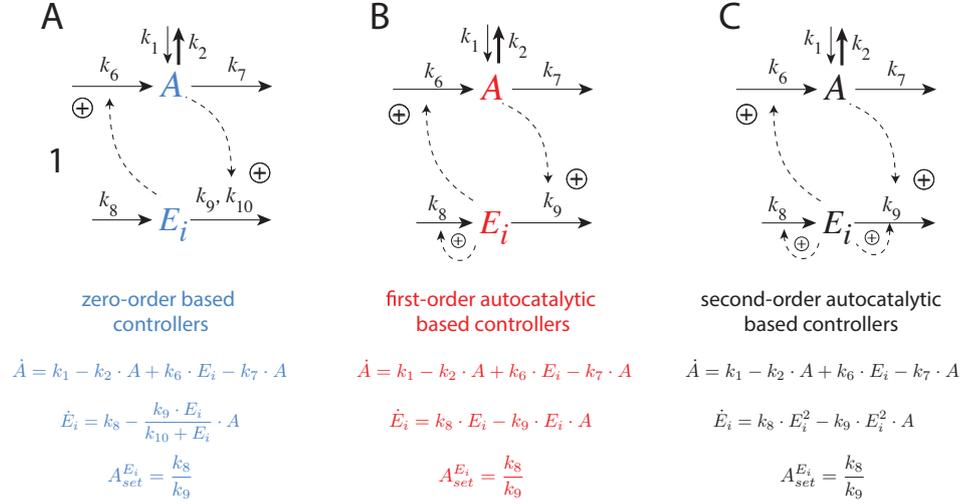
Figure 2.1: The three different kinetic implementations of integral control for motif 1. **A** Topology and rate equations of the zero-order implementation. **B** Topology and rate equations of the first-order autocatalytic implementation. **C** Topology and rate equations of the second-order autocatalytic implementation.

We observe from figure 2.1 the important result that the expressions for the set-point of A is unchanged regardless of the kinetic implementation of E. The same conclusion applies for motif 4 in figure 2.2.

Rate equations were solved numerically using the Fortran subroutine LSODE [116] in conjunction with Absoft's Pro Fortran compiler. All rate constants and concentrations are given in arbitrary units (au).
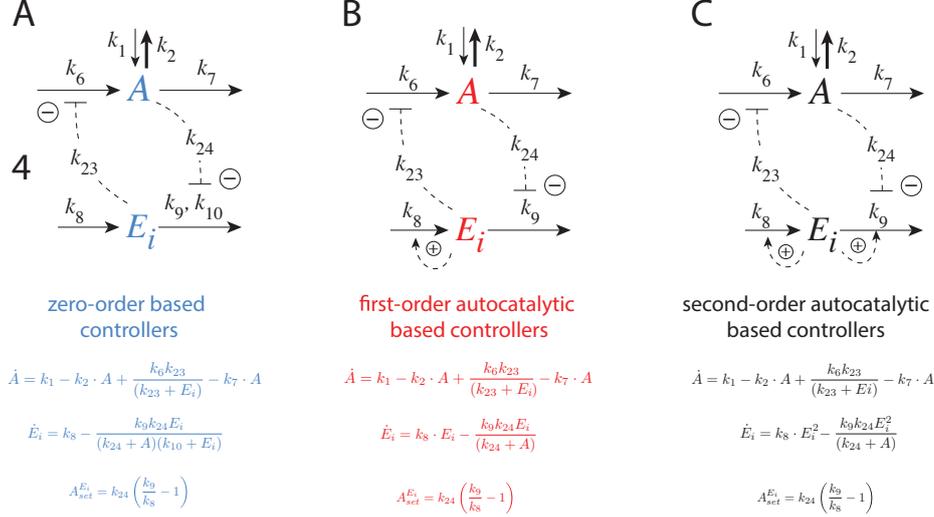
Figure 2.2: The three different kinetic implementations of integral control for motif 4. **A** Topology and rate equations of the zero-order implementation. **B** Topology and rate equations of the first-order autocatalytic implementation. **C** Topology and rate equations of the second-order autocatalytic implementation.

2.2 Paper II

In paper II we proposed a mathematical model for the regulation of glucose uptake and the regulation of concentration for intermediates in glycolysis during growth in cancer cells. The study includes a collection of data comparing differential gene expression of key genes associated with glucose uptake and glycolysis in cancerous and non-cancerous cells. The data highlights differences between normal cells and cancer cells and is the basis for the proposed model.

2.2.1 Differential gene expression

The Expression Atlas is a database launched by the European Bioinformatics Institute (EMBL-EBI) in 2013. It is an open science resource providing information on gene and protein expression in animal and plant samples of different cell types, organism parts, developmental stages, diseases, and other conditions [113]. The database contains thousands of selected microarray and RNA-sequencing datasets that are manually curated, annotated, checked for high quality, and processed using standardized

analysis methods [113] such as DESeq2 [96] with independent filtering [21]. These analysis methods take into account data of small replicate numbers, discreteness, large dynamic range, and the presence of outliers, before the data is subjected to normal statistical analysis like t-tests. For genes of interest, users can view baseline expression in tissues, and differential expression for biologically meaningful pairwise comparisons [113].

The Expression Atlas database was used in this study to collect differential gene expression data comparing cancer cells with normal (i.e. non-cancerous) cells, across a variety of tissues and cell types. The genes of interest included the solute carrier SLC2A gene family, HK1-3, GCK, PFKM, PFKP, PKM, and PKLR genes. The SLC2A gene family encodes for the family of glucose transporters, GLUTs; HK1-3 encodes for hexokinase isoforms 1-3; GCK encodes for glucokinase; PFKM encodes for 6-phosphofructokinase; PFKP encodes for phosphofructokinase; PKM encodes for the pyruvate kinase M (muscle) isoforms; and PKLR encodes for pyruvate kinase R (red blood cells) and L (liver) isoforms. We curated the data to ensure only experiments comparing cancer cells with their counterparting normal cells were included. Differential gene expression experiments with drug treatments were removed. Expression Atlas reports experiment results as log2-fold changes. In this paper, we report the arithmetic mean of log2-fold changes (i.e. log2 of the geometric mean fold change) for each gene across all experiments.

2.2.2   Computational methods

The proposed mathematical model form a system of ODEs that was solved numerically as an initial value problem using Matlab R2018a and the ode45 ODE solver, based on the Dormand-Prince (4, 5) pair [133]. Initial values and parameters for all simulations are provided in the Supporting Material of the paper. Simulation results are given in arbitrary units (arb. unit). Reaction rates are expressed as concentrations per unit of time.

2.3   Paper III

Paper III is based on experimental results of glutamine metabolism in two colorectal cancer cell lines. By using a Seahorse XFp metabolic flux analyzer (Agilent Technologies, USA), we obtained data of oxygen consumption rates and extracellular acidification rates in real time. By using different

inhibitors, we were able to isolate key pathways involved in glutamine metabolism and to investigate the difference in glucose and glutamine metabolism between the two cell lines. Note that paper III is a methodology paper, and has an extensive methods section where the rational behind the sequential addition of each metabolite and inhibitor is covered in more detail.

In the next section, a brief introduction to the Seahorse XFp metabolic flux analyzer is given. Then the target sites of the inhibitors and metabolites are presented, followed by the experimental prosedure for preparation of the cells. Finally, the protocols and the inhibitors are described, together with the data management procedure and the expressions used to calculate each flux.

2.3.1 Seahorse XFp metabolic flux analyzer

The Seahorse XFp metabolic flux analyzer measures the oxygen consumption rate (OCR) and the extracellular acidification rate (ECAR) of live cells in a well plate. Measurements are done in real time, and the analyzer is capable of automatically adding new metabolites or inhibitors to the wells with live cells during the experiments. ECAR is measured as a change in extracellular pH, where the change is caused by the extrusion of one proton (H^+) that is secreted with each lactate molecule. The change in OCR is caused by a change in the oxygen consumption of the mitochondria. Thus, ECAR is a proxy for lactate secretion, and OCR a proxy for TCA cycle activity. In order to block glucose's contribution to either ECAR and OCR we used the inhibitor 2-DeoxyGlucose (2-DG). We are then left with an estimate of glutamine as the carbon and energy source. The pathways of glutamine catabolism (paths 1-5 and then further into 6, 7a or 7b) are shown in figure 2.3 together with the inhibitors used in the study.

The ability to measure ECAR and OCR in real time to get dynamic time-series data made it appealing for us to use a Seahorse XFp metabolic flux analyzer in this study. The Seahorse XFp analyzer has become a popular tool to measure the metabolism of glucose and how it is directed to fermentation or oxidation in cancer cells [175], but has not yet been used extensively to study glutamine metabolism. While the producer of the instrument, Agilent, provides readily made kits with inhibitors and detailed protocols to study glucose metabolism, they do not provide the same types of kits to study glutamine metabolism. We thus had to select inhibitors and make our own protocols for studying glutamine metabolism,

and specifically the flux through the three branches from malate (see section 1.8 in the introduction).
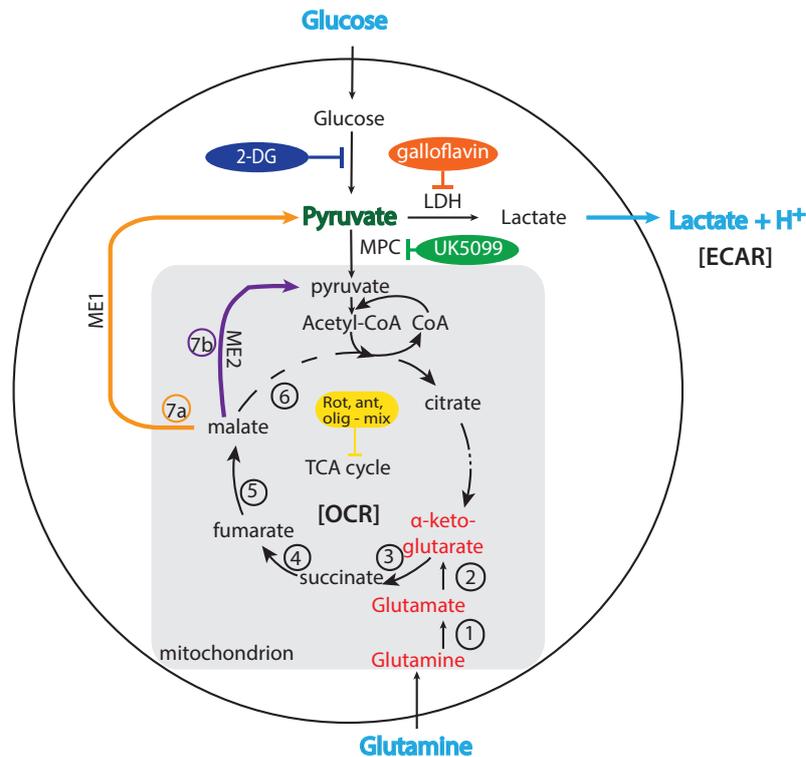
Figure 2.3: Simplified structure of glycolysis and the tricarboxylic acid (TCA) cycle of a cell. Glutamine is converted to glutamate in the mitochondria, and follow paths 1-6 to anaplerotically supply the TCA cycle with intermediates. Alternatively, it can follow path 7a via malic enzyme 1 (ME1) to enter the cytosol and eventually be turned into pyruvate and then lactate, which is subsequently secreted. Yet another alternative is path 7b via malic enzyme 2 (ME2) to non-glycolytic pyruvate, which in turn is converted into acetyl-CoA, closing the TCA cycle. The inhibitors used in this study are given at their respective target sites.

Up to four different solutions can be added sequentially from four different ports on the Searhorse XFp metabolic flux analyzer. As an example from one of the protocols in our experiments, the cells started in a media without glutamine, where glutamine then was added as the first injectant. This allowed the isolated reading of glutamine-induced OCR and ECAR changes. As indicated in figure 2.3, we have in this study used the following four

inhibitors:

(i) 2-DG, which inhibits the first step of glycolysis

(ii) a mixture of three electron transport chain inhibitors, i.e., rotenone, antimycin A and oligomycin

(iii) galloflavin (GF), which inhibits lactate dehydrogenase (LDH)

(iv) UK5099, which inhibits the mitochondrial pyruvate carrier (MPC)

2-DG and the three electron transport chain inhibitors have previously been used by Agilent, and are provided in commercial kits. The two last inhibitors, GF and UK5099, are new to this type of experiments, and to our knowledge, we are the first to use these inhibitors in this setting.

2.3.2 Protocols and glutamine flux estimation

The *Basic inhibition protocol* was used to calculate the total use of glutamine (Gln). The protocol is given in table 2.1 below.

Table 2.1: Basic inhibition protocol using the LDH inhibitor galloflavin to assess glutamine's contribution to ECAR and OCR using different concentrations of glutamine (0, 2 or 4 mM Gln). The cells start out in a media without glutamine and glucose in the experiment, but have been pregrown in high glucose (HG, 25 mM) and 2 mM glutamine. Each step marks the addition of a metabolite or inhibitor at the given timepoint. All ports are filled with 25 μL, and each new addition increases the well volume respectively.

Step	Compound	[Port]	[Well]	Vol well
0, t = 0 min	-	-	-	180 μL
1, t = 24 min	Glutamine	0, 16.4, 32.8 mM	0, 2, 4 mM	205 μL
2, t = 42 min	Glucose	80 mM	10 mM	230 μL
3, t = 66 min	2-DG	1 M	100 mM	255 μL
4, t = 84 min	Galloflavin	1.1 mM	100 μM	280 μL

The expression for calculating the total glutamine oxidation through path 6 and 7b is given as,

$$\text{Total Gln ox.} = \text{OCR}_{+\text{Gln}} - \text{OCR}_{\text{start}} \qquad (2.4)$$

where OCR_{+Gln} is the measured OCR after the addition of glutamine and OCR_{start} is the measured OCR prior to the addition of glutamine.

The *Extended inhibition protocol* was used to calculate the use of glutamine metabolism through ME1 (path 7a) or ME2 (path 7b). The protocol is given table 2.2 below.

Table 2.2: Extended inhibition protocol using the MPC inhibitor UK5099 and the LDH inhibitor galloflavin to assess glutamine's contribution to ECAR and OCR. Cells are pregrown in low glucose (LG, 5 mM) or high glucose (HG, 25 mM), and the starting media in the experiments contains the same concentration of glucose as the cells have been pregrown in. Each step marks the addition of a metabolite or inhibitor, at the given timepoint. All ports are filled with 25 μL, and each new addition increases the well volume respectively.

Step	Compound	[Port]	[Well]	Vol well
0, t = 0 min	-	-	-	180 μL
1, t = 18 min	2-DG	1 M	100 mM	205 μL
2, t = 48 min	Galloflavin	1 mM	100 μM	230 μL
3, t = 66 min	UK5099	2 mM	200 μM	255 μL
4, t = 84 min	Rotenone	10 μM	1 μM	280 μL
	Antimycin A	10 μM	1 μM	
	Oligomycin	30 μM	3 μM	

The expression for calculating the lactic fermentation (ECAR) of glutamine through ME1 (path 7a) is given as,

$$\text{ME1 Gln ferm.} = ECAR_{+2DG} - ECAR_{+GF} \tag{2.5}$$

where $ECAR_{+2DG}$ is the measured ECAR after the addition of 2-DG and $ECAR_{+GF}$ is the measured ECAR after the addition of galloflavin.

Finally, the expression for calculating the oxidation of glutamine through ME2 (path 7b) is given as,

$$\text{ME2 Gln ox.} = OCR_{+UK5099} - OCR_{+Rot,Ant,Oli} \tag{2.6}$$

where $OCR_{+UK5099}$ is the measured OCR after the addition of UK5099 and $OCR_{+Rot,Ant,Oli}$ is the measured OCR after the addition of the rotenone, antimycin A and oligmycin mixture.

2.3.3 Cell line culturing

Two colorectal cancer cell lines, Caco2 (Merck) and HCT116 (Merck) were donated by Oddmund Nordgård from the cell lab at Stavanger University Hospital. The cells were grown in DMEM without glutamine or glucose (Corning), with addition of 10% FBS (Biowest) and 5% PenStrep (Biowest). Glucose and glutamine were added fresh, with 25 mM glucose and 2 mM L-glutamine used for the normal growth media. Once 70% confluent, cells were split and seeded for experiments.

2.3.4 Preperation of cells for Seahorse experiments

Cells were seeded in Seahorse 8 well cartridges. Caco2 cells were seeded at 15000 cells per well in 80 μL of media and HCT116 cells were seeded at 10000 cells per well in 80 μL media. The difference in seeding density was to ensure that the measurements were within the linear range of the device in OCR readings, and to ensure sufficient confluency for the monolayer that was measured. The wells were coated with collagen 24 hours prior to seeding, to assure better attachment. The cells were either grown in low glucose (LG, 5 mM) media or high glucose (HG, 25 mM) media, together with 2 mM Gln in the cartridge wells for 24 hours prior to experiments. The medium was replaced by 180 μL serum-free Seahorse medium 1 hour before the experiment, and incubated in a CO_2-free incubator. Glutamine and glucose were added to the Seahorse base medium according to the protocols, and the pH was adjusted to 7.4 using NaOH.

2.3.5 Units and normalization of ECAR and OCR measurements

Protein content was measured using the Pierce BCA Protein Assay Kit (ThermoFisher, USA) in a microplate setting directly into the Seahorse-well plates. The protein measurements from each well was used to normalize ECAR and OCR values. The first datapoint from each measurement series was set to 100 % to ease the comparison between the cell lines, and the percentage-wise contribution of each inhibitor. The two last datapoints in each measurement series were used to calculate the effect of the inhibitors (in percent), working in duplets for the basic inhibition protocol (two 0 mM Gln wells, two 2 mM Gln wells and two 4 mM Gln wells), and triplicates for the extended inhibition protocol (three LG wells and three HG wells).

Chapter 3

Results

This chapter summarizes the main results from the three papers that make up this thesis.

3.1 Paper I – Performance of Homeostatic Controller Motifs Dealing with Perturbations of Rapid Growth and Depletion

As explained in section 2.1 and exemplified in figures 2.1 and 2.2, three variants of each of the eight controller motifs from figure 1.4 were examined in this study. Each controller motif was exposed to

- a linear increase in k_1 or k_2 as given by equation 2.1

- an exponential increase in k_1 or k_2 as given by equation 2.2

- a hyperbolic increase in k_1 or k_2 as given by equation 2.3

The main results regarding how each motif cope with these perturbations are summarized in table 3.1. As we see from table 3.1, the controller motifs are organized in pairs consisting of one inflow and one outflow controller. This organization is based on the signaling between A and E, where

- motifs 1 and 5 are based on activation between A and E, and activation from E to the compensatory flux of A

- motifs 2 and 6 are based on activation between A and E, and inhibition from E to the compensatory flux of A

- motifs 3 and 7 are based on inhibition between A and E, and activation from E to the compensatory flux of A

Table 3.1: Summarized results from the simulations of all controller motifs.

controller motifs	time dependence of k_1/k_2 Increase	type of integral control implementation		
		zero-order	first-order	second-order
1, 5 (Figure 3, SI2, SI3)	linear	constant A-offset, dependent on $\dot{k}_1/\dot{k}_2$	functional controller	functional controller
	exponential	controller breakdown	constant A-offset, dependent on k_1/k_2	functional controller
	hyperbolic	controller breakdown	controller breakdown	constant or small increasing A-offset
2, 6 (Figure 5, SI4, SI5)	linear	functional controller, breakdown at high k_1/k_2 values	functional controller, breakdown at high k_1/k_2 values	constant or increasing A-offset
	exponential	functional controller, breakdown at high k_1/k_2 values	breakdown at high k_1/k_2 values	controller breakdown
	hyperbolic	breakdown at high k_1/k_2 values	breakdown at high k_1/k_2 values	controller breakdown
3, 7 (Figure 7, SI6, SI7)	linear	constant A-offset, dependent on $\dot{k}_1/\dot{k}_2$	functional controller	functional controller
	exponential	controller breakdown	constant A-offset, dependent on k_1/k_2	functional controller
	hyperbolic	controller breakdown	controller breakdown	constant or small increasing A-offset
4, 8 (Figure 9, SI8, SI9)	linear	functional controller, breakdown at high k_1/k_2 values	functional controller, breakdown at high k_1/k_2 values	controller breakdown
	exponential	breakdown at high k_1/k_2 values	controller breakdown	controller breakdown
	hyperbolic	breakdown at high k_1/k_2 values	controller breakdown	controller breakdown

- motifs 4 and 8 are based on inhibition between A and E, and inhibition from E to the compensatory flux of A

The response to either linear, exponential or hyperbolic increases in k_1 or k_2 are given in the table for the zero-, first-, and second-order kinetic implementations. A controller is considered *functional* when the offset between A and the controller's set-point, A_{set}, decreases with time. On the other hand, controller *breakdown* occurs when the offset in A from A_{set} increases monotonically with time.

One of the main results we can extract from table 3.1, is that controllers with activating kinetics between E and the compensatory flux (motifs 1, 3, 5 and 7), are able to cope with rapidly growing perturbations under the condition that the integral control implementation is at least of the same kinetic order as the perturbation (right part of table 3.1). Another interesting result is found for the controllers where the compensatory flux is inhibited by the controller species E (motifs 2, 4, 6 and 8). Since these controllers already have an inherent hyperbolic rate law in their compensatory fluxes (see equation 3.1 below and the related discussion), the zero-order implementations of these controllers are actually able to cope with the applied time perturbations in k_1 and k_2. However, these controllers face a problem as the perturbation levels drive the controller species E to such low levels that the compensatory fluxes become saturated and the controller breaks down. For these controllers, the zero-order implementation of integral control provides the best control design, as higher-order implementation of integral control hinders an effective decrease in E.

These differences in controller behaviour can be illustrated using the results from the simulations of controller motifs 1 (see figure 3.1) and 4 (see figure 3.2). The kinetic implementations of these motifs were presented in figures 2.1 and 2.2 in section 2.1.
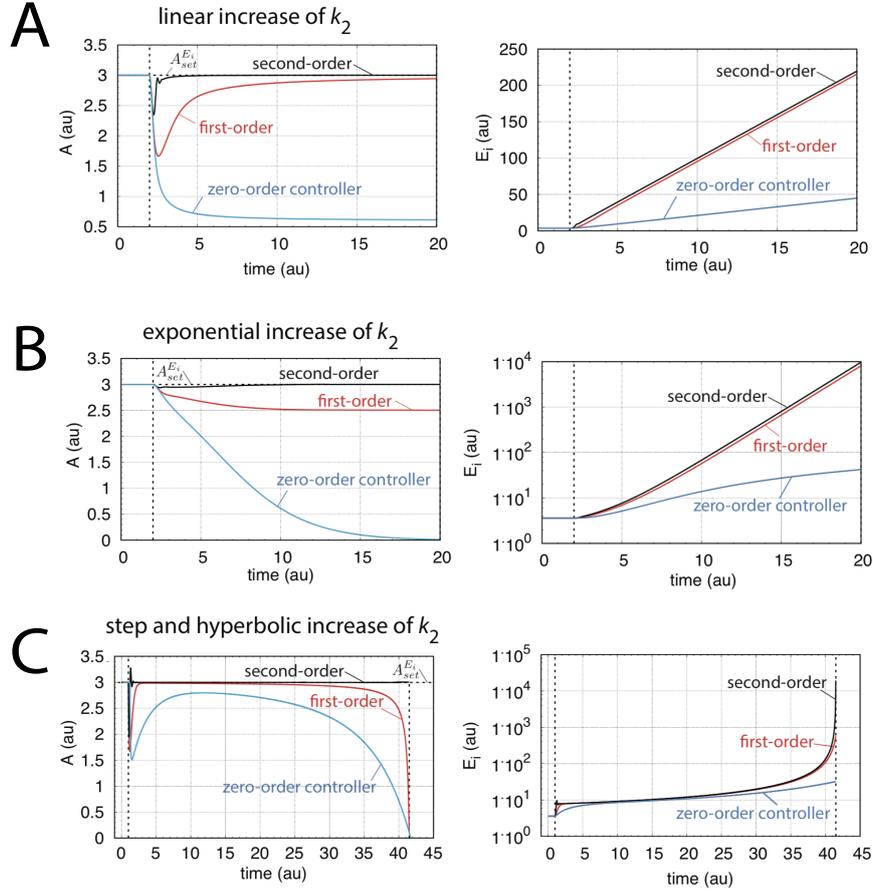
Figure 3.1: Performance of zero-, first-, and second-order kinetic implementations of integral control in controller motif 1. **A** Simulations of A and E_i during a linear increase in k_2. **B** Simulations of A and E_i during an exponential increase in k_2. **C** Simulations of A and E_i during a hyperbolic increase in k_2. Rate equations for k_2 are described in section 2.1, equations 2.1 - 2.3.

From the simulations of motif 1 in figure 3.1, we observe that the second-order controller outperforms the zero- and first-order controllers for all types of perturbations. The first-order controller produces a constant offset from the set-point $A_{set}^{E_i}$ during the exponential increase in k_2. For the hyperbolic increase in k_2, the first-order controller breaks down. The zero-order controller produces a constant offset from the set-point $A_{set}^{E_i}$ during the linear increase in k_2 and breaks down for the exponential and hyperbolic increases in k_2.
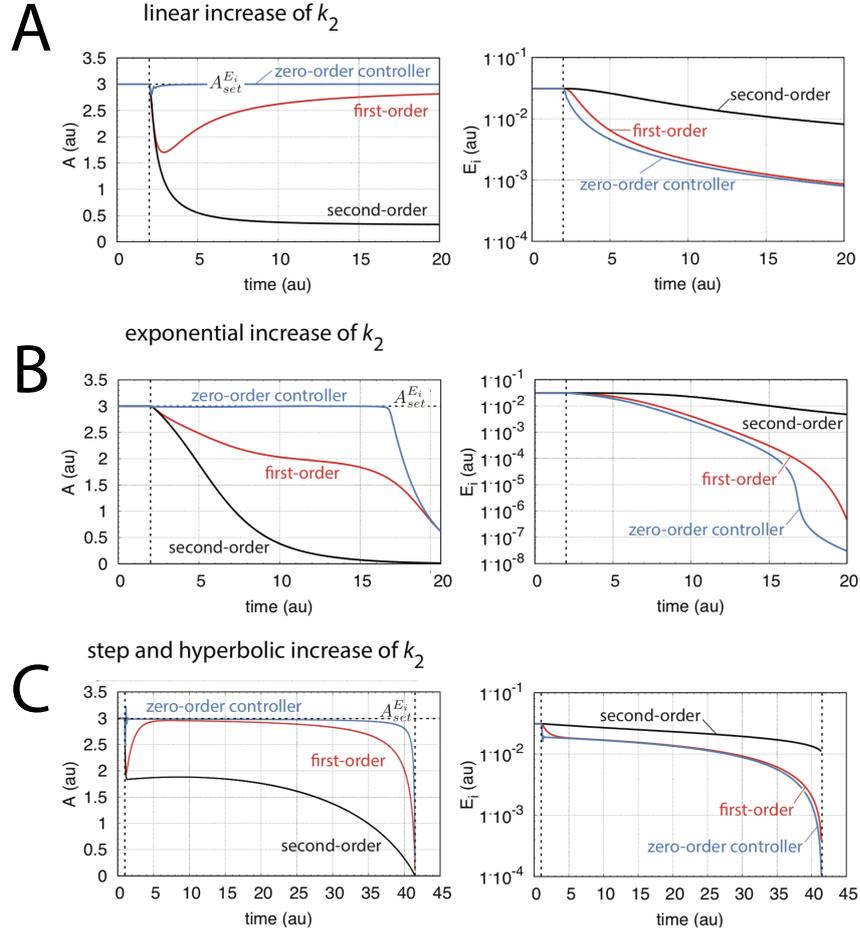
Figure 3.2: Performance of zero-, first-, and second-order kinetic implementations of integral control in controller motif 4. **A** Simulations of A and E_i during a linear increase in k_2. **B** Simulations of A and E_i during an exponential increase in k_2. **C** Simulations of A and E_i during a hyperbolic increase in k_2. Rate equations for k_2 are described in section 2.1, equations 2.1 - 2.3.

From the simulations of motif 4 in figure 3.2, we observe that the zero-order controller outperforms the first- and second-order controllers for all type of perturbations. As mentioned above, this is due to the inherent hyperbolic expression being a part of the inhibitory action E has on the compensatory flux in these controllers, i.e.,

$$f(E) = \frac{K_i^E}{K_i^E + E} \tag{3.1}$$

where K_i^E is the inhibition constant, corresponding to k_{23} in figure 2.2. This implies that inhibition adds a hyperbolic term to the overall controller motif functionality, and our results are therefore in accordance with the internal model principle (IMP) described in section 1.4. This is furthermore verified through the observations of the second-order controller of motifs 1, 3, 5 and 7, which have the ability to increase A by increasing E hyperbolically to compensate for the hyperbolic perturbation given in k_1 or k_2.

3.2 Paper II – Exploring Mechanisms of Glucose Uptake Regulation and Dilution Resistance in Growing Cancer Cells

The mathematical model in this study was built in a stepwise manner, illustrated by the three versions A, B and C shown in figure 3.3. By simulating each model under step perturbations in glucose supply, with or without growth conditions (volume increase), we were able to jugde and compare their performances.

The results indicate that the simplest structure (**model A**) was not able to show any regulatory mechanisms with respect to changes in glucose supply or during growth (see fig. 5 in paper II).

In order to improve the regulatory performance of the model, we considered the AMPK-related signaling effects shown in figure 1.11. Based on the overall function of these parallell pathways, we added a negative feedback structure from G6P to GLUT1 in **model B**. This feedback structure corresponds to inflow controller motif 3 from figure 1.4. From the simulations of **model B**, we observed homeostatic control of G6P for a stepwise increase in glucose supply, but not during growth. Further investigations of **model B** revealed that the dilution of HK2 during growth effectively limited the glycolytic flux. We therefore added a regulatory loop between this enzym and cellular glucose (Glc) in **model C**. The details on how HK2 functions as an integral controller is given in the supplementary information of the paper.

The simulation results from **model C** is shown in figure 3.4. The simulation is divided into four phases. In the first phase (white area), the
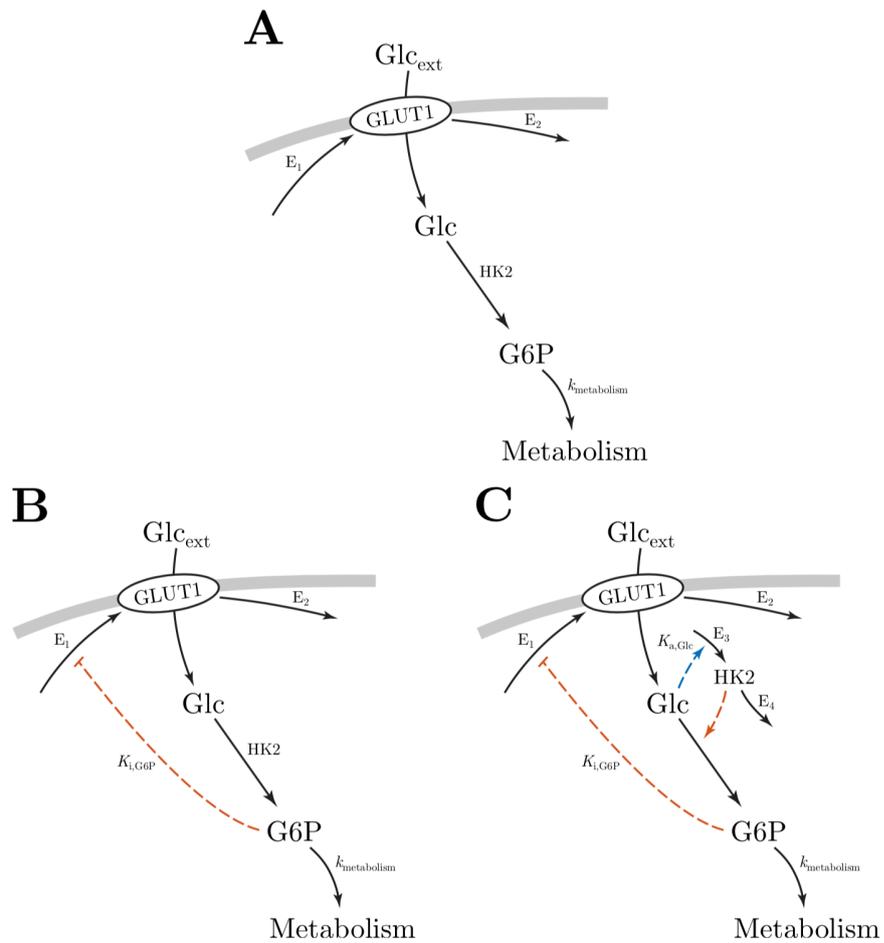
Figure 3.3: The three versions of the glucose uptake model. **Model A** includes only the uptake and supply of glucose to metabolism. **Model B** includes feedback inhibition from G6P to GLUT1 mediated glucose uptake. **Model C** includes in addition the regulatory feedback by HK2 on intracellular glucose levels. *Metabolism* is the model sink of metabolites downstream of G6P.
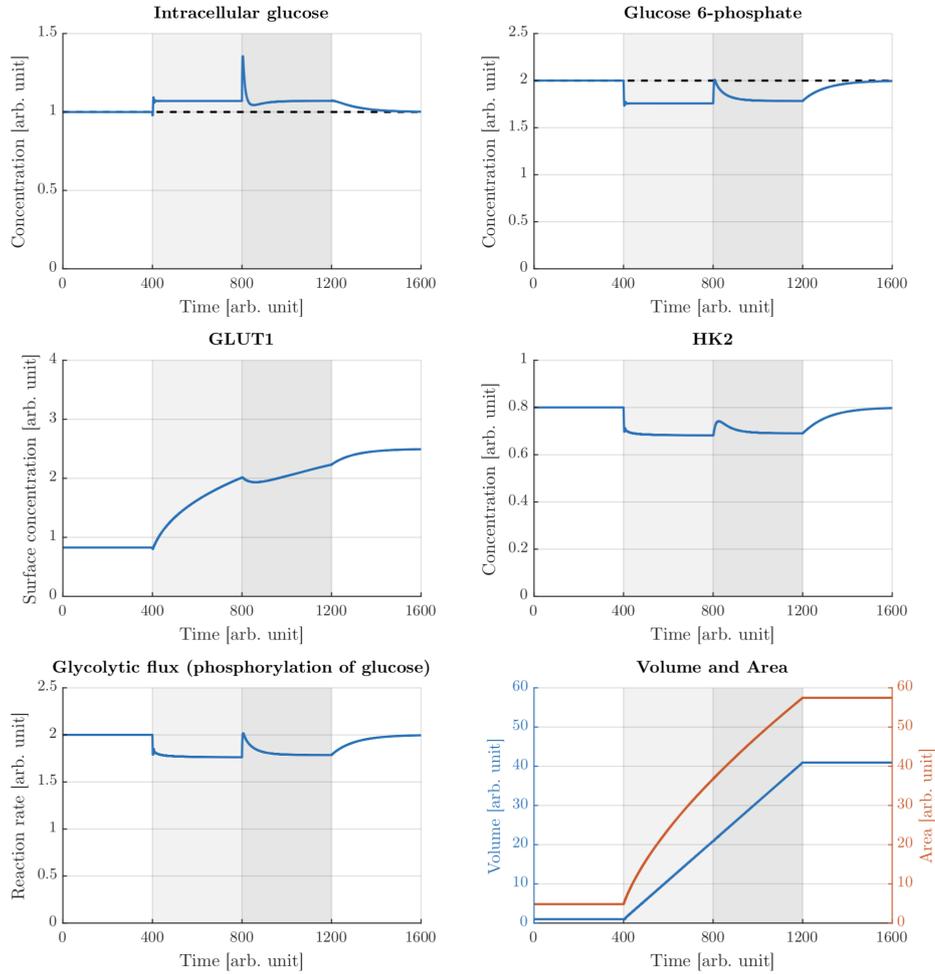
Figure 3.4: Simulation results of **model C**. Initially, the cellular volume is kept constant, and the system has settled at steady state (white area). In the second phase (light gray area), the cellular volume increases linearly. During this phase, metabolite levels and the glycolytic flux are maintained at constant levels, however, with offsets from the steady state values associated with constant volume. In the third phase (dark gray area), the concentration of extracellular glucose is increased while the volume is still increasing. Finally, in the fourth phase the growth is terminated, and we see that metabolite levels and the glycolytic flux return to steady state values associated with constant volume.

volume is kept constant and the system has settled at steady state. In the second phase (light gray area), the cellular volume increases linearly and we note that the glycolytic flux is shifted by an offset compared to the case without growth (seen in the lower left panel). We also note that the other intracellular metabolites are shifted accordingly. In the third phase (dark gray area), the extracellular glucose concentration is increased in a step from 5 to 20 (data not shown). As a consequence, there is a temporary drop in the GLUT1 concentration, though there is no permanent change for the other intracellular metabolites during this phase. In other words, it seems that the control mechanisms attempt to bring the system back to the steady state associated with growth (light gray area), and not to the steady state associated with constant volume (first white area). This again, suggests that the growth associated offset is in fact a change in set-point, rather than the inability to maintain the glycolytic flux during growth. In the last phase (white area) the growth is terminated, and the metabolite levels and the glycolytic flux return to values associated with constant volume. Compared to the conditions in the first phase, the total volume is increased and the extracellular glucose concentration is at a higher level.

The Expression Atlas database was used to collect differential gene expression data comparing cancer cells with normal cells. Average log2-fold changes for key genes associated with glucose uptake and glycolysis are shown in figure 3 in paper II, and the values largely mirrors the reported rewiring of glycolysis in cancer (see section 1.7 in the introduction). There is a clear upregulation of GLUT1 with a 0.73 log2-fold higher expression, and of HK2 with a 1.0 log2-fold higher expression. Thus, our proposed model C appears to include the key components for glucose uptake in cancer. PFKP (phosphofructokinase) and PKM (pyruvate kinase M) are also upregulated with a 0.20 and 1.33 log2-fold higher expression, respectively. These two enzymes are likely to play a role in maintaining a high flux through glycolysis downstream of G6P but are not included in our model.

3.3 Paper III – Using UK5099 and galloflavin to examine glutamine metabolism through sequential inhibition in a real time setting

In order to make protocols that can be used to estimate how much glutamine is used in the mitochondria and how much glutamine-derived pyruvate is secreted as lactate, we have incorporated the use of two new inhibitors:

galloflavin and UK5099. Galloflavin inhibits both isoforms of lactate dehydrogenase (LDH) [99], and has as far as we know never been used in a Seahorse XFp setting before. UK5099 inhibits the mitochondrial pyruvate carrier (MPC) [70] and has not been used on its own as an acute injectant in Seahorse XFp metabolic flux measurements. The inhibitors were titrated, and concentrations suitable for Seahorse experiments were found.

We made two new protocols: the *basic inhibition protocol* which is used to calculate the total oxidation of glutamine, and the *extended inhibition protocol* which is used to calculate glutamine metabolism through ME1 (path 7a) and ME2 (path 7b). The protocols are explained in detail in section 2.3.2 of this thesis and in paper III itself.

We used our protocols to examine glutamine metabolism in two colorectal cancer cells lines, Caco2 and HCT116. The results are shown in detail in the following sections, but in short: We found that the more aggressive cancer cell line, HCT116 [177], primarily metabolized glutamine to fuel the TCA cycle through path 6 and 7b. Addition of glutamine increased the oxidative metabolism in HCT116 cells with almost 50 % and oxidation of glutamine contributes to just above 30 % of the total oxidative metabolism (see table 3 in paper III). In the less aggressive and more differentiated Caco2 cells [177] on the other hand, glutamine does not contribute to more than approximately 5 % of the total oxidative metabolism. The results are reversed for how much glutamine metabolism (path 7a) contribute to the total amount of fermentation of pyruvate to lactate. Glutamine makes up only around 5 % of lactate fermentation in HCT116, but significantly more, around 17 % in Caco2 (see table 4 in paper III).

3.3.1 Results from the basic inhibition protocol

The real-time measurements gathered from the experiments done with the basic inhibition protocol are shown in figure 3.5. In this protocol the cells start out in a media without glutamine and glucose.

The glutamine (Gln) addition only increased the ECAR for the 2 mM Gln wells of HCT116 (fig 3.5A), and actually decreased the ECAR for the 2 mM and 4 mM Gln wells for Caco2 (fig. 3.5C).

Glutamine increased the OCR for HCT116 (fig. 3.5B), and the effect is clearly different compared to the cells that got no glutamine added (0 mM) which had a continued decline in OCR (fig. 3.5B). It does however not seem to be a difference between the 2 and 4 mM Gln wells. For Caco2 cells
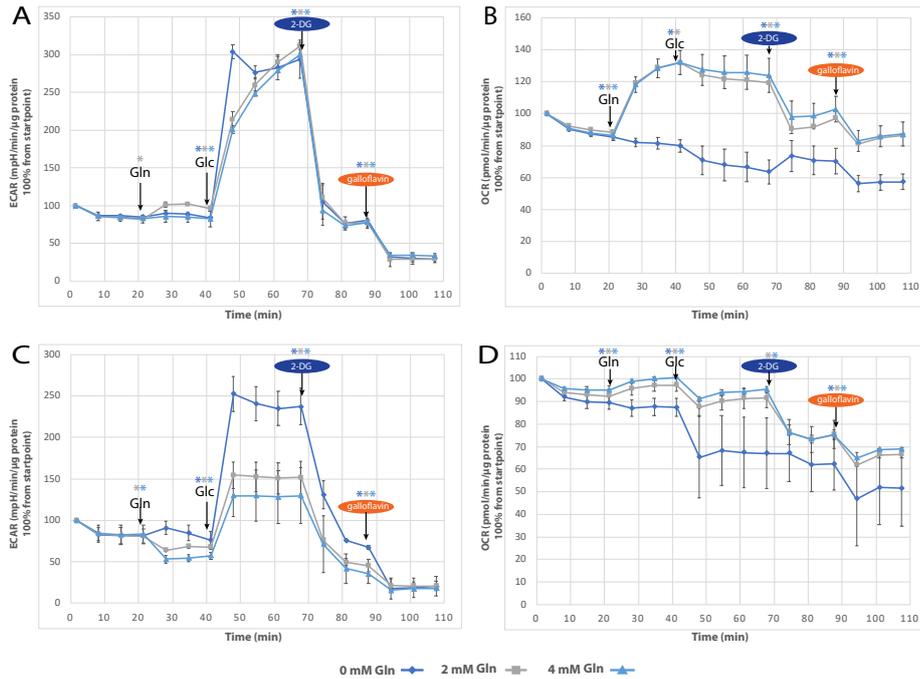
Figure 3.5: A ECAR HCT116 (mpH/min/μg protein in % from startpoint), **B** OCR HCT116 (pmol/min/μg protein in % from startpoint), **C** ECAR Caco2 (mpH/min/μg protein in % from startpoint), **D** OCR Caco2 (pmol/min/μg protein in % from startpoint). Measurements from 10 000 HCT116 cells per well and 15 000 Caco2 cells per well, using the basic inhibition protocol, in duplicates. Additions are 0, 2 or 4 mM glutamine (Gln) (t = 24 min) as indicated by each group, followed by 10 mM glucose (Glc) (t = 42 min), 2-deoxyglucose (2-DG) (t = 66 min) and the LDH inhibitor galloflavin (t = 84 min). Significant changes between the two last datapoints from before and after each addition are marked by * in the respective color for the 0 mM Gln, 2 mM Gln and 4 mM Gln wells.

43

there seemed to be only a slight (but significant) increase in OCR when glutamine was added (fig 3.5D). The increase in OCR after addition of glutamine is significantly different between the two cell lines, indicating that Caco2 does not oxidize as much glutamine in the mitochondria as HCT116.

Using equation 2.4 and the measured OCR rates after the addition of glutamine (OCR_{+OCR}), we calculated the contribution of glutamine to the total oxidative metabolism for both cell lines and found that it made out approximately 30 % of the total OCR for HCT116 cells and only 5 % of the total OCR for Caco2 cells.

The glucose addition yielded a large increase in the ECAR readings for both cell lines, but the increase was relatively higher for cells that had received less glutamine in the previous addition for Caco2 cells (fig. 3.5C) whereas no such dependence of glutamine level was seen for HCT116 cells (fig. 3.5A). The glucose addition gave a small dip in the OCR measurements for both cell lines and for all wells (figs. 3.5B and D).

After the 2-DG addition, glucose's contribution to ECAR is blocked, and the ECAR levels drop to approximately the same level as before the glucose addition was made (figs. 3.5A and C). The OCR also drops for the 2 mM Gln and 4 mM Gln wells of both cell lines (figs. 3.5B and D) after the 2-DG addition.

Once galloflavin is added, LDH is blocked, and the cells are not able to convert pyruvate to lactate. We are thus left with a measurement of the background acidification rate (figs. 3.5A and C). Galloflavin also causes the OCR to drop for all wells (figs. 3.5B and D).

The results from the basic inhibition protocol show that HCT116 use more glutamine to fuel the TCA cycle, through path 6 + 7b, than Caco2 cells do. It also provides an insight into how much glucose is fermented to lactate (ECAR), and how this is different depending on the glutamine concentration for Caco2, but not for HCT116. It seems like HCT116 cells maximize the use of media components, seen by a large increase in OCR after the glutamine addition for both the 2 mM Gln wells and the 4 mM Gln wells (fig. 3.5B), as well as by a large increase in ECAR after the glucose addition (fig. 3.5A). Caco2 cells on the other hand, only maximize the ECAR after the glucose addition in the wells that were depleted of nutrients (0 mM Gln wells) (fig. 3.5C). For Caco2, the cells with 0 mM glutamine increased their ECAR much more than the cells with 2 mM, which again increased their ECAR more than the cells with 4 mM glutamine. For

HCT116 cells, on the other hand, the ECAR reading was similar for all wells (fig. 3.5A). It seems that glutamine in HCT116 has a clear contribution to OCR whereas glucose has a clear contribution to ECAR, and that HCT116 in this way metabolizes glutamine and glucose more independently of each other than what Caco2 does.

3.3.2 Results from the extended inhibition protocol

The real-time measurements gathered from the experiments done with the basic inhibition protocol are shown in figure 3.5. In this protocol the cells start out in a media with 2 mM glutamine and either 5 mM glucose (low glucose, LG) or 25 mM glucose (high glucose, HG).

2-DG lowered the ECAR of HCT116 cells to an average of 12 % from the total ECAR (fig. 3.6A), which is a significantly larger reduction than an average of 33 % for Caco2 cells (fig. 3.6C). 2-DG also lowered the OCR (figs. 3.6B and D) to around 85% for Caco2 cells and 96% for HCT116 cells from the total OCR. The reduction in OCR indicates that when glycolysis is blocked upstream, it also affects the pyruvate availability downstream for oxidative phosphorylation. The decrease in OCR was significant for all measurement series, except for the HG HCT116 wells.

Estimations of glutamine's contribution to ECAR through the ME1 and path 7a (see fig. 2.3) are calculated using equation 2.5. The calculations show that glutamine in HCT116 cells contribute to approximately 5 % of the total lactate production, whereas glutamine in Caco2 cells contribute to approximately 17 % of the total lactate production (see table 3.3 in paper III).

Next, UK5099 was added to block cytosolic pyruvate from entering the mitochondria through MPC. The OCR for HCT116 and Caco2 was significantly reduced by UK5099 (figs. 3.6B and D). Also, ECAR dropped significantly for both cell lines (figs. 3.6A and C).

Finally, by adding the electron transport chain inhibitors Rotenone, Antimycin A and Oligomycin (see fig. 2.3 for target sites), we can estimate the flow of glutamine through ME2 and path 7b by using equation 2.6. The calculations show that HCT116 cells metabolize approximately 8 % of their total oxidative phophorylation through path 7b, whereas Caco2 cells metabolize approximately 4.5 % of their total oxidative phosphorylation through path 7b.
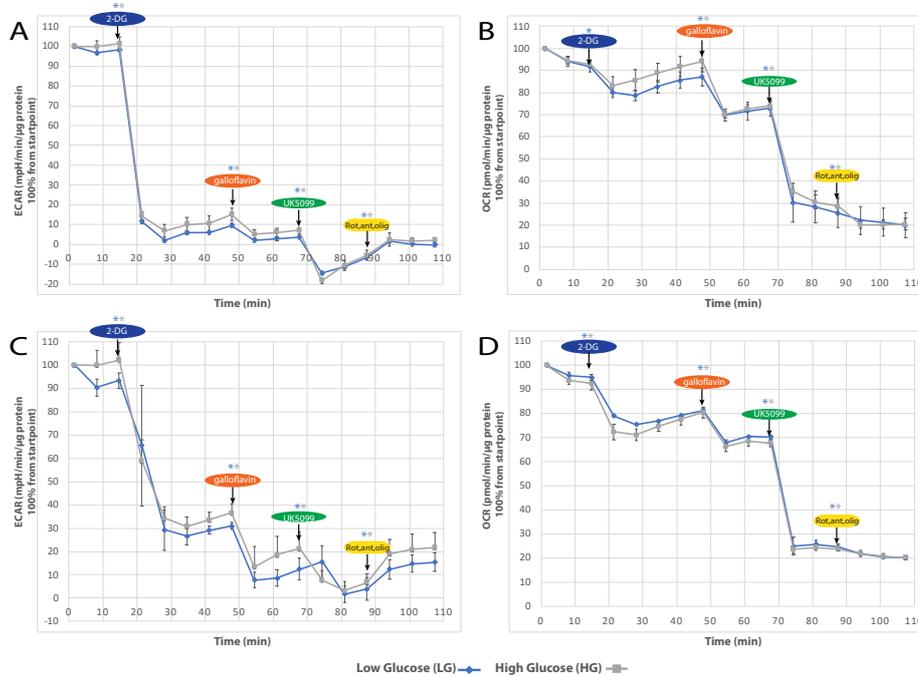
Figure 3.6: A ECAR HCT116 (mpH/min/μg protein in % from startpoint), **B** OCR HCT116 (pmol/min/μg protein in % from startpoint), **C** ECAR Caco2 (mpH/min/μg protein in % from startpoint), **D** OCR Caco2 (pmol/min/μg protein in % from startpoint). Measurements from 10 000 HCT116 cells per well and 15 000 Caco2 cells per well, using the extended inhibition protocol. Cells were pregrown either low glucose (LG, 5 mM) or high glucose (HG, 25 mM) and also ran in LG and HG accordingly. Additions were 2-deoxyglucose (2-DG) (t = 18 min) followed the LDH inhibitor galloflavin (t = 48 min), the MPC inhibitor UK5099 (t = 66 min), and finally the electron transport chain inhibitors rotenone, antimycin and oligomycin (Rot,Ant,Olig) (t = 84 min). Significant changes between the two last datapoints from before and after each addition are marked by * of the respectful color between LG and HG.

The results of the extended inhibition protocol show that Caco2 cells secrete more glutamine-derived lactate via ME1 and path 7a, than HCT116 cells do. Furthermore the results also show that HCT116 cells have more TCA cycle activity after the addition of UK5099, and therefore oxidize more glutamine via ME2 and path 7b than Caco2 cells do.

Chapter 4

Discussion and concluding remarks

This chapter will first summarize the main contributions of each paper and evaluate the results in a broader perspective. Then, to extend on our work on glutamine metabolism in cancer, we will look into a possible control mechanism for glutamine and glutamate uptake to the mitochondria. It is reasonable to assume that the control mechanisms for glutamine uptake in cancer cells are altered to better support growth, much like the system for glucose uptake examined in paper II. Finally, we will discuss our general approach and its limitations.

4.1 Paper I – How internal structure and kinetics affects the performance of biological controllers

Paper I explores some of the inner properties of the controller motifs, specifically how the structural and kinetic properties affects and limits the ability to compensate for time varying perturbations. The controllers are capable of maintaining homeostasis if they are able to produce a compensatory flux that matches the perturbation. This depends on the combination of the underlying kinetics of the production and removal rates of the controller species E, and the way E acts on the compensatory flux.

The controllers that have a compensatory flux that is inhibited by the controller species (motifs 2, 4, 6 and 8) all face the problem that a continuously increasing perturbation will eventually drive the level of E so low that the compensatory flux saturates. This leads to a noticeable controller breakdown, not observed in the simulations of activating controllers (motifs

1, 3, 5 and 7). However, in a real physiological setting it is obvious that the compensatory flux at some point will saturate also for the activating controllers. Either because of saturation in the flux itself, or because of saturation in the level of E; a cell or organism will eventually reach a limit in the capacity to produce more E. Thus, there will be an observable breakdown also in the controllers that have a compensatory flux activated by the controller species. Seen in retrospect, it can be argued that the activating controllers, for this reason, should have been modeled with actual saturation kinetics in the expression for the compensatory flux instead of a pure linear dependence on E[1].

In the end of the discussion section of paper I, we comment that saturation-related breakdown behavior can be analogous to Selye's General Adaptation Syndrome (GAS) [132]: "When continuously exposed to stress (cold, drugs, or forced work), Selye observed that animals show a certain reaction pattern: during the first phase, the so-called "alarm reaction", animals react to the stressor and prepare for physical activity; during the second phase, termed the "stage of resistance", animals have adapted to the stressor and are in a stage of apparent well-being similar to the unstressed animals; in the final phase, the "stage of exhaustion", the resistance collapses and animals die. Selye interpreted the surprising collapse as a loss of "adaptation energy" [63, 131, 132]. The breakdown seen in the controllers when a continuously increasing perturbation after some time drives the controller species and the compensatory flux into saturation can similarly be seen as a "loss of adaptation energy", i.e., that the controllers have exhausted their ability to compensate."

The two-component controller motifs studied in paper I are sometimes referred to as inflow-outflow motifs, as they act through either a compensatory inflow or a compensatory outflow flux [50]. They are however, of course, not the only type of regulatory network motifs [3, 102, 118]. Krishnan and Floros recently published a large study that examined how different types of motifs reacted to different types of disturbances or stimuli [87]. Their study included two-component inflow-outflow motifs and three-component variants with an added node, in addition to so-called *transcritical circuits*, *incoherent feedforwards motifs*, and other networks. The transcritical circuit involves three species, A, B and C, where the conversion from B to C is facilitated by an autocatalytic feedback. The incoherent feedforward motifs

---

[1]Our group has looked into the effect of saturable activation kinetics in other works [121, 122]

considered were all three-node systems with a topology in which two different links from the input-receiving node ends at the output-transmitting node. The cumulative sign of the two pathways have different signs (one positive and one negative) [97]. Krishnan and Floros also examined how the different motifs reacted to ramp perturbations, i.e., linear increase in perturbation strength, and found, like us, that the two-component inflow-outflow motifs with zero-order kinetics[2] are not able to compensate for ramp perturbations that act on A. They did not consider two-component motifs with higher-order kinetics in the controller species. However, they found that inflow-outflow motifs with three nodes, transcritical circuits with three nodes, and feedforward motifs with three nodes, are all able to compensate for ramp perturbations (with some limitations in where the perturbation disturbs the system). It is interesting that three node networks are better to compensate for ramp disturbances, albeit not surprising as more nodes in the feedback loop from the disturbance to the compensatory flow makes the compensatory flow able to mimic a broader class of signals. Our group has also previously shown that three node inflow-outflow motifs are able to compensate for ramp disturbances when the feedback path has double integral action [147].

4.2 Paper II – Regulation of glucose uptake and metabolic changes in growing cancer cells

In paper II, we studied the rewiring of glycolysis in cancer, both by literature studies and analysis of public gene expression data in the Expression Atlas database. Based on this, we constructed a mathematical model of glucose uptake and added regulatory mechanisms to it in a stepwise manner to investigate the role of each mechanism. We showed that while negative feedback from downstream glycolytic metabolites to glucose transporters (model B) is sufficient for homeostatic control of glycolysis in a constant cellular volume, it is not enough to achieve homeostatic control during growth. Simulations using our models show that negative feedback regulation of intermediate glycolytic enzymes (HK2) together with negative feedback regulation of glucose transporters (GLUT1) give homeostatic control during growth (model C).

The two control mechanisms examined in this paper form two controller motifs; the regulation of GLUT1 acts as an inflow controller (motif 3) of the

---

[2]See model DR12.M1 and DR12.M4, and figure 2 in their study.

glycolytic intermediate G6P; and the regulation of HK2 acts as an outflow controller (motif 5) of intracellular glucose. Both of the two controllers are modeled with zero-order kinetics with respect to the controller species, as there are no indications in the literature that either GLUT1 or HK2 has a direct autocatalytic effect on its own production. Growth is modeled as a linear increase in cellular volume, and thus acts as a ramp perturbation on the regulatory system. The observation that the negative feedback through GLUT1 alone is unable to compensate for this linear increase in cellular volume is in line with our results from paper I.

A general problem of trying to build and set up simple conceptual models of regulatory systems in cells, like in this study, is that it is unavoidable that some information is left out of the model. In this work, we based our reasoning for the negative feedback through GLUT1 on AMPK related pathways and signaling (see section 1.7 and fig. 1.11). However, there are also other pathways that are rewired in cancer that affect GLUT1 [172]. One transcription factor known to act as an ocongene when mutated is the mammalian target of rapamycin (mTOR). mTOR activates GLUT1 expression, as well as inducing the expression of other glycolytic enzymes under normoxic conditions [172, 176]. In fact, mTOR is activated by AMPK silencing, which means that even if AMPK becomes downregulated and cannot act positively to mobilize more GLUT1 to the surface, mTOR can [72]. Although we based our reasoning on AMPK mediated feedback, the feedback from G6P to the synthesis of GLUT1 is modeled directly, and AMPK is not actually included in the model.

Another interesting factor related to regulation of glucose uptake in cancer cells is the hypoxia inducible factor 1-α (HIF-1α), which is involved in the progression of many cancers [39]. It has actually been suggested that HIF-1α produces a positive feedforward loop between glycolytic intermediates and GLUT1 [41, 49]. It would in a future extension of our work be interesting to look closer into what role this HIF-1α pathway can play. An intriguing question is whether a positive loop would destabilize the entire feedback structure in the model, or if it maybe could act as an inner autocatalytic loop and give the controller motif better regulatory properties against ramp perturbations. Could an inner positive feedback have a similar or related effect to what autocatalytic synthesis and first-order removal of the controller species were shown to provide in paper I?

The genes involved in glycolysis which are typically upregulated in cancer were identified from the average genetic expression in a variety of different cell types and tissues. There are, as also shown by our own study of

two different cancer cell lines in paper III, metabolic differences between cancer cells. Although an increased reliance on glycolysis and lactic acid fermentation is considered a hallmark of cancer [93, 152], our paper does not examine whether the expression of individual genes related to glycolysis are correlated. In order to do so, a full multivariate analysis is necessary. However, we checked the data for GLUT1 and HK2 individually for some of the studies from the Expression Atlas database, and found that GLUT1 and HK2 expression correlated in 14 out of 16 studies (compared to normal cells). Furthermore, in 9 out of the 14 studies, the expression of GLUT1 and HK2 was higher than in the corresponding normal cells, whereas it was lower in the remaining 5 studies. On average we found a 0.73 2-log fold higher expression of GLUT1 in cancer cells and 1.0 2-log fold higher HK2 expression in cancer cells.

4.3 Paper III – Experimental analysis of glutamine metabolism in cancer cells

The experimental study of paper III allowed us to investigate how two cancer cell lines that differ in growth rates and differentiation grade, also differ in glutamine metabolism. As a mean to uncover this redirection of fluxes, we used a Seahorse XFp analyzer and two new inhibitors, i.e., UK5099 and galloflavin, for the mitochondrial pyruvate carrier (MPC) and the lactate dehydrogenase enzyme (LDH), respectively.

One of the uncertainties related to such experiments is whether or not each inhibitor functions as planned, i.e., fully inhibiting the pathway or causing adverse off-target effects. Hence, in order to ensure that the correct amount of galloflavin and UK5099 were added, both inhibitors were titrated. Since we only considered short time scales and not prolonged effects of the inhibitors, we opted for concentrations that were higher than those used in other experimental settings (see discussion in paper III). Another concern related to this type of experiments is that the relative change caused by the addition of a metabolite or inhibitor is not independent from the prior additions. All of the inhibitors and metabolites are added in the same, small media reservoir, and as the cells also consume metabolites over the time-course of the experiment, an addition may not yield the same result whether it is added in the beginning of the experiment or at the end.

Our study on redirection of metabolic flux is, among other things, based on inhibition of pyruvate, which is one of the most important intermediates

in the central carbon metabolism. Thus, an interesting extension of this study would be to add exogenous pyruvate to the cells in the experiments. It is found that in human embryonic cells, exogenous pyruvate lowered the ECAR and increased the OCR in Seahorse experiments [136]. Another alternative is to add galactose instead of glucose [2], which suppresses the glycolytic ATP production. In this situation, the cells would be forced to use oxidative phosphorylation and, as such, would provide valuable insight into basic energy requirements [123]. Thus, there are much to be revealed by carefully designed experiments using sequential addition of inhibitors and/or metabolites.

Other techniques that can be used to measure the flux through metabolic pathways include mass spectrometry (MS) and nuclear magnetic resonance (NMR). MS and MNR allow for carbon tracing of metabolic pathways, which means that the specific pathways an added metabolite follows can be mapped in detail [62, 100]. A limitation of MS, however, is that this technique require the cells to be harvested and thus provides only snapshots of the metabolic states. On the other hand, by real time NMR and Seahorse experiments, the metabolic state of cells can be analyzed in real-time, while the cells are still growing. Since the data is obtained in real time, the dynamics and compensatory actions of the cell's regulatory machinery during media perturbations can be revealed. Interestingly, our findings from the Seahorse experiments agree with results obtained by carbon tracing of glutamine. In fact, Yang et al found in a trace study that glutamine's contribution to the TCA cycle varied between 15 and 40 % of the total TCA intermediate pool in different ovarian cancer cells [167]. This is in line with our findings in paper III where we report a TCA cycle contribution of around 5 % for Caco2 (fig. 3.5D) and 30 % for HCT116 (fig. 3.5B).

4.3.1 Regulation of glutamine uptake based on a possible controller motif

A logical further extension of the work presented in this thesis is to explore the regulation of glutamine uptake to the mitochondria. The metabolism of glutamine is, as shown in paper III, different in different cancer cell lines. It would be interesting to do a closer study on the rewiring of glutamine metabolism in cancer, and to examine regulatory mechanisms in a similar way to what we have done for glucose metabolism in paper II. One potential use of the results obtained in this thesis is to explore the regulation of glutamine uptake into the mitochondria, by the use of an extended model

that includes regulation of both glucose and glutamine. Such a model could further be parameterized with realistic model parameters from Seahorse experiments.

From a mass balance perspective, it is evident that glutamine uptake into the mitochondria is linked to the glutamine uptake rate into the cytosol. Glutamine is transported into the cytosol by the Alanine, Serine, Cysteine Transporter 2 (ASCT2)[3] [95, 128]. The literature suggests that the uptake of extracellular glutamine is saturated at concentrations around 1-2 mM [65, 71, 127, 173]. This concentration region fits well with our results from the basic inhibition protocol, which showed that neither Caco2 nor HCT116 cells exhibited a difference in OCR when exposed to 4 mM versus 2 mM of glutamine, see figure 3.5B and C[4]. Glutamine is converted to glutamate in the intermembrane space of the mitochondria by the enzyme glutaminase (Gase) [101, 129], and the conversion releases one molecule of ammonium for each molecule of glutamine. Deberardinis and Cheng reported that the rate of ammonia secretion into the extracellular space is about 75% of the rate of glutamine uptake in glioblastoma cells (brain cancer), a number consistent with a high fraction of glutamine being metabolized in the mitochondria [47].

Glutamate is further transported from the intermembrane space and into the mitochondria by mitochondrial glutamate carriers. The two main human isoforms of the glutamate carrier are known as GC1 (SLC25A22) and GC2 (SLC25A18). Their respective K_M/V_{max} values for glutamate uniport uptake are approximately K_M=5 mM/V_{max}=12 μmol/min/g protein and K_M=0.3 mM/V_{max}=4 μmol/min/g protein [57]. Glutamate carriers have been reported to be upregulated in a number of tumors and cancer cell lines. In fact, SLC25A22 mRNA expression is upregulated in colorectal cancer, where the expression level is linked to cancer aggressiveness through proliferation and migration [92, 162]. Glutamate can also be transported into the mitochondria by the Aspartate-glutamate carrier (AGC1/SLC25A12) which transports one glutamine molecule into the mitochondria in exchange for one aspartate molecule transported out of the mitochondria [75]. SLC25A12 is also upregulated in many cancers [6, 75] and is believed to be tightly

---

[3]Glutamine is the preferred substrate of this transporter even though it is not included in the name; the transporter is called ASCT2 for historical reasons [128].

[4]Note that the slightly higher OCR rate of the HCT116 cells exposed to 4 mM glutamine compared to those exposed to 2 mM, in figure 3.5C, seems not to be caused by different concentrations of glutamine as the difference was already established before the glutamine addition.

regulated in different tissues under physiological and pathological conditions because of the link between cytosolic metabolism and mitochondrial metabolism [73, 74, 76]. Another human isoform, AGC2/SLC25A13, has been found to be upregulated in some colorectal cancer cell lines and downregulated in others depending on nutrient availablility [103]. In DLD1 cells, the mRNA level of SLC25A13 decreased during glucose-deprived conditions relative to the levels in glucose- and glutamine-containing conditions. The opposite effect was found in HT29 cells [103], which highlights how various cancer cell lines may interchange glucose for glutamine.

Based on the discussion above, we speculate that the mitochondrial glutamate carrier may be an important regulator of glutamine metabolism in cancer, with a functionality described by one of our controller motifs. Figure 4.1 shows a possible scheme where the synthesis of the glutamate carrier depends on mitochondrial concentration of glutamate, an arrangement similar to the regulation of GLUT1 in paper II. Whether or not the mitochondrial concentration of glutamate actually affect the transcriptional level of the carrier remains unknown, and the arrangement is at this stage only speculation.

4.4   The bottom up systems biology approach

"All models are wrong, but some are useful" - George E.P. Box [22]

There are different modeling approaches used in systems biology [34, 45, 77], ranging from large scale models built from the top down to include every molecule, enzyme and pathway in a metabolic network, to models with only a few key components and interactions built gradually in a bottom up fashion. Even if these kind of models are different in scope, a common denominator is that mathematical models in systems biology are intended to be a description of *why the biological system behaves the way it does.* The models are in other words mechanistic and can be used to understand and predict the behavior of the system [77]. Both large and small scale systems biology models are thus structurally different from purely empirical models with limited relation to the actual biological system. Empirical models are adapted to mimic an experimental observation, e.g., a generic set of mathematical equations with adjustable parameters fitted to match a certain behavior.
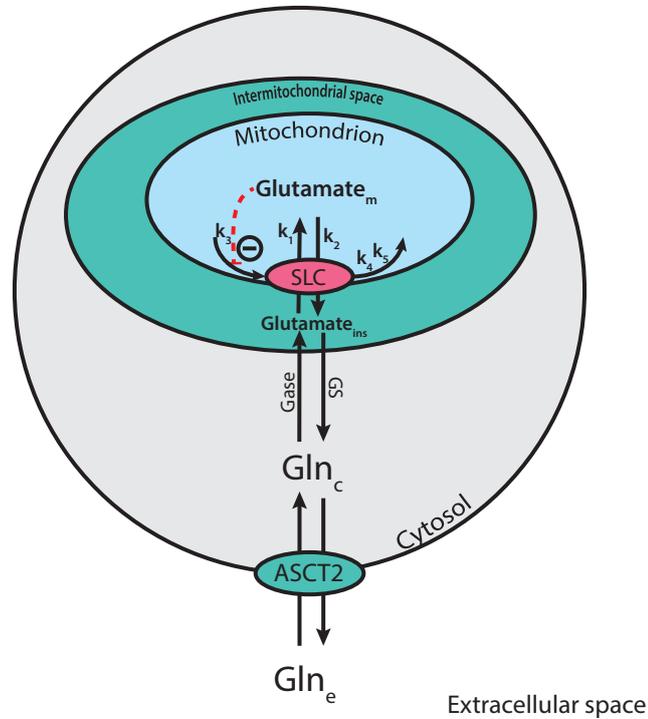
Figure 4.1: Suggestion of glutamate uptake regulation by mitochondrial glutamate carriers (SLCs). The uptake of glutamate from the inner mitochondrial space through membrane-bound carriers could be regulated in the way depicted with the rate constants k_{1-5}. The control structure is similar to the inflow controller motif 3, and thus the regulation of GLUT1 from paper II. Glutamate is produced from glutamine by glutaminase (Gase) and glutamine synthetase (GS) is an enzyme that catalyzes the reverse reaction. ASCT2 is the cytosolic transporter of glutamine.

The work in this thesis uses a bottom up approach where key components are presented as state variables in ordinary differential equations (ODEs), which describe the behavior of key components and their interactions. We have in the work presented in paper I and paper II made step by step changes in the structure of the models, and then evaluated each step based on the simulation results.

4.4.1 Limitations in our approach

One of our goals in this work has been to investigate the *structural* properties of regulatory networks. Parameters, such as rate constants and enzymatic properties, have been given values which produce a model response typical for a wide range of parameter values. For this reason, we have chosen to use *arbitrary units* [au.] in the studies of paper I and II. This again implies that the numerical values from our simulations are not in correspondence with actual molecular concentrations or metabolic fluxes. For the study in paper II in particular, we acknowledge that future work should be to parameterize the models with experimentally measured kinetic parameters. Nevertheless, we do not expect that such a re-parameterization will alter the results we have already found. The mechanisms in model B will for example still not be able to compensate enough to maintain a high glycolytic flux during volume growth [5].

One of the main modeling assumptions adopted in our models is the concept of irreversible reactions. Depending on the purpose of the model, this can be a questionable assumption, as all chemical reactions have finite standard Gibbs energies. The assumption is still commonly used because it simplifies, and because many reactions are practically irreversible, at least at physiological conditions [16, 37]. However, there are circumstances where this assumption must be handled with care. An example of such is the GLUT1 mediated glucose transport, modeled in paper II to be independent of the intracellular glucose concentration. As long as the level of intracellular glucose is kept low by the conversion to glucose-6-phosphate by hexokinase, this model assumption is valid. If, however, the hexokinase conversion is limited, the intracellular glucose concentration would increase to levels above the extracellular concentration. In fact, this is the case when model B is exposed to a linear increase in cell volume (see figure 5 in paper II). Reversibility comes with extra complexity, and it can be challenging to parameterize reversible reactions with biologically relevant parameter values as these may not be available from experimental measurements [37].

Our approach of using ordinary differential equations has two essential limitations that may be of concern for some biological systems. The

---

[5]At least not unless the parameters create a big separation of time scales between the metabolic system and the disturbing volume growth. If the disturbance changes slowly (e.g., over days) compared to the response time of the regulatory system (e.g., minutes), the system will have time to adapt and reach a near stationary state that follows the slowly changing disturbance.

first is the assumption that state variables and reactions are continuous. It is true that molecules are discrete, and that reactions are stochastic events that occur only when two molecules collides with kinetic energy large enough to break chemical bonds and form new ones. How well the behavior of a stochastic biological system follows a deterministic ODE-model depends on the amount of molecules, the volume, the mixing, and the time resolution. A general rule of thumb is that it is safe to use ODEs as long as the concentrations are larger than about 10 nM [141][6]. Stochastic models of reaction networks can be difficult to solve and analyze [66, 148], but improved methods have been suggested [66], and also used to study controller motifs for regulation [25, 26]. The second limitation is that ODE-models do not capture spatial information and have an inherent assumption that reactions occur in well mixed compartments with evenly distributed concentrations of chemical species. Spatial models with partial differential equations have been used in studies of sensing mechanisms [86, 91] and recently also in a study of adaptation to spatial disturbances [87].

While considering the limitations of our approach it is crucial to not forget the quote from George E. P. Box and that models are not only measured by their correctness, but also for their usefulness. A simple deterministic model of a few key elements in a metabolic pathway may be less correct than a larger stochastic and spatial model of the same pathway, but the simpler model can be easier to interpret and understand. Furthermore, it is noteworthy to remember that most experiments are also in a way models. A cell culture for example only mimics the cells in the human body [151], and an experimental procedure is a controlled way to test or examine a certain phenomena.

---

[6]A concentration of 10 nM corresponds to 8190 molecules ($1.36 \cdot 10^{-20}$ mol) for a Caco2 cell with a volume of approximately 1360 μm^3 [105].

Bibliography

[1] **Agafonov O, Selstø CH, Thorsen K, Xu XM, Drengstig T, Ruoff P**. The organization of controller motifs leading to robust plant iron homeostasis. *PloS one* 11: e0147120. 2016.

[2] **Aguer C, Gambarotta D, Mailloux RJ, Moffat C, Dent R, McPherson R, Harper ME**. Galactose enhances oxidative metabolism and reveals mitochondrial dysfunction in human primary muscle cells. *PloS one* 6. 2011.

[3] **Ahnert SE, Fink T**. Form and function in gene regulatory networks: the structure of network motifs determines fundamental properties of their dynamical state space. *Journal of The Royal Society Interface* 13: 20160179. 2016.

[4] **Almquist J, Cvijovic M, Hatzimanikatis V, Nielsen J, Jirstrand M**. Kinetic models in industrial biotechnology–improving cell factory performance. *Metabolic engineering* 24: 38–60. 2014.

[5] **Alon U**. *An introduction to systems biology: design principles of biological circuits.* London, UK: Chapman and Hall/CRC. 2006.

[6] **Amoedo N, Punzi G, Obre E, Lacombe D, De Grassi A, Pierri C, Rossignol R**. AGC1/2, the mitochondrial aspartate-glutamate carriers. *Biochimica et Biophysica Acta (BBA)-Molecular Cell Research* 1863: 2394–2412. 2016.

[7] **Andrews NC, Schmidt PJ**. Iron homeostasis. *Annu Rev Physiol* 69: 69–85. 2007.

[8] **Ang J, McMillen DR**. Physical constraints on biological integral control design for homeostasis and sensory adaptation. *Biophysical journal* 104: 505–515. 2013.

[9] **Åström KJ, Murray RM**. *Feedback systems: an introduction for scientists and engineers.* New Jersey: Princeton university press. 2010.

[10] **Baetica AA, Westbrook A, El-Samad H**. Control theoretical concepts for synthetic and systems biology. *Current Opinion in Systems Biology.* 2019.

[11] **Barkai N, Leibler S**. Robustness in simple biochemical networks. *Nature* 387: 913. 1997.

[12] **Barnes K, Ingram JC, Porras OH, Barros LF, Hudson ER, Fryer LG, Foufelle F, Carling D, Hardie DG, Baldwin SA**. Activation of GLUT1 by metabolic and osmotic stress: potential involvement of AMP-activated protein kinase (AMPK). *Journal of cell science* 115: 2433–2442. 2002.

[13] **Bayley JP, Devilee P**. The Warburg effect in 2012. *Current opinion in oncology* 24: 62–67. 2012.

[14] **Belay T, Aviles H, Vance M, Fountain K, Sonnenfeld G**. Catecholamines and in vitro growth of pathogenic bacteria: enhancement of growth varies greatly among bacterial species. *Life sciences* 73: 1527–1535. 2003.

[15] **Berg JM SL Tymoczko JL**. The Biosynthesis of Amino Acids. In: *Biochemistry. 5th edition.* chap. 24. New York: W H Freeman. 2002.

[16] **Berg JM SL Tymoczko JL**. The Glycolytic Pathway Is Tightly Controlled. In: *Biochemistry. 5th edition.* chap. 16. New York: W H Freeman. 2002.

[17] **Berg JM SL Tymoczko JL**. The Regulation of Cellular Respiration Is Governed Primarily by the Need for ATP. In: *Biochemistry. 5th edition.* chap. 18. New York: W H Freeman. 2002.

[18] **Berridge MJ, Bootman MD, Roderick HL**. Calcium: calcium signalling: dynamics, homeostasis and remodelling. *Nature reviews Molecular cell biology* 4: 517. 2003.

[19] **Björklund M**. Cell size homeostasis: Metabolic control of growth and cell division. *Biochimica et Biophysica Acta (BBA)-Molecular Cell Research* 1866: 409–417. 2019.

[20] **Borb AA, Achermann P**. Sleep homeostasis and models of sleep regulation. *Journal of biological rhythms* 14: 559–570. 1999.

[21] **Bourgon R, Gentleman R, Huber W**. Independent filtering increases detection power for high-throughput experiments. *Proceedings of the National Academy of Sciences* 107: 9546–9551. 2010.

[22] **Box GE, Draper NR, et al.** *Empirical model-building and response surfaces* vol. 424. New York, USA: Wiley. 1987.

[23] **Boyman O, Krieg C, Homann D, Sprent J**. Homeostatic maintenance of T cells and natural killer cells. *Cellular and molecular life Sciences* 69: 1597–1608. 2012.

[24] **Brand A, Singer K, Koehl GE, Kolitzus M, Schoenhammer G, Thiel A, Matos C, Bruss C, Klobuch S, Peter K, et al.** LDHA-associated lactic acid production blunts tumor immunosurveillance by T and NK cells. *Cell metabolism* 24: 657–671. 2016.

[25] **Briat C, Gupta A, Khammash M**. Antithetic integral feedback ensures robust perfect adaptation in noisy biomolecular networks. *Cell systems* 2: 15–26. 2016.

[26] **Briat C, Gupta A, Khammash M**. Antithetic proportional-integral feedback for reduced variance and improved control performance of stochastic reaction networks. *Journal of The Royal Society Interface* 15: 20180079. 2018.

[27] **Brown RS, Wahl RL**. Overexpression of glut-1 glucose transporter in human breast cancer an immunohistochemical study. *Cancer* 72: 2979–2985. 1993.

[28] **Cannon WB**. Organization for physiological homeostasis. *Physiological reviews* 9: 399–431. 1929.

[29] **Cannon WB**. *The wisdom of the body.* New York: Norton & Co. 1939.

[30] **Chang YL, Gao HW, Chiang CP, Wang WM, Huang SM, Ku CF, Liu GY, Hung HC**. Human Mitochondrial NAD (P)+–Dependent Malic Enzyme Participates in Cutaneous Melanoma Progression and Invasion. *Journal of Investigative Dermatology* 135: 807–815. 2015.

[31] **Chen L, Wang RS, Zhang XS**. *Biomolecular networks: methods and applications in systems biology* vol. 10. New Jersey: John Wiley & Sons. 2009.

[32] **Christensen CD, Hofmeyr JHS, Rohwer JM**. Tracing regulatory routes in metabolism using generalised supply-demand analysis. *BMC systems biology* 9: 89. 2015.

[33] **Clegg JS, Jackson SA, Fendl K**. Effects of reduced cell volume and water content on glycolysis in L-929 cells. *Journal of cellular physiology* 142: 386–391. 1990.

[34] **Cobelli C, Carson E**. *Introduction to modeling in physiology and medicine.* Massachusetts, USA: Academic Press. 2019.

[35] **Cook GM, Morgan HW**. Hyperbolic growth of Thermoanaerobacter thermohydrosulfuricus (Clostridium thermohydrosulfuricum) increases ethanol production in pH-controlled batch culture. *Applied microbiology and biotechnology* 41: 84–89. 1994.

[36] **Cornish-Bowden A**. *Fundamentals of enzyme kinetics* vol. 510. Weinheim, Germany: Wiley-Blackwell. 2012.

[37] **Cornish-Bowden A, Cárdenas ML**. Information transfer in metabolic pathways: effects of irreversible steps in computer models. *European Journal of Biochemistry* 268: 6616–6624. 2001.

[38] **Cosentino C, Bates D**. *Feedback control in systems biology.* Florida, USA: Crc Press. 2011.

[39] **Courtnay R, Ngo DC, Malik N, Ververis K, Tortorella SM, Karagiannis TC**. Cancer metabolism and the Warburg effect: the role of HIF-1 and PI3K. *Molecular biology reports* 42: 841–851. 2015.

[40] **Dai Z, Shestov AA, Lai L, Locasale JW**. A flux balance of glucose metabolism clarifies the requirements of the Warburg effect. *Biophysical journal* 111: 1088–1100. 2016.

[41] **Dang CV, Kim Jw, Gao P, Yustein J**. The interplay between MYC and HIF in cancer. *Nature Reviews Cancer* 8: 51–56. 2008.

[42] **Davies SP, Hawley SA, Woods A, Carling D, Haystead TA, Hardie DG**. Purification of the AMP-activated protein kinase on ATP-γ-Sepharose and analysis of its subunit structure. *European journal of biochemistry* 223: 351–357. 1994.

[43] **de Alteriis E, Carteni F, Parascandola P, Serpa J, Mazzoleni S**. Revisiting the Crabtree/Warburg effect in a dynamic perspective: a fitness advantage against sugar-induced cell death. *Cell Cycle* 17: 688–701. 2018.

[44] **De Deken R**. The Crabtree effect: a regulatory system in yeast. *Microbiology* 44: 149–156. 1966.

[45] **De Jong H**. Modeling and simulation of genetic regulatory systems: a literature review. *Journal of computational biology* 9: 67–103. 2002.

[46] **de Padua MC, Delodi G, Vučetić M, Durivault J, Vial V, Bayer P, Noleto GR, Mazure NM, Ždralević M, Pouysségur J**. Disrupting glucose-6-phosphate isomerase fully suppresses the "Warburg effect" and activates OXPHOS with minimal impact on tumor growth except in hypoxia. *Oncotarget* 8: 87623. 2017.

[47] **DeBerardinis RJ, Cheng T**. Q's next: the diverse functions of glutamine in metabolism, cell biology and cancer. *Oncogene* 29: 313. 2010.

[48] **Deboer T**. Sleep homeostasis and the circadian clock: Do the circadian pacemaker and the sleep homeostat influence each others functioning? *Neurobiology of sleep and circadian rhythms* 5: 68–77. 2018.

[49] **Denko NC**. Hypoxia, HIF1 and glucose metabolism in the solid tumour. *Nature Reviews Cancer* 8: 705–713. 2008.

[50] **Drengstig T, Jolma IW, Ni XY, Thorsen K, Xu XM, Ruoff P**. A basic set of homeostatic controller motifs. *Biophys J* 103: 2000–2010. 2012.

[51] **Drengstig T, Ni X, Thorsen K, Jolma I, Ruoff P**. Robust adaptation and homeostasis by autocatalysis. *The Journal of Physical Chemistry B* 116: 5355–5363. 2012.

[52] **Dubitzky W, Wolkenhauer O, Yokota H, Cho KH**. *Encyclopedia of systems biology.* New York: Springer Publishing Company, Incorporated. 2013.

[53] **Eigen M, Biebricher CK, Gebinoga M, Gardiner WC**. The hypercycle. Coupling of RNA and protein biosynthesis in the infection cycle of an RNA bacteriophage. *Biochemistry* 30: 11005–11018. 1991.

[54] **El-Samad H, Goff J, Khammash M**. Calcium homeostasis and parturient hypocalcemia: an integral feedback perspective. *Journal of theoretical biology* 214: 17–29. 2002.

[55] **Fernandez-de Cossio-Diaz J, Vazquez A**. A physical model of cell metabolism. *Scientific reports* 8. 2018.

[56] **Ferrell Jr JE**. Perfect and near-perfect adaptation in cell signaling. *Cell Systems* 2: 62–67. 2016.

[57] **Fiermonte G, Palmieri L, Todisco S, Agrimi G, Palmieri F, Walker JE**. Identification of the mitochondrial glutamate transporter bacterial expression, reconstitution, functional characterization, and tissue distribution of two human isoforms. *Journal of Biological Chemistry* 277: 19289–19294. 2002.

[58] **Francis BA, Wonham WM**. The internal model principle of control theory. *Automatica* 12: 457–465. 1976.

[59] **Franck U**. Feedback kinetics in physicochemical oscillators. *Berichte der Bunsengesellschaft für physikalische Chemie* 84: 334–341. 1980.

[60] **Galbo T, Perry RJ, Nishimura E, Samuel VT, Quistorff B, Shulman GI**. PP2A inhibition results in hepatic insulin resistance despite Akt2 activation. *Aging (Albany NY)* 5: 770. 2013.

[61] **Ginneken V**. Targeting tumor metabolism: A biochemical explanation related to a systems biology lipidomics based approach. *J Mol Biomark Diagn S* 2: 2. 2017.

[62] **Glish GL, Vachet RW**. The basics of mass spectrometry in the twenty-first century. *Nature reviews drug discovery* 2: 140–150. 2003.

[63] **Gorban AN, Tyukina TA, Smirnova EV, Pokidysheva LI**. Evolution of adaptation mechanisms: Adaptation energy, stress, and oscillating death. *Journal of theoretical biology* 405: 127–139. 2016.

[64] **Grabellus F, Nagarajah J, Bockisch A, Schmid KW, Sheu SY**. Glucose transporter 1 expression, tumor proliferation, and iodine/glucose uptake in thyroid cancer with emphasis on poorly differentiated thyroid carcinoma. *Clinical nuclear medicine* 37: 121–127. 2012.

[65] **Grewer C, Grabsch E**. New inhibitors for the neutral amino acid transporter ASCT2 reveal its Na+-dependent anion leak. *The Journal of physiology* 557: 747–759. 2004.

[66] **Gupta A, Briat C, Khammash M**. A scalable computational framework for establishing long-term behavior of stochastic reaction networks. *PLoS computational biology* 10. 2014.

[67] **Hardie DG**. AMP-activated/SNF1 protein kinases: conserved guardians of cellular energy. *Nature reviews Molecular cell biology* 8: 774–785. 2007.

[68] **Haspel HC, Mynarcik DC, Ortiz PA, Honkanen RA, Rosenfeld MG**. Glucose deprivation induces the selective accumulation of hexose transporter protein GLUT-1 in the plasma membrane of normal rat kidney cells. *Molecular Endocrinology* 5: 61–72. 1991.

[69] **Hay N**. Reprogramming glucose metabolism in cancer: can it be exploited for cancer therapy? *Nature Reviews Cancer* 16: 635. 2016.

[70] **Hildyard JC, Ämmälä C, Dukes ID, Thomson SA, Halestrap AP**. Identification and characterisation of a new class of highly specific and potent inhibitors of the mitochondrial pyruvate carrier. *Biochimica et Biophysica Acta (BBA)-Bioenergetics* 1707: 221–230. 2005.

[71] **Hiller G, Clark D, Blanch H**. Cell retention, chemostat studies of hybridoma cells-analysis of hybridoma growth and metabolism in continuous suspension culture in serum-free medium. *Biotechnology and bioengineering* 42: 185–195. 1993.

[72] **Holczer M, Hajdú B, Lőrincz T, Szarka A, Bánhegyi G, Kapuy O**. A Double Negative Feedback Loop between mTORC1 and AMPK Kinases Guarantees Precise Autophagy Induction upon Cellular Stress. *International journal of molecular sciences* 20: 5543. 2019.

[73] **Iacobazzi V, Infantino V, Castegna A, Menga A, Palmieri EM, Convertini P, Palmieri F**. Mitochondrial carriers in inflammation induced by bacterial endotoxin and cytokines. *Biological chemistry* 398: 303–317. 2017.

[74] **Iacobazzi V, Infantino V, Costanzo P, Izzo P, Palmieri F**. Functional analysis of the promoter of the mitochondrial phosphate carrier human gene: identification of activator and repressor elements and their transcription factors. *Biochemical Journal* 391: 613–621. 2005.

[75] **Infantino V, Dituri F, Convertini P, Santarsiero A, Palmieri F, Todisco S, Mancarella S, Giannelli G, Iacobazzi V**. Epigenetic up-regulation and functional role of the mitochondrial aspartate/glutamate carrier isoform 1 in hepatocellular carcinoma. *Biochimica et Biophysica Acta (BBA)-Molecular Basis of Disease* 1865: 38–47. 2019.

[76] **Infantino V, Pierri CL, Iacobazzi V**. Metabolic routes in inflammation: the citrate pathway and its potential as therapeutic target. *Current medicinal chemistry* 26: 7104–7116. 2019.

[77] **Ingalls BP**. *Mathematical modeling in systems biology: an introduction*. Massachusetts, USA: MIT press. 2013.

[78] **Isidori A, Byrnes CI**. Output regulation of nonlinear systems. *IEEE transactions on Automatic Control* 35: 131–140. 1990.

[79] **Israelsen WJ, Vander Heiden MG**. ATP consumption promotes cancer metabolism. *Cell* 143: 669–671. 2010.

[80] **Jeon SM**. Regulation and function of AMPK in physiology and diseases. *Experimental & molecular medicine* 48: e245. 2016.

[81] **Johnson KA, Goody RS**. The original Michaelis constant: translation of the 1913 Michaelis–Menten paper. *Biochemistry* 50: 8264–8269. 2011.

[82] **Jolma IW, Ni XY, Rensing L, Ruoff P**. Harmonic oscillations in homeostatic controllers: Dynamics of the p53 regulatory system. *Biophysical journal* 98: 743–752. 2010.

[83] **Jonnalagadda SS**. Glutamine. In: *Sports nutrition: fats and proteins*, edited by Driskell J chap. 9. Florida, USA: CRC Press. 2007.

[84] **Kabashima T, Kawaguchi T, Wadzinski BE, Uyeda K**. Xylulose 5-phosphate mediates glucose-induced lipogenesis by xylulose 5-phosphate-activated protein phosphatase in rat liver. *Proceedings of the National Academy of Sciences* 100: 5107–5112. 2003.

[85] **Kotas ME, Medzhitov R**. Homeostasis, inflammation, and disease susceptibility. *Cell* 160: 816–827. 2015.

[86] **Krishnan J**. Signal processing through a generalized module of adaptation and spatial sensing. *Journal of theoretical biology* 259: 31–43. 2009.

[87] **Krishnan J, Floros I**. Adaptive information processing of network modules to dynamic and spatial stimuli. *BMC systems biology* 13: 32. 2019.

[88] **Kroemer G, Pouyssegur J**. Tumor cell metabolism: cancer's Achilles' heel. *Cancer cell* 13: 472–482. 2008.

[89] **Lage R, Diéguez C, Vidal-Puig A, López M**. AMPK: a metabolic gauge regulating whole-body energy homeostasis. *Trends in molecular medicine* 14: 539–549. 2008.

[90] **Lang F, Busch GL, Ritter M, Volkl H, Waldegger S, Gulbins E, Haussinger D**. Functional significance of cell volume regulatory mechanisms. *Physiological reviews* 78: 247–306. 1998.

[91] **Levchenko A, Iglesias PA**. Models of eukaryotic gradient sensing: application to chemotaxis of amoebae and neutrophils. *Biophysical journal* 82: 50–63. 2002.

[92] **Li X, Chung AC, Li S, Wu L, Xu J, Yu J, Wong C, Cai Z**. LC-MS-based metabolomics revealed SLC25A22 as an essential regulator of aspartate-derived amino acids and polyamines in KRAS-mutant colorectal cancer. *Oncotarget* 8: 101333. 2017.

[93] **Liberti MV, Locasale JW**. The Warburg effect: how does it benefit cancer cells? *Trends in biochemical sciences* 41: 211–218. 2016.

[94] **Lin J, Amir A**. Homeostasis of protein and mRNA concentrations in growing cells. *Nature communications* 9: 4496. 2018.

[95] **Liu Y, Zhao T, Li Z, Wang L, Yuan S, Sun L**. The role of ASCT2 in cancer: A review. *European journal of pharmacology* 837: 81–87. 2018.

[96] **Love MI, Huber W, Anders S**. Moderated estimation of fold change and dispersion for RNA-seq data with DESeq2. *Genome biology* 15: 550. 2014.

[97] **Ma W, Trusina A, El-Samad H, Lim WA, Tang C**. Defining network topologies that can achieve biochemical adaptation. *Cell* 138: 760–773. 2009.

[98] **Macheda ML, Rogers S, Best JD**. Molecular and cellular regulation of glucose transporter (GLUT) proteins in cancer. *Journal of cellular physiology* 202: 654–662. 2005.

[99] **Manerba M, Vettraino M, Fiume L, Di Stefano G, Sartini A, Giacomini E, Buonfiglio R, Roberti M, Recanatini M**. Galloflavin (CAS 568-80-9): a novel inhibitor of lactate dehydrogenase. *ChemMedChem* 7: 311–317. 2012.

[100] **Marion D**. An introduction to biological NMR spectroscopy. *Molecular & Cellular Proteomics* 12: 3006–3025. 2013.

[101] **Matés JM, Di Paola FJ, Campos-Sandoval JA, Mazurek S, Márquez J**. Therapeutic targeting of glutaminolysis as an essential strategy to combat cancer. In: *Seminars in cell & developmental biology.* Elsevier. 2019.

[102] **Milo R, Shen-Orr S, Itzkovitz S, Kashtan N, Chklovskii D, Alon U**. Network motifs: simple building blocks of complex networks. *Science* 298: 824–827. 2002.

[103] **Miyo M, Konno M, Nishida N, Sueda T, Noguchi K, Matsui H, Colvin H, Kawamoto K, Koseki J, Haraguchi N, et al.** Metabolic adaptation to nutritional stress in human colorectal cancer. *Scientific reports* 6: 38415. 2016.

[104] **Molenaar D, Van Berlo R, De Ridder D, Teusink B**. Shifts in growth strategies reflect tradeoffs in cellular economics. *Molecular systems biology* 5. 2009.

[105] **Moyes S, Smyth S, Shipman A, Long S, Morris J, Carr K**. Parameters influencing intestinal epithelial permeability and microparticle uptake in vitro. *International journal of pharmaceutics* 337: 133–141. 2007.

[106] **Murai S, Ando A, Ebara S, Hirayama M, Satomi Y, Hara T**. Inhibition of malic enzyme 1 disrupts cellular metabolism and leads to vulnerability in cancer cells in glucose-restricted conditions. *Oncogenesis* 6: e329–e329. 2017.

[107] **Muzzey D, Gómez-Uribe CA, Mettetal JT, van Oudenaarden A**. A systems-level analysis of perfect adaptation in yeast osmoregulation. *Cell* 138: 160–171. 2009.

[108] **Nakashima C, Yamamoto K, Fujiwara-Tani R, Luo Y, Matsushima S, Fujii K, Ohmori H, Sasahira T, Sasaki T, Kitadai Y, et al.** Expression of cytosolic malic enzyme (ME 1) is associated with disease progression in human oral squamous cell carcinoma. *Cancer science* 109: 2036–2045. 2018.

[109] **Ni XY, Drengstig T, Ruoff P**. The control of the controller: molecular mechanisms for robust perfect adaptation and temperature compensation. *Biophysical journal* 97: 1244–1253. 2009.

[110] **Palmer BF**. Regulation of potassium homeostasis. *Clinical Journal of the American Society of Nephrology* 10: 1050–1060. 2015.

[111] **Panda S, Hogenesch JB, Kay SA**. Circadian rhythms from flies to human. *Nature* 417: 329–335. 2002.

[112] **Pedersen PL, Mathupala S, Rempel A, Geschwind J, Ko YH**. Mitochondrial bound type ii hexokinase: a key player in the growth and survival of many cancers and an ideal prospect for therapeutic intervention. *Biochimica et Biophysica Acta (BBA)-Bioenergetics* 1555: 14–20. 2002.

[113] **Petryszak R, Keays M, Tang YA, Fonseca NA, Barrera E, Burdett T, Fullgrabe A, Fuentes AMP, Jupp S, Koskinen S, et al.** Expression Atlas update an integrated database of gene and protein expression in humans, animals and plants. *Nucleic acids research* 44: D746–D752. 2015.

[114] **Price GM, Halliday D, Pacy PJ, Quevedo MR, Millward DJ**. Nitrogen homoeostasis in man: influence of protein intake on the amplitude of diurnal cycling of body nitrogen. *Clinical Science* 86: 91–102. 1994.

[115] **Rabinovitch RC, Samborska B, Faubert B, Ma EH, Gravel SP, Andrzejewski S, Raissi TC, Pause A, Pierre JS, Jones RG**. AMPK maintains cellular metabolic homeostasis through regulation of mitochondrial reactive oxygen species. *Cell reports* 21: 1–9. 2017.

[116] **Radhakrishnan K, Hindmarsh AC**. Description and use of LSODE, the Livermore solver for ordinary differential equations. *NASA Reference Publication*. 1993.

[117] **Rastogi RP**. Time order, chemical oscillations. In: *Introduction to non-equilibrium physical chemistry*. Amsterdam, Netherlands: Elsevier. 2007.

[118] **Reed M, Best J, Golubitsky M, Stewart I, Nijhout HF**. Analysis of homeostatic mechanisms in biochemical networks. *Bulletin of mathematical biology* 79: 2534–2557. 2017.

[119] **Ren JG, Seth P, Clish CB, Lorkiewicz PK, Higashi RM, Lane AN, Fan TWM, Sukhatme VP**. Knockdown of malic enzyme 2 suppresses lung tumor growth, induces differentiation and impacts PI3K/AKT signaling. *Scientific reports* 4: 5414. 2014.

[120] **Rensing L, Jaeger NI**. *Temporal Order: Proceedings of a Symposium on Oscillations in Heterogeneous Chemical and Biological Systems, University of Bremen, September 17–22, 1984* vol. 29. New York: Springer Science & Business Media. 2012.

[121] **Risvoll GB, Drengstig T**. The impact of signalling kinetics on controller motif performance. In: *Proceedings of the 58th Conference on Simulation and Modelling (SIMS 58) Reykjavik, Iceland, September 25th–27th, 2017* 138 343–349. Linköping University Electronic Press. 2017.

[122] **Risvoll GB, Thorsen K, Ruoff P, Drengstig T**. Variable setpoint as a relaxing component in physiological control. *Physiological reports* 5: e13408. 2017.

[123] **Rossignol R, Gilkerson R, Aggeler R, Yamagata K, Remington SJ, Capaldi RA**. Energy substrate modulates mitochondrial structure and oxidative capacity in cancer cells. *Cancer research* 64: 985–993. 2004.

[124] **Ruderman NB, Julia Xu X, Nelson L, Cacicedo JM, Saha AK, Lan F, Ido Y**. AMPK and SIRT1: a long-standing partnership? *American Journal of Physiology-Endocrinology and Metabolism* 298: E751–E760. 2010.

[125] **San-Millán I, Brooks GA**. Reexamining cancer metabolism: lactate production for carcinogenesis could be the purpose and explanation of the Warburg Effect. *Carcinogenesis* 38: 119–133. 2017.

[126] **Sarfraz I, Rasul A, Hussain G, Hussain SM, Ahmad M, Nageen B, Jabeen F, Selamoglu Z, Ali M**. Malic enzyme 2 as a potential therapeutic drug target for cancer. *IUBMB life* 70: 1076–1083. 2018.

[127] **Sarkar A**. Cells in artificial environment. In: *Animal Stem Cells* chap. 4. New Dehli, India: Discovery Publishing House Pvt. Limited. 2009.

[128] **Scalise M, Pochini L, Console L, Losso MA, Indiveri C**. The human SLC1A5 (ASCT2) amino acid transporter: From function to structure and role in cell biology. *Frontiers in cell and developmental biology* 6: 96. 2018.

[129] **Scalise M, Pochini L, Galluccio M, Console L, Indiveri C**. Glutamine transport and mitochondrial metabolism in cancer cell growth. *Frontiers in oncology* 7: 306. 2017.

[130] **Seborg DE, Mellichamp DA, Edgar TF, Doyle III FJ**. *Process dynamics and control*. New Jersey, USA: John Wiley & Sons. 2010.

[131] **Selye H**. Adaptation energy. *Nature* 141: 926–926. 1938.

[132] **Selye H**. *The stress of life*. New York: McGraw-Hill Education. 1956.

[133] **Shampine LF, Reichelt MW**. The matlab ode suite. *SIAM journal on scientific computing* 18: 1–22. 1997.

[134] **Shestov AA, Liu X, Ser Z, Cluntun AA, Hung YP, Huang L, Kim D, Le A, Yellen G, Albeck JG, et al.** Quantitative determinants of aerobic glycolysis identify flux through the enzyme GAPDH as a limiting step. *Elife* 3: e03342. 2014.

[135] **Skogestad S, Postlethwaite I**. *Multivariable Feedback Control: Analysis*. New Jersey, USA: John Wiley & Sons. 2005.

[136] **Song C, Xu F, Ren Z, Zhang Y, Meng Y, Yang Y, Lingadahalli S, Cheung E, Li G, Liu W, et al.** Elevated Exogenous Pyruvate Potentiates Mesodermal Differentiation through Metabolic Modulation and AMPK/mTOR Pathway in Human Embryonic Stem Cells. *Stem cell reports* 13: 338–351. 2019.

[137] **Sontag ED**. Adaptation and regulation with signal detection implies internal model. *Systems & control letters* 50: 119–126. 2003.

[138] **Stoltzman CA, Kaadige MR, Peterson CW, Ayer DE**. MondoA senses non-glucose sugars regulation of thioredoxin-interacting protein (TXNIP) and the hexose transport curb. *Journal of Biological Chemistry* 286: 38027–38034. 2011.

[139] **Stoltzman CA, Peterson CW, Breen KT, Muoio DM, Billin AN, Ayer DE**. Glucose sensing by MondoA: Mlx complexes: a role for hexokinases and direct regulation of thioredoxin-interacting protein expression. *Proceedings of the National Academy of Sciences* 105: 6912–6917. 2008.

[140] **Sweetlove LJ, Fernie AR**. The role of dynamic enzyme assemblies and substrate channelling in metabolic regulation. *Nature communications* 9: 2136. 2018.

[141] **Szallasi Z P Stelling J**, editor. *Modeling molecular interaction networks with nonlinear ordinary differential equations.* Florida, USA: CRC Press. 2006.

[142] **Thorsen K**. Controller motifs for homeostatic regulation and their applications in biological systems. 2015.

[143] **Thorsen K, Drengstig T, Ruoff P**. Transepithelial glucose transport and Na+/K+ homeostasis in enterocytes: an integrative model. *American Journal of Physiology-Cell Physiology* 307: C320–C337. 2014.

[144] **Thorsen K, Drengstig T, Ruoff P**. The effect of integral control in oscillatory and chaotic reaction kinetic networks. *Physica D: Nonlinear Phenomena* 393: 38–46. 2019.

[145] **Thorsen K, Risvoll GB, Tveit DM, Ruoff P, Drengstig T**. Tuning of physiological controller motifs. In: *Proceedings of The 9th EUROSIM Congress on Modelling and Simulation, EUROSIM 2016, The 57th SIMS Conference on Simulation and Modelling SIMS 2016* 142 31–37. Linköping University Electronic Press. 2018.

[146] **Thorsen K, Ruoff P, Drengstig T**. Control theoretic properties of physiological controller motifs. In: *2013 International Conference on System Science and Engineering (ICSSE)* 165–170. IEEE. 2013.

[147] **Thorsen K, Ruoff P, Drengstig T**. Antagonistic regulation with a unique setpoint, integral and double integral action. *bioRxiv* 248682. 2018.

[148] **Tian T, Burrage K**. Stochastic models for regulatory networks of the genetic toggle switch. *Proceedings of the national Academy of Sciences* 103: 8372–8377. 2006.

[149] **Traut T**. Properties and evolution of allosteric enzymes. In: *Allosteric Regulatory Enzymes* chap. 4. New York: Springer. 2008.

[150] **Tzur A, Kafri R, LeBleu VS, Lahav G, Kirschner MW**. Cell growth and size homeostasis in proliferating animal cells. *Science* 325: 167–171. 2009.

[151] **Uysal O, Sevimli T, Sevimli M, Gunes S, Sariboyaci AE**. *Cell and Tissue Culture: The Base of Biotechnology.* Amsterdam, Netherlands: Elsevier. 2018.

[152] **Vander Heiden MG, Cantley LC, Thompson CB**. Understanding the Warburg effect: the metabolic requirements of cell proliferation. *science* 324: 1029–1033. 2009.

[153] **Vander Heiden MG, DeBerardinis RJ**. Understanding the intersections between metabolism and cancer biology. *Cell* 168: 657–669. 2017.

[154] **Vazquez A, Oltvai ZN**. Molecular crowding defines a common origin for the Warburg effect in proliferating cells and the lactate threshold in muscle physiology. *PloS one* 6: e19538. 2011.

[155] **Visioli A**. Basic of PID control. In: *Practical PID control* chap. 1. New York: Springer Science & Business Media. 2006.

[156] **Warburg O**. The metabolism of carcinoma cells. *The Journal of Cancer Research* 9: 148–163. 1925.

[157] **Warburg O**. On the origin of cancer cells. *Science* 123: 309–314. 1956.

[158] **Wehrle JP, Ng CE, McGovern KA, Aiken NR, Shungu DC, Chance EM, Glickson JD**. Metabolism of alternative substrates and the bioenergetic status of EMT6 tumor cell spheroids. *NMR in Biomedicine: An International Journal Devoted to the Development and Application of Magnetic Resonance In Vivo* 13: 349–360. 2000.

[159] **Wilkie J, Johnson M, Reza K**. *Control Engineering. An Introductory Course.* New York: Palgrave. 2002.

[160] **Wise DR, Thompson CB**. Glutamine addiction: a new therapeutic target in cancer. *Trends in biochemical sciences* 35: 427–433. 2010.

[161] **Witte D, Ali N, Carlson N, Younes M**. Overexpression of the neutral amino acid transporter ASCT2 in human colorectal adenocarcinoma. *Anticancer research* 22: 2555–2557. 2002.

[162] **Wong CC, Qian Y, Li X, Xu J, Kang W, Tong JH, To KF, Jin Y, Li W, Chen H, et al.** SLC25A22 promotes proliferation and survival of colorectal cancer cells with KRAS mutations and xenograft tumor progression in mice via intracellular synthesis of aspartate. *Gastroenterology* 151: 945–960. 2016.

[163] **Wu N, Zheng B, Shaywitz A, Dagon Y, Tower C, Bellinger G, Shen CH, Wen J, Asara J, McGraw TE, et al.** AMPK-dependent degradation of TXNIP upon energy stress leads to enhanced glucose uptake via GLUT1. *Molecular cell* 49: 1167–1175. 2013.

[164] **Xi X, Han J, Zhang JZ**. Stimulation of glucose transport by AMP-activated protein kinase via activation of p38 mitogen-activated protein kinase. *Journal of Biological Chemistry* 276: 41029–41034. 2001.

[165] **Yamamoto T, Seino Y, Fukumoto H, Koh G, Yano H, Inagaki N, Yamada Y, Inoue K, Manabe T, Imura H**. Over-expression of facilitative glucose transporter genes in human cancer. *Biochemical and biophysical research communications* 170: 223–230. 1990.

[166] **Yang L, Bashir R**. Electrical/electrochemical impedance for rapid detection of foodborne pathogenic bacteria. *Biotechnology advances* 26: 135–150. 2008.

[167] **Yang L, Moss T, Mangala LS, Marini J, Zhao H, Wahlig S, Armaiz-Pena G, Jiang D, Achreja A, Win J, et al.** Metabolic shifts toward glutamine regulate tumor growth, invasion and bioenergetics in ovarian cancer. *Molecular systems biology* 10. 2014.

[168] **Yang Z, Xiong HR**. Culture conditions and types of growth media for mammalian cells. *Biomedical Tissue Culture* 1: 3–18. 2012.

[169] **Yi TM, Huang Y, Simon MI, Doyle J**. Robust perfect adaptation in bacterial chemotaxis through integral feedback control. *Proceedings of the National Academy of Sciences* 97: 4649–4653. 2000.

[170] **Young CD, Nolte EC, Lewis A, Serkova NJ, Anderson SM**. Activated Akt1 accelerates MMTV-c-ErbB2 mammary tumourigenesis in mice without activation of ErbB3. *Breast Cancer Research* 10: R70. 2008.

[171] **Yu D, Shi X, Meng G, Chen J, Yan C, Jiang Y, Wei J, Ding Y**. Kidney-type glutaminase (GLS1) is a biomarker for pathologic diagnosis and prognosis of hepatocellular carcinoma. *Oncotarget* 6: 7619. 2015.

[172] **Yu L, Chen X, Sun X, Wang L, Chen S**. The glycolytic switch in tumors: how many players are involved? *Journal of Cancer* 8: 3430. 2017.

[173] **Zeng AP, Deckwer WD, Hu WS**. Determinants and rate laws of growth and death of hybridoma cells in continuous culture. *Biotechnology and bioengineering* 57: 642–654. 1998.

[174] **Zhang F, Du G**. Dysregulated lipid metabolism in cancer. *World journal of biological chemistry* 3: 167. 2012.

[175] **Zhang J, Zhang Q**. *Using seahorse machine to measure OCR and ECAR in cancer cells.* New York: Springer. 2019.

[176] **Zhou QL, Jiang ZY, Holik J, Chawla A, Hagan GN, Leszyk J, Czech MP**. Akt substrate TBC1D1 regulates GLUT1 expression through the mTOR pathway in 3T3-L1 adipocytes. *Biochemical Journal* 411: 647–655. 2008.

[177] **Zhuang K, Zhang J, Xiong M, Wang X, Luo X, Han L, Meng Y, Zhang Y, Liao W, Liu S**. CDK5 functions as a tumor promoter in human colorectal cancer via modulating the ERK5–AP-1 axis. *Cell death & disease* 7: e2415. 2016.

Paper 1:
The Performance of Homeostatic Controller Motifs Dealing with Perturbations of Rapid Growth and Depletion

J. Phys. Chem. B 2017, 121, 25, 6097-6107

Paper 2:
Exploring Mechanisms of Glucose Uptake Regulation and Dilution Resistance in Growing Cancer Cells

Article

Exploring Mechanisms of Glucose Uptake Regulation and Dilution Resistance in Growing Cancer Cells

Daniel M. Tveit[1], Gunhild Fjeld[2], Tormod Drengstig[1], Fabian V. Filipp[3], Peter Ruoff[2], and Kristian Thorsen[1,*]

[1]Department of Electrical Engineering and Computer Science, University of Stavanger, Stavanger, Norway
[2]Centre for Organelle Research, University of Stavanger, Stavanger, Norway
[3]Systems Biology and Cancer Metabolism, Program for Quantitative Systems Biology, University of California Merced, Merced, CA, USA
[*]Correspondence: kristian.thorsen@uis.no

ABSTRACT   Most cancer cells rely on aerobic glycolysis and increased glucose uptake for the production of biosynthetic precursors needed to support rapid proliferation. Increased glucose uptake and glycolytic activity may result in intracellular acidosis and increase of osmotically active substances, leading to cell swelling. This causes dilution of cellular constituents, which can markedly influence cellular reactions and the function of proteins, and hence, control mechanisms used by cancer cells to maintain a highly glycolytic phenotype must be robust to dilution. In this paper, we review the literature on cancer cell metabolism and glucose uptake, and employ mathematical modeling to examine control mechanisms in cancer cell metabolism that show robust homeostatic control in the presence of dilution. Using differential gene expression data from the Expression Atlas database, we identify the key components of glucose uptake in cancer, in order to guide the construction of a mathematical model. By simulations of this model we show that while negative feedback from downstream glycolytic metabolites to glucose transporters is sufficient for homeostatic control of glycolysis in a constant cellular volume, it is necessary to control intermediate glycolytic enzymes in order to achieve homeostatic control during growth. With a focus on glucose uptake in cancer, we demonstrate a systems biology approach to the identification, reduction, and analysis of complex regulatory systems.

SIGNIFICANCE   Rapid proliferation and increased glycolytic activity in cancer cells lead to dilution of cellular constituents, which can markedly influence cellular reactions and the function of proteins. Therefore, control mechanisms used by cancer cells to maintain a highly glycolytic phenotype must be robust to dilution. We construct a mathematical model of glucose uptake in cancer, and using a systems biology approach to the analysis of regulatory networks, identify the presence of integral control motifs as a means for achieving dilution resistance. Furthermore, we show that while negative feedback from downstream glycolytic metabolites to glucose transporters is sufficient for homeostatic control of glycolysis in a constant cellular volume, it is necessary to control intermediate glycolytic enzymes to achieve homeostatic control during growth.

INTRODUCTION

It is well established that cell swelling and shrinkage affect important cellular functions, in part by dilution and concentration of cellular compounds (1–4). Such changes in concentration can markedly influence the function of intracellular proteins (1). This has been demonstrated in studies on the effect of volume change on enzyme reactions in solitary vesicles, showing that there is a significant impact on the dynamical and steady state behavior of these reactions (5). The significance of dilution due to growth is emphasized by the cell-size control mechanism employed in budding-yeast. In these cells, the concentration of a cell cycle activator maintained at a constant level during growth relative to a growth diluted inhibitor provides a measurement of cell volume and a molecular mechanism for cell-size control (6, 7). Although most proteins are maintained at constant concentrations in growing cells, owing to mRNA amounts and number of ribosomes increasing with cell size, we lack an understanding of the molecular mechanisms that coordinate biosynthesis to achieve constant protein concentrations during growth (7, 8). Investigations into the performance of so-called integral control motifs (ICMs) have revealed mechanisms by which robustness to dilution can be achieved (9, 10). In this paper, we look into homeostatic mechanisms regulating glucose uptake in rapidly growing cancer cells. We identify the presence of ICMs as part of glucose uptake in cancer, and investigate how homeostatic control of metabolite and protein concentrations is achieved in the presence of dilution due to growth.

Most cancer cells show an increased uptake and metabolism of glucose, a phenotype that can be detected by [18]fluoro-deoxyglucose positron emission tomography (FDG-PET) (11–13). This growth mode relies on a balanced production of cellular components to avoid molecular crowding and solvent capacity constraints (14, 15). The cell represents a tiny reagent reservoir and is reliant on a balanced influx and efflux of compounds to support growth rates corresponding to that seen in cancer. Thus, as the cell expands, its constituents need to increase at the same rate to meet the growth requirements, meaning a proportional increase in nucleic acids, polysaccharides, proteins, and lipids (16). Aside from biomass formation for the purpose of growth, metabolism also affects cell volume through uptake of nutrients, by creation of osmotically active substances, developing intracellular acidosis, and by depletion of available ATP (1, 17, 18). In fact, increased cellular volume appears to be required for proliferation, and hypertonic shrinkage inhibits cell proliferation, whereas slight osmotic swelling has the opposite effect (1). In contrast, differentiation is followed by cell shrinkage in a number of cells (1).

In the following, we take a look at some key elements of the rewiring of glycolysis that produce the increased glycolytic activity seen in cancer. Next, we look at the various control mechanisms in place that maintain this increased glucose uptake and metabolic activity. We then focus our attention to glucose uptake, and show that differential gene expression of cancer and normal cells corroborate the reported rewiring in cancer. With this information, we construct a mathematical model of glucose uptake in cancer, formulated as a system of ordinary differential equations (ODEs). We construct the model in a stepwise manner, where each step adds a layer of regulation to the model. This is done in order to investigate the role each control mechanism serve. We show how dilution is incorporated into the model, and run simulations for each step of model construction. Finally, we show how control mechanisms of glucose uptake in cancer form ICMs, and how this enables robust homeostatic control of glycolysis, even in the presence of dilution.

Rewiring of Glycolysis in Cancer

Cancer cells show an increased reliance on glycolysis and lactic acid fermentation, even in the presence of oxygen, and a more glycolytic phenotype is persistent with a more aggressive cancer cell type (12, 19, 20). This is known as the Warburg effect, or aerobic glycolysis, and is necessary in order to meet the increased demands of rapid proliferation (11). In cancer cells, the Warburg effect is in supplement to oxidative phosphorylation rather than a replacement (21). This is in contrast to normal cells that maintain a high rate of glycolysis at the expense of oxidative phosphorylation; a phenomenon known as the Crabtree effect (21). However, in the hypoxic tumor microenvironment, cancer cells naturally show a decreased reliance on oxidative phosphorylation (21, 22). The increased glycolytic flux in cancer supplies biosynthetic pathways with precursors, meets the increased bioenergetic demand of proliferation, and contributes to tumor invasion through the excretion of lactate and consequent acidification of the tumor microenvironment (11, 12, 21, 23, 24). The mechanisms that reprogram metabolism in cancer are often cancer-specific, nevertheless, there are common hallmarks, notably a shift towards protein isoforms that promote biosynthesis and proliferation (11, 21).

In the first step of glycolysis, glucose is transported into the cell. The GLUT (gene symbol *SLC2A*) family of glucose transporters are membrane-spanning proteins facilitating the transport of sugars across biological membranes along the concentration gradient (25, 26). GLUT1 is one of 14 currently identified GLUT proteins expressed in humans, and is expressed in almost every tissue (27–30). Together with its high affinity for glucose, this gives GLUT1 a clear role in the basal glucose uptake of most tissues (25, 28, 29). Elevated expression of GLUT1 has been reported in most cancers, and the expression level correlates reciprocally with the survival of cancer patients (12, 23, 30). Hypoxia-inducible factor-1 (HIF-1), a dimer of HIF-1α and HIF-1β, is one of the factors responsible for upregulating GLUT1 in tumor cells (12, 21, 30, 31). HIF-1β is constitutively expressed, whereas HIF-1α is regulated through oxygen-dependent and oxygen-independent mechanisms (31). GLUT1 expression is upregulated through hypoxia-response elements on the GLUT1 promoter that bind HIF-1 (30). HIF-1α has increased levels in most cancers, which provides a mechanism by which cancer cells overexpress GLUT1 (12, 30, 31). Other factors known to cause overexpression and translocation of GLUT1 to the cell membrane in cancer include the oncoprotein c-Myc, protein kinase Akt/PKB, and oncogenic KRAS and BRAF (12, 21, 30).

Glycolysis consists of several reversible reactions and three (essentially) irreversible reactions (see Figure 1). Because they are irreversible, these three reactions represent committed steps of glycolysis, and the enzymes that drive these reactions function as gatekeepers of glycolysis and have a key role in regulating the glycolytic flux (21). In the first irreversible reaction of glycolysis, glucose is phosphorylated to glucose 6-phosphate (G6P) by hexokinase, coupled to the dephosphorylation of ATP (13, 32, 33). Hexokinase 2 (HK2) is one of four isoforms of hexokinase found in mammalian tissue (13). HK2 has a very high affinity for glucose, with a Michaelis constant (K_M value) of 0.02–0.03 mM (13, 32). To support increased glucose uptake in cancer, HK2 is overexpressed and bound to the outer mitochondrial membrane protein voltage-dependent anion channel (VDAC) (13, 21, 32). VDAC supplies HK2 with ATP by recruiting help from ATP synthase and adenine nucleotide translocator, resulting in a mechanism that rapidly converts glucose to G6P (13). HK2 is product inhibited by G6P, however, it is likely that this inhibition is minimal due to rapid utilization of G6P in cancer cells (21, 32).

The second irreversible reaction of glycolysis is catalyzed by phosphorfructokinase 1 (PFK1), and is the phosphorylation of fructose 6-phosphate (F6P) to fructose 1,6-bisphosphate (F1,6BP) with the concomitant dephosphorylation of ATP (21, 33, 34). PFK1 is a tetrameric enzyme that exists in liver (PFKL), muscle (PFKM), and platelet (PFKP) isoforms in mammalian cells (21, 34, 35). PFK1 expression is upregulated in cancer cells, and increased expression of the PFKP isoform is a characteristic feature of cancer (34, 35). Krüppel-like factor 4 (KLF4), which has elevated levels in certain cancer types, has been shown to activate transcription of the *PFKP* gene by directly binding to its promoter (34). In addition, PFK1 is allosterically activated by fructose 2,6-bisphosphate (F2,6BP), which shows increased generation associated with overexpression of the phosphofructokinase 2 (PFK2) isoform PFKFB3 in cancer (21).

The third irreversible reaction of glycolysis is the conversion of phosphoenolpyruvate (PEP) to pyruvate by the transfer of a phosphoryl group to ADP (21, 33). Cancer cells control this reaction by expressing the low-affinity M2 isoform of pyruvate kinase (PKM2) (11, 21). The PKM2 tetramer is allosterically regulated by various metabolites and responds to nutritional and stress signals, whereas the normal M1 isoform of pyruvate kinase (PKM1) is a constitutively active tetramer (21, 36). The regulation of PKM2 enables cancer cells to dictate the flow of carbon into biosynthetic pathways and adapt to different conditions of nutrient availability and anabolic demands (11, 21, 36). Additionally, PKM2 is regulated between its metabolically active tetrameric form and metabolically inactive dimeric form, where the PKM2 dimer is imported into the nucleus and stimulates transcription of glycolytic genes (36).

In addition to the key regulatory enzymes of glycolysis described above, other important glycolytic enzymes are also upregulated in cancer. For example, of the lactate dehydrogenases (LDHs), LDHA is the predominantly expressed isozyme in cancer (21). LDHA has a high affinity for pyruvate, and favors the conversion of pyruvate to lactate (21). Enolase 1 (ENO1) is induced in cancer cells through HIF-1α overexpression (30, 31). Aldolase A (ALDOA) is the predominant aldolase isoform expressed in hepatoma and gastric cancer tissues, and favors the cleaving of F1,6BP (21, 37). Taken together, the glycolytic isoforms expressed in cancer show a concerted effort to increase glycolytic activity and promote production of biosynthetic precursors. A schematic of glycolysis is shown in Figure 1, highlighting some of the key isoforms that are commonly overexpressed in cancer.

Regulation of Glucose Uptake in Cancer

We now focus our attention to glucose uptake and the initial steps of glycolysis, and discuss the control mechanisms that regulate glucose uptake in cancer. Although key glycolytic enzymes are upregulated in cancer, they are still involved in metabolic regulation and respond to signals such as nutritional and oxidative stress, however, this regulation changes to favor proliferation (11, 21, 36, 38). Regulation of nutrient transporters by the availability of nutrients is a phenomenon observed in bacteria and yeast, and similarly, an inhibitory effect of glucose on GLUT1 expression has been observed in several mammalian cell lines (39, 40). To study the effect of glucose on GLUT1 expression, cells have been subjected to glucose deprivation experiments, with the common result that GLUT1 content at the cell surface is increased (39, 41–45). This is achieved by different mechanisms, including increased GLUT1 mRNA transcription and stability, increased protein synthesis or decreased protein degradation, and translocation of the transporter to the cell membrane (39).

Extracellular glucose supply directly affects the intracellular glucose level (46). Thus, it is possible that GLUT1 content at the cell surface is regulated in some way by the intracellular level of glucose, as has been previously suggested (41, 47). In fact, comparisons of mammary tumors and normal mammary tissue in mice have shown that increased GLUT1 level correlates with decreased intracellular glucose level and increased glycolytic activity (38). One way in which intracellular glucose affects GLUT1 expression is via AMP-activated protein kinase (AMPK) (48). AMPK is comprised of one catalytic α-subunit, and two regulatory subunits, β and γ (48, 49). Intracellular glucose regulates AMPK activity in a few different ways: An abundance of glucose will quickly be phosphorylated to G6P by HK2. G6P is then used to supply glycolysis, lowering the AMP/ATP and ADP/ATP ratios, keeping AMPK from being activated by the binding of AMP and ADP (48). High glucose levels and increased biomass generation also reduce the NAD+/NADH ratio, which indirectly inhibits AMPK through silent information regulator T1 (SIRT1) and serine-threonine liver kinase B1 (LKB1) (21, 48, 50, 51). Downstream of G6P, the accumulation of diacylglycerol (DAG) and glycogen both lead to inhibition of AMPK. DAG inhibits AMPK by activating protein kinase C (PKC), which in turn induces the inhibitory phosphorylation of the AMPK α-subunit, while glycogen inhibits AMPK by binding to the β-subunit (48). In addition, activation of protein phosphatase 2A (PP2A) as a result of high glucose levels inhibits AMPK (48, 52, 53).

AMPK in turn has been shown to affect GLUT1 expression (54). One mechanism by which this happens is by increasing the degradation of thioredoxin interacting protein (TXNIP). TXNIP can bind directly to GLUT1 and induce internalization, as well as reduce GLUT1 mRNA level (48, 55). Another suggested mechanism is that downstream of AMPK, p38 mitogen-activated protein kinase (MAPK) activation leads to enhancement of GLUT1 mediated glucose transport (56).

Another important aspect of glucose uptake is the regulation of HK2, as it drives the first committed step of glycolysis and maintains a high concentration gradient of glucose across the cell membrane, thereby driving the facilitated diffusion

Tveit et al.
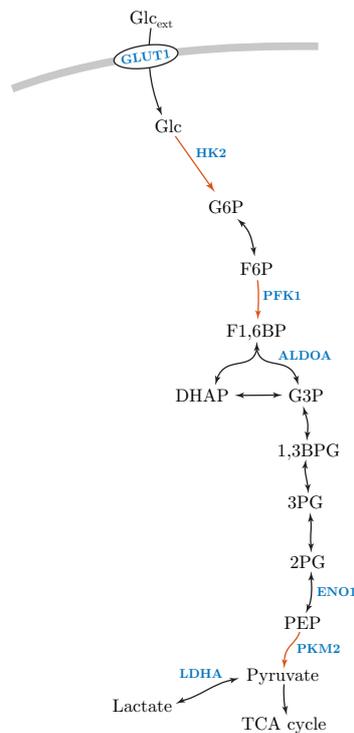
Figure 1: Schematic of glycolysis with some of the commonly overexpressed isoforms in cancer highlighted in blue. Reactions highlighted in red indicate the committed steps of glycolysis. Abbreviations: Extracellular glucose (Glc_{ext}), glucose transporter 1 (GLUT1), glucose (Glc), hexokinase 2 (HK2), glucose 6-phosphate (G6P), fructose 6-phosphate (F6P), phosphofructokinase 1 (PFK1), fructose 1,6-bisphosphate (F1,6BP), aldolase A (ALDOA), dihydroxyacetone phosphate (DHAP), glyceraldehyde 3-phosphate (G3P), 1,3-bisphosphoglycerate (1,3BPG), 3-phosphoglycerate (3PG), 2-phosphoglycerate (2PG), enolase 1 (ENO1), phosphoenolpyruvate (PEP), pyruvate kinase M2 (PKM2), lactate dehydrogenase A (LDHA), tricarboxylic acid cycle (TCA cycle).

of glucose by GLUT1 (21, 57, 58). Activators of the HK2 promoter include glucose, insulin, glucagon, p53, cAMP, and hypoxic conditions (13, 32, 59). Interestingly, it is glucose rather than downstream glycolytic metabolites that activate the HK2 promoter (13, 32, 59–61). Together with the fact that HK2 phosphorylates glucose to G6P in a reaction that is essentially irreversible, these two compounds form a stabilizing feedback connection (13, 62). Additionally, the binding of HK2 to the outer mitochondrial membrane via VDAC helps prevent apoptosis in cancer cells (13, 32). Together with the diminished inhibition (or possibly saturated inhibition) of HK2 by G6P that is associated with mitochondrial bound HK2, this gives a clear role for HK2 in promoting a malignant phenotype (32, 63–65).

The control mechanisms discussed above are summarized in Figure 2A. Here, glucose uptake and supply to metabolism includes regulatory pathways that inhibit GLUT1 mediated glucose uptake via AMPK, as well the stabilizing feedback connection formed by glucose and HK2. The mechanisms that affect AMPK depend on the production of G6P, and therefore, G6P represents the potential for these mechanisms to ultimately affect GLUT1 mediated glucose uptake. Before we can construct a mathematical model of the system in Figure 2A, activating and inhibiting pathways need to be translated into reactions that

can be described by reaction kinetic equations. To this end, parallel pathways with similar overall effects are grouped together, shown in Figure 2B. These combined pathways are then turned into activating or inhibiting reactions affecting generation or removal reactions of the compounds considered, shown in Figure 2C. The conversion of the system in Figure 2B to the system in Figure 2C preserves the effect one compound has on another, however, this conversion is not unique. For example, a negative effect of G6P on GLUT1 content at the cell surface could also be achieved if G6P activates the degradation or internalization of GLUT1 (62). Additionally, the activating and inhibiting reactions of Figure 2C do not need to represent the same molecular mechanisms. For example, the generation of G6P is driven by the phosphorylation of glucose by HK2, whereas glucose induces HK2 generation by activating the HK2 promoter. We use the system in Figure 2C as a simplified representation of glucose uptake in cancer, and as a basis for our mathematical model.
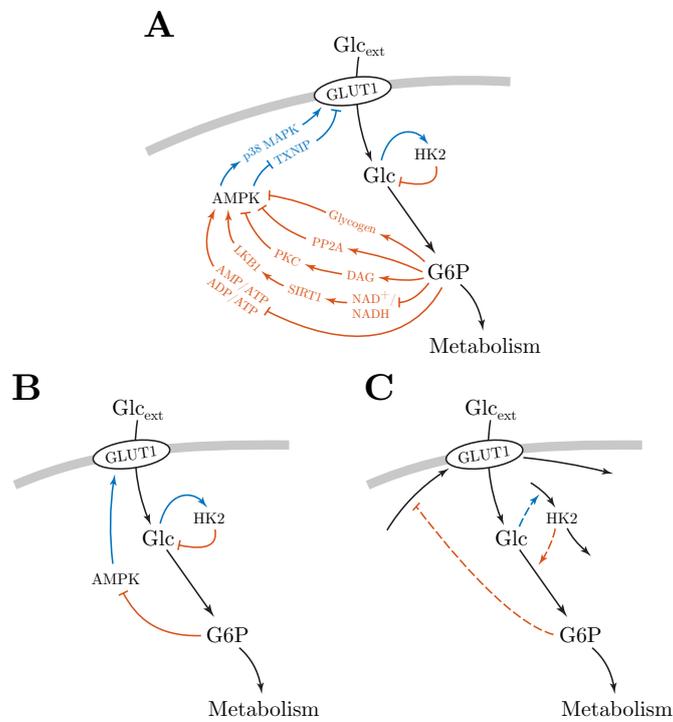
Figure 2: Panel A summarizes the control mechanisms of glucose uptake in cancer reported in the literature. Line marker-ends indicate the effect one compound has on another, arrowhead for positive and flat head for negative. Colored pathways indicate the overall effect of that pathway, blue for positive and red for negative. Black lines represent the flow of glucose to metabolism. Panel B shows colored pathways grouped together based on similar overall effects. Panel C shows the system in panel B translated into a form where activating and inhibiting effects act on reactions generating and turning over compounds. This allows for the system to be described by a simplified mathematical model using reaction kinetic equations.

Tveit et al.

METHODS

Differential Gene Expression

Expression Atlas was used to collect differential gene expression data comparing cancer cells with normal (i.e. non-cancerous) cells, across a variety of tissues and cell types. Expression Atlas is an open science resource providing information on gene and protein expression in animal and plant samples of different cell types, organism parts, developmental stages, diseases, and other conditions (66). Expression Atlas contains thousands of selected microarray and RNA-sequencing datasets that are manually curated, annotated, checked for high quality, and processed using standardized analysis methods (66). For genes of interest, users can view baseline expression in tissues, and differential expression for biologically meaningful pairwise comparisons (66).

Differential expression data of the *SLC2A* gene family, *HK1-3*, *GCK*, *PFKM*, *PFKP*, *PKM*, and *PKLR* genes in human was gathered from the Expression Atlas database. We curated the data to ensure only experiments comparing cancer cells with normal cells were included. Differential gene expression experiments with drug treatments were removed. Expression Atlas reports experiment results as $\log_2$-fold changes. In this paper, we report the arithmetic mean of $\log_2$-fold changes (i.e. $\log_2$ of the geometric mean fold change) for each gene across all experiments. Additional genes were analyzed, but due to low number of experiments (less than 5), are not included in the main results (see Section S1 in the Supporting Material).

Computational Methods

Systems of ODEs are solved numerically in initial value problems using Matlab R2018a and the ode45 ODE solver, based on the Dormand-Prince (4, 5) pair (67). Initial values and parameters for all simulations are provided in the Supporting Material. Simulation results are given in arbitrary units (arb. unit). Reaction rates are expressed as concentrations per unit of time.

RESULTS AND DISCUSSION

Corroborating the Reported Rewiring of Glycolysis in Cancer

Average $\log_2$-fold changes for key genes associated with glucose uptake and glycolysis, across a variety of tissues and cell types, are shown in Figure 3. The differential gene expression data largely corroborates the reported rewiring of glycolysis in cancer discussed above. Namely, a shift towards GLUT1 (*SLC2A1* gene) mediated glucose uptake, predominant expression of the PKM2 (PKM1 and PKM2 are different splicing products of the *PKM* gene (21)) isoform, and overexpression of HK2. We also found a slight upregulation of the *PFKP* gene in cancer, consistent with previous studies (34). Hence, the model proposed in Figure 2C appears to include the key components of glucose uptake in cancer, and provides a good basis for mathematical modeling.

The results also shows an increased *HK3* transcript abundance in cancer. This is not surprising, since it has been shown that HK3 is upregulated by hypoxia, partially through HIF dependent signaling (68). Whereas HK2 bind to the outer mitochondrial membrane, HK3 does not (13, 68). A consequence of mitochondrial bound HK2 is the prevention of cell death by inhibiting formation of the mitochondrial permeability transition pore (MPTP) complex (13, 68). On the other hand, HK3 overexpression promotes cell survival in response to oxidative stress, decreases the production of reactive oxygen species (ROS), perserves mitochondrial membrane potential, and promotes mitochondrial biogenesis (68). Therefore, it is likely that HK2 and HK3 serve different, but complementary, roles in maintaining a highly glycolytic phenotype and promoting cancer cell survival. Notably, inhibition of glucose or G6P binding to the regulatory half of HK3 (N-terminal domain) impairs catalysis in the catalytic half (C-terminal domain), suggesting a cooperative effect of glucose binding in the regulatory half to subsequent binding in the catalytic half (68). Hence, it appears that HK3 interacts with glucose in a similar way to that of HK2 in Figure 2. As a result, we will only consider HK2 in the following mathematical modeling, but note that HK2 can be thought of as a pool of both HK2 and HK3.

Modeling Rate Expressions in a Changing Volume

When modeling rate expressions in a changing volume, care must be taken so that concentrations are handled in the correct way. As an example we show how this is done for a simple enzyme reaction. The Michaelis–Menten equation describes the rate of an enzyme reaction, assuming steady state for the substrate-enzyme complex (69)

$$v = \frac{k_{\text{cat}} \cdot c_{\text{E}} \cdot c_{\text{S}}}{K_{\text{M}} + c_{\text{S}}} \tag{1}$$

where v is the reaction rate, k_{cat} is the catalytic constant (or turnover number), K_{M} is the Michaelis constant, c_{E} is the (total) concentration of enzyme, and c_{S} is the concentration of substrate. We start by considering some compound x in a changing
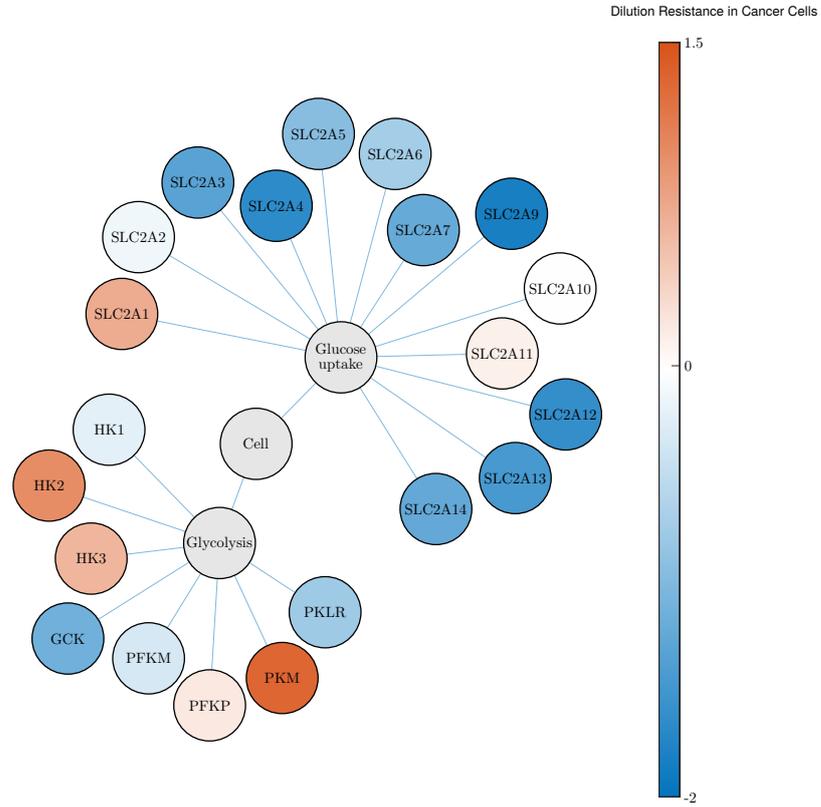
Figure 3: Differential gene expression of key genes associated with glucose uptake and glycolysis. The differential gene expression compares cancer cells with normal cells, across a variety of tissues and cell types, reported as the average $\log_2$-fold change of several experiments. Upregulation in cancer cells is indicated by red, and downregulation by blue. White indicates no change. The differential gene expression corroborates the reported rewiring of glycolysis in cancer. Namely, a shift towards GLUT1 (*SLC2A1* gene) mediated glucose uptake, overexpression of HK2, and a predominant reliance on PKM2 (PKM1 and PKM2 are different splicing products of the *PKM* gene (21)). We also found upregulation of the *HK3* and *PFKP* genes. See Section S1 in the Supporting Material for information on the individual differential gene expression experiments.

volume. Using the product rule, we express the change in concentration of x as

$$n_x(t) = c_x(t) \cdot V(t) \tag{2}$$

$$\dot{n}_x(t) = \dot{c}_x(t) \cdot V(t) + c_x(t) \cdot \dot{V}(t) \tag{3}$$

$$\dot{c}_x(t) = \frac{\dot{n}_x(t)}{V(t)} - c_x(t) \cdot \frac{\dot{V}(t)}{V(t)} \tag{4}$$

where n_x is the amount of compound, c_x is the concentration of compound, and V is the volume. We use dot notation to indicate time derivative. The first term of Eq. 4 is identical to the time derivative of c_x in a constant volume, while the second term represents the dilution of c_x (10). We will call this the *dilution term*. Using Eq. 1, we express the differential equation of a

Tveit et al.

product P being formed by an enzyme reaction in a changing volume by introducing the dilution term from Eq. 4 (5)

$$\dot{c}_P(t) = \frac{k_{cat} \cdot c_E(t) \cdot c_S(t)}{K_M + c_S(t)} - c_P(t) \cdot \frac{\dot{V}(t)}{V(t)} \tag{5}$$

It is important to note that all constituents of the enzyme reaction, i.e. product, enzyme, and substrate, are diluted as the volume increases. This means that even if an enzyme is present in constant amount, a large enough volume increase can effectively stop the enzyme reaction by dilution of the enzyme concentration (5).

Modeling Glucose Uptake in Cancer
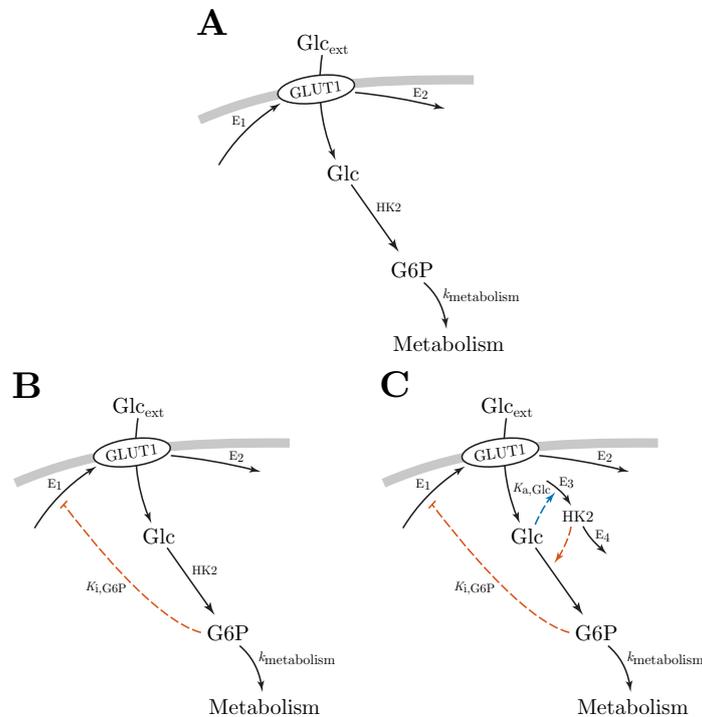
Figure 4: The mathematical model of glucose uptake is constructed in three steps. Panel A shows the first step, with only the uptake and supply of glucose to metabolism. The second step is shown in panel B, which includes feedback inhibition from G6P to GLUT1 mediated glucose uptake. Panel C shows the final step, where the model also includes the stabilizing feedback connection formed by HK2 and intracellular glucose.

We construct the mathematical model of glucose uptake in three steps, starting with glucose uptake and supply to metabolism without any of the control mechanisms discussed above. This system is shown in Figure 4A. Assuming low intracellular concentration of glucose due to rapid conversion by HK2, facilitated diffusion of glucose by GLUT1 can be approximated by the Michaelis–Menten equation (57, 58). In this first step of model construction, we assume that HK2 is not being generated and turned over (and therefore, HK2 synthesis is not activated by intracellular glucose), and that the concentration of HK2 simply dilutes as the cellular volume increases. The phosphorylation of glucose to G6P is modeled by the Michaelis–Menten equation,

and the sink reaction to metabolism is modeled by a first order reaction with rate constant $k_{\text{metabolism}}$. GLUT1 is assumed to be generated and turned over in reactions driven by enzymes E_1 and E_2, respectively, but feedback inhibition from G6P is omitted for the time being. The enzymes E_1 and E_2 are themselves present in constant amounts only (i.e. their concentrations simply dilute with increasing volume). We assume the production of GLUT1 is proportional to the concentration of E_1, and that the degradation of GLUT1 by E_2 is given by a Michaelis–Menten-type process. We are considering a growing cell, which introduces the dilution term from Eq. 4. The dynamical model is given by the following system of ODEs

$$\dot{c}_{\text{Glc}}(t) = \frac{k_{\text{cat,GLUT1}} \cdot c_{\text{GLUT1}}(t) \cdot c_{\text{Glc,ext}}(t)}{K_{\text{M,GLUT1}} + c_{\text{Glc,ext}}(t)} \cdot \frac{A(t)}{V(t)} - \frac{k_{\text{cat,HK2}} \cdot c_{\text{HK2}}(t) \cdot c_{\text{Glc}}(t)}{K_{\text{M,HK2}} + c_{\text{Glc}}(t)} - c_{\text{Glc}}(t) \cdot \frac{\dot{V}(t)}{V(t)} \qquad (6)$$

$$\dot{c}_{\text{G6P}}(t) = \frac{k_{\text{cat,HK2}} \cdot c_{\text{HK2}}(t) \cdot c_{\text{Glc}}(t)}{K_{\text{M,HK2}} + c_{\text{Glc}}(t)} - k_{\text{metabolism}} \cdot c_{\text{G6P}}(t) - c_{\text{G6P}}(t) \cdot \frac{\dot{V}(t)}{V(t)} \qquad (7)$$

$$\dot{c}_{\text{GLUT1}}(t) = k_{\text{cat,1}} \cdot c_{E,1}(t) \cdot \frac{V(t)}{A(t)} - \frac{k_{\text{cat,2}} \cdot c_{E,2}(t) \cdot c_{\text{GLUT1}}(t)}{K_{\text{M,2}} + c_{\text{GLUT1}}(t)} \cdot \frac{V(t)}{A(t)} - c_{\text{GLUT1}}(t) \cdot \frac{\dot{A}(t)}{A(t)} \qquad (8)$$

where c_{Glc} and c_{G6P} are concentrations in the cellular volume V, whereas c_{GLUT1} is a concentration at the cell surface A. As a consequence, the import of glucose is converted by the factor $\frac{A}{V}$ to a flux given with respect to the cellular volume. Similarly, the generation and degradation of GLUT1 are converted by the factor $\frac{V}{A}$ to fluxes with respect to the cell surface area, since the enzymes generating and turning over GLUT1 are situated inside the cell. HK2, E_1, and E_2 are not assumed to be generated and turned over, and their concentrations dilute from some initial concentrations as the cellular volume increases. These concentrations are given by $c_x(t) = n_x/V(t)$ ($x = \text{HK2}, E_1, E_2$), where n_x is the amount of compound x (constant quantities).

We call the system of ODEs given by Eqs. 6–8 *model A*, corresponding to the system shown in Figure 4A. This model only describes the uptake of glucose and supply to metabolism, without any control mechanisms in place. To examine the regulatory mechanisms of glucose uptake, we build on this model, and add feedback inhibition from G6P to GLUT1 production. This feedback is based on the many pathways that regulate GLUT1 mediated glucose uptake via AMPK, summarized in Figure 2A. This way, a reduction in G6P level will reduce inhibition of GLUT1 production, thereby increasing GLUT1 mediated glucose uptake. We model this feedback by allosteric inhibition (specifically, a special case of mixed inhibition) of the reaction producing GLUT1 (69, 70). The model is shown in Figure 4B, and given by Eqs. 6–7, and the additional ODE

$$\dot{c}_{\text{GLUT1}}(t) = k_{\text{cat,1}} \cdot c_{E,1}(t) \cdot \frac{K_{\text{i,G6P}}}{K_{\text{i,G6P}} + c_{\text{G6P}}(t)} \cdot \frac{V(t)}{A(t)} - \frac{k_{\text{cat,2}} \cdot c_{E,2}(t) \cdot c_{\text{GLUT1}}(t)}{K_{\text{M,2}} + c_{\text{GLUT1}}(t)} \cdot \frac{V(t)}{A(t)} - c_{\text{GLUT1}}(t) \cdot \frac{\dot{A}(t)}{A(t)} \qquad (9)$$

where $K_{\text{i,G6P}}$ is the inhibition constant for the allosteric inhibition of GLUT1 production by G6P. We call this *model B*.

We simulate models A and B in three phases (Figure 5): In the first phase (white area, $t = [0, 50]$), the cellular volume is kept constant. In the second phase (light gray area, $t = [50, 100]$), we still maintain a constant cellular volume, and probe the regulatory function of the feedback inhibition in model B by reducing the extracellular glucose concentration by 75% at the start of the phase. In the third phase (dark gray area, $t = [100, 150]$), we investigate the effect of dilution on the two models by increasing the cellular volume linearly. The simulation results are shown in Figure 5, with initial values and parameters provided in Table S1 in the Supporting Material. Dashed red lines show the dynamical response of model A, and solid blue lines show model B. The bottom right plot of cellular volume (solid black line) and surface area (dashed black line) is the same for both simulations. In the first phase (white area), the cellular volume is constant and both systems have settled at steady state, producing a constant glycolytic flux (represented by the phosphorylation of glucose). At the start of the second phase (light gray area), extracellular glucose concentration is reduced while the cellular volume remains constant. Comparing the two models, we see that model A shows no adaptation to such a perturbation in glucose supply, resulting in reduced metabolite levels (intracellular glucose and G6P) and glycolytic flux. Model B, however, is able to fully compensate for the reduction in glucose supply. This is achieved by increasing the surface concentration of GLUT1, thereby increasing GLUT1 mediated glucose uptake to match the previous uptake rate of the system. In the final phase of the simulations (dark gray area), cellular volume starts to increase linearly. Although neither of the models are able to compensate for dilution, in the case of model B, GLUT1 production is increased in an attempt to mitigate the effect of dilution. However, this compensatory response is not being effectuated as the level of HK2 is not being maintained, resulting in reduced glycolytic flux as the concentration of HK2 dilutes. The simulation results show that feedback inhibition from downstream glycolytic metabolites to glucose transporters is sufficient for homeostatic control of glycolysis in a constant volume, consistent with principles of metabolic regulation by negative feedback (71, 72). The regulation of glucose transporters by feedback inhibition is, however, not sufficient to maintain a constant glycolytic flux during growth. It appears that control of HK2 may be necessary for homeostatic control during growth.

In order to compensate for dilution, we extend model B, and add activation of HK2 synthesis by intracellular glucose. As mentioned earlier, this forms a stabilizing feedback connection together with the phosphorylation of glucose to G6P (62). This
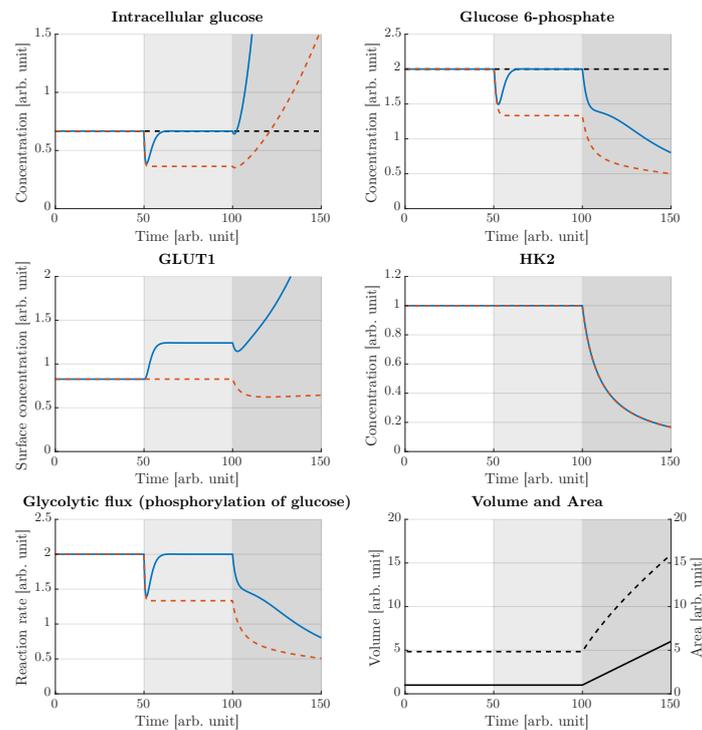
Figure 5: Simulation results of model A (dashed red lines) and model B (solid blue lines). The bottom right plot of volume (solid black line) and surface area (dashed black line) is the same for the two simulations. Initially, the cellular volume is kept constant and the systems have settled at steady state (white area, $t = [0, 50]$). At the start of the second phase (light gray area, $t = [50, 100]$), extracellular glucose concentration is reduced by 75%. Whereas model A shows no adaptation in this phase, model B is able to regulate intracellular glucose and G6P levels back to pre-perturbed values (dashed black lines), and maintain homeostatic control of glycolysis (regulation of the glycolytic flux). In the last phase (dark gray area, $t = [100, 150]$), the cellular volume starts to increase linearly. Neither of the models are able to compensate for dilution, however, GLUT1 mediated glucose uptake is increased in model B, but due to dilution of HK2 this compensatory response is not being effectuated. Note that due to dilution of HK2, intracellular glucose accumulates in the final phase. Such an accumulation can not go on forever, and as the concentration of intracellular glucose approaches that of extracellular glucose, our assumption of GLUT1 mediated glucose uptake following the Michaelis–Menten equation will break down. A similar limit for the surface concentration of GLUT1 will also likely be approached. Nevertheless, the simulation results are able to show that models A and B do not achieve homeostatic control of glysolysis in the presence of dilution. Initial values and parameters are provided in Table S1 in the Supporting Material.

feedback connection stabilizes the level of HK2 in the presence of dilution, such that the concentration of HK2 remains more or less constant during growth, providing robustness to dilution in the first irreversible step of glycolysis. In turn, this robustness allows GLUT1 mediated glucose uptake to regulate the glycolytic flux during growth. With this addition it is necessary to add reactions generating and turning over HK2, so that activation by intracellular glucose can be mediated through these reactions. The activation of HK2 synthesis is modeled by allosteric activation (specifically, a special case of mixed activation) (69, 70).

We assume the synthesis and degradation of HK2 are driven by enzymes E_3 and E_4, respectively, where the synthesis is proportional to the level of E_3, and the degradation by E_4 follows a Michaelis–Menten-type process. The model is shown in Figure 4C and given by Eqs. 6–7, 9, and the following ODE describing the change in HK2 concentration

$$\dot{c}_{HK2}(t) = k_{cat,3} \cdot c_{E,3}(t) \cdot \frac{c_{Glc}(t)}{K_{a,Glc} + c_{Glc}(t)} - \frac{k_{cat,4} \cdot c_{E,4}(t) \cdot c_{HK2}(t)}{K_{M,4} + c_{HK2}(t)} - c_{HK2}(t) \cdot \frac{\dot{V}(t)}{V(t)} \qquad (10)$$

where $K_{a,Glc}$ is the activation constant for the allosteric activation of HK2 synthesis by intracellular glucose. The enzymes E_i (i = 1, 2, 3, 4) are not assumed to be generated and turned over, and their concentrations dilute as the volume increases. These concentrations are given by $c_{E,i}(t) = n_{E,i}/V(t)$ (i = 1, 2, 3, 4), where $n_{E,i}$ (the amount of E_i) are constant quantities. We call this *model C*.

We simulate model C in four phases (Figure 6): In the first phase (white area, $t = [0, 400]$), the volume is kept constant. In the second phase (light gray area, $t = [400, 800]$), we increase the volume linearly to investigate whether model C is able to maintain homeostatic control of glycolysis during growth. While the volume is still increasing, extracellular glucose concentration is increased 4-fold at the start of the third phase (dark gray area, $t = [800, 1200]$). Finally, in the last phase (white area, $t = [1200, 1600]$), volume increase is stopped. The simulation results are shown in Figure 6, with initial values and parameters provided in Table S2 in the Supporting Material. The bottom right plot shows volume (solid black line) and surface area (dashed black line) during the simulation. In the first phase (white area), the system has settled at steady state, producing a constant glycolytic flux. In the second phase (light gray area), we see that model C is able to compensate for dilution and produce a constant glycolytic flux, however, steady state values are shifted compared to steady state values without growth (dashed black lines in intracellular glucose and G6P plots). These growth associated offsets could indicate the inability of the control mechanisms to fully compensate for dilution. However, they could also represent set-point changes during the growth phase. To investigate the cause of the growth associated offsets, we increase extracellular glucose concentration as the cellular volume is growing. This is done at the start of the third phase (dark gray area). Due to the subsequent increase in glucose uptake, a sudden reduction in the surface concentration of GLUT1 follows. Nevertheless, the surface concentration of GLUT1 continues to increase throughout this phase in order to compensate for dilution. Interestingly, it seems that the control mechanisms attempt to bring the system back to steady state values associated with growth, not steady state values associated with constant volume. If the latter were true, we would not expect to see the regulatory action in Figure 6 bringing intracellular glucose and G6P levels away from steady state values associated with constant volume (dashed black lines). This suggests that the growth associated offsets may be caused by set-point changes, rather than the inability to maintain the glycolytic flux during growth. Finally, the first phase is repeated and the volume is kept constant again, but is now much larger (white area). In this phase, we see that metabolite levels and the glycolytic flux return to steady state values associated with constant volume. This is achieved by the increase of surface concentration of GLUT1 during the growth phase, which is made possible due to the relationship between cellular volume and cell surface area (see Section S2 in the Supporting Material). Thus, the growth associated offsets appears to be dependent on the rate of volume increase, not the total volume.

Taken together, the simulation results of models A, B, and C in Figure 5 and Figure 6 show that while negative feedback from downstream metabolites to nutrient transporters is sufficient for homeostatic control in a constant volume, it is necessary to stabilize the concentrations of intermediate enzymes in order to achieve homeostatic control during growth. The simulations also demonstrate that during the growth phase, growth associated offsets from steady state values associated with constant volume are observed, and that these offsets appears to be caused by set-point changes that are dependent on the growth rate. Importantly, investigations into control mechanisms similar to the ones identified in this paper, have shown that growth associated offsets become negligible if the kinetics of the controller species behave on a timescale much faster than cell growth (9, 10, 73–75). These control mechanisms, called ICMs, achieve robust homeostatic control due to a negative feedback structure that includes integral action. In the following, we take a closer look at the function of such ICMs and show how the control mechanisms discussed above realize integral action and dilution resistance.

A Closer Look at Integral Control Motifs

Asymptotic regulation is the notion that a regulation error approaches zero, i.e. the output perfectly reaches a desired reference, as time tends to infinity (76). If asymptotic regulation is achieved in the presence of disturbances, asymptotic disturbance rejection (also called robustness) is achieved (76). In the case of constant reference signal, or set-point, and constant disturbance, asymptotic regulation and disturbance rejection can be achieved by integral action (76). A block diagram of negative feedback with integral action is shown in Figure 7. For a system subject to disturbance w, the output y is to be regulated to a set-point r. This is achieved by comparing the system output to the set-point, giving the regulation error $e = r - y$. The integral controller integrates the regulation error, producing the control action input u to the system. Thus, when the system output deviates from the set-point, the regulation error is non-zero, which produces a change in the control action. Because the feedback is negative,

Tveit et al.
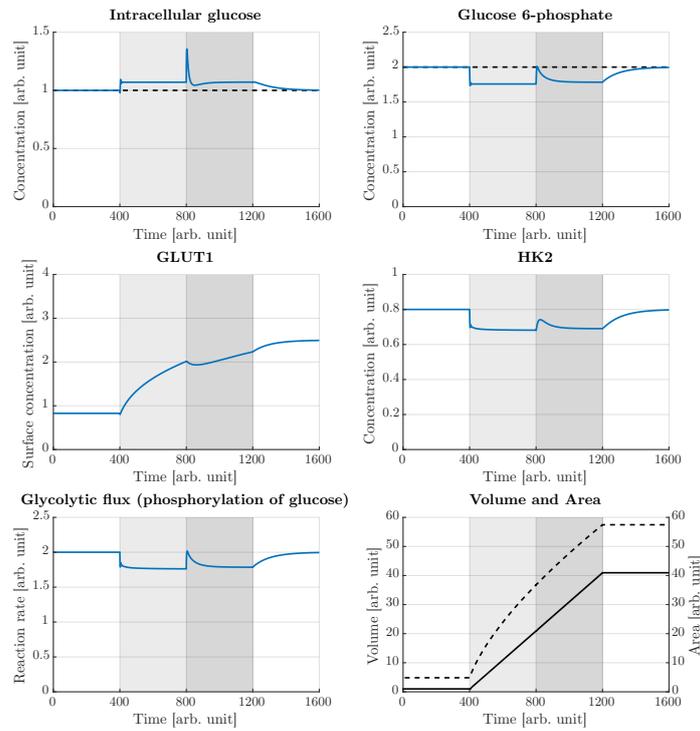
Figure 6: Simulation results of model C. The bottom right plot shows volume (solid black line) and surface area (dashed black line) during the simulation. Initially, the cellular volume is kept constant, and the system has settled at steady state (white area, $t = [0, 400]$). In the second phase (light gray area, $t = [400, 800]$), the cellular volume increases linearly. During this phase, metabolite levels and the glycolytic flux are maintained at constant levels, however, with offsets from steady state values associated with constant volume (dashed black lines in intracellular glucose and G6P plots). At the start of the third phase (dark gray area, $t = [800, 1200]$), as the volume is still increasing, the concentration of extracellular glucose is increased 4-fold. Interestingly, the system is regulated back to steady state values associated with growth, and away from steady state values associated with constant volume. This suggests that the growth associated offsets are caused by set-point changes. Finally, the first phase is repeated, and the volume is kept constant (white area, $t = [1200, 1600]$). In this phase we see that metabolite levels and the glycolytic flux return to steady state values associated with constant volume. This indicates that the growth associated offsets are dependent on the growth rate, rather than the total volume. Initial values and parameters are provided in Table S2 in the Supporting Material.

this change in control action counteracts the deviation of the system output from the set-point. Importantly, when the system output reaches the desired set-point, the output is maintained exactly at the set-point, as the "memory" element of the integral controller stores the accumulated regulation error (9). The block diagram in Figure 7 suggests a constant integral gain G_i, though this gain can be variable, often referred to as gain scheduling (62, 76). The mathematical description of the integral controller, called the integral control law, is given by

$$\dot{u}(t) = G_i \cdot (r - y(t)) \tag{11}$$
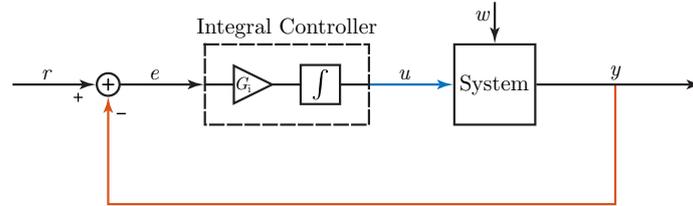
Figure 7: Block diagram of negative feedback with integral action. The system output y is fed back (red output feedback) and compared to the reference signal r to produce the regulation error $e = r - y$. The regulation error is multiplied by an integral gain G_i and integrated over time to produce the control action u (blue system input). In the presence of an uncontrolled disturbance w (black disturbance input), a deviation in system output from the reference will cause a non-zero regulation error. This produces a change in the control action, and since the feedback is negative, this control action functions to contract the deviation in system output from the reference.

Investigations into robust homeostatic systems have revealed several motifs that include negative feedback with integral action (9, 62, 77, 78). The control mechanisms considered in this paper correspond to a class of ICMs called homeostatic controller motifs (62). It has been shown that these homeostatic controller motifs are robust to all parameter perturbations that do not destroy the stability of the system (79). For example, feedback inhibition from G6P to GLUT1 generation produces the same structure as that of Figure 7. Red output feedback corresponds to the inhibition of GLUT1 generation by G6P, the integral controller block corresponds to GLUT1 level, blue system input corresponds to GLUT1 mediated glucose uptake, and the system block corresponds to the level of G6P. The black disturbance input corresponds to perturbations made in extracellular glucose and cellular volume. By manipulating Eq. 9, we show that GLUT1 functions as an integral controller for G6P level

$$\dot{c}_{\text{GLUT1}}(t) = k_{\text{cat},1} \cdot c_{E,1}(t) \cdot \frac{K_{\text{i,G6P}}}{K_{\text{i,G6P}} + c_{\text{G6P}}(t)} \cdot \frac{V(t)}{A(t)} - \frac{k_{\text{cat},2} \cdot c_{E,2}(t) \cdot c_{\text{GLUT1}}(t)}{K_{\text{M},2} + c_{\text{GLUT1}}(t)} \cdot \frac{V(t)}{A(t)} - c_{\text{GLUT1}}(t) \cdot \frac{\dot{A}(t)}{A(t)} \tag{12}$$

$$\approx k_{\text{cat},1} \cdot c_{E,1}(t) \cdot \frac{K_{\text{i,G6P}}}{K_{\text{i,G6P}} + c_{\text{G6P}}(t)} \cdot \frac{V(t)}{A(t)} - k_{\text{cat},2} \cdot c_{E,2}(t) \cdot \frac{V(t)}{A(t)} - c_{\text{GLUT1}}(t) \cdot \frac{\dot{A}(t)}{A(t)} \tag{13}$$

$$= G_{\text{i}}(t) \cdot \left(c_{\text{G6P,set}} - \dot{A}(t) \cdot o_{\text{G6P}}(t) - c_{\text{G6P}}(t) \right) \tag{14}$$

where we make the simplification $K_{\text{M},2} \ll c_{\text{GLUT1}}$. The following definitions are made

$$G_{\text{i}}(t) = \frac{1}{A(t)} \cdot \frac{k_{\text{cat},2} \cdot n_{E,2}}{K_{\text{i,G6P}} + c_{\text{G6P}}(t)} \tag{15}$$

$$c_{\text{G6P,set}} = \frac{k_{\text{cat},1} \cdot n_{E,1} - k_{\text{cat},2} \cdot n_{E,2}}{k_{\text{cat},2} \cdot n_{E,2}} \cdot K_{\text{i,G6P}} \tag{16}$$

$$o_{\text{G6P}}(t) = \frac{K_{\text{i,G6P}} + c_{\text{G6P}}(t)}{k_{\text{cat},2} \cdot n_{E,2}} \cdot c_{\text{GLUT1}}(t) \tag{17}$$

The set-point for G6P level, $c_{\text{G6P,set}}$, is given entirely by parameters associated with GLUT1 generation and degradation. This means that perturbations in G6P are fully compensated for, as the set-point remains unchanged for such perturbations (73). In the case without growth, $\dot{A} = 0$, Eq. 14 is reduced to the same form as the integral control law in Eq. 11. In the case with growth, a growth associated offset, $\dot{A} \cdot o_{\text{G6P}}$, is introduced. However, if the reaction rates for the generation and degradation of GLUT1 behave on a timescale much faster than the rate of dilution, o_{G6P} is small, and the growth associated offset becomes negligible. ICMs with controller reactions much faster than the rate of dilution are called quasi-ICMs, and characteristically show small growth associated offsets (9). One mechanism of regulating GLUT1 and HK2 activity is through translocation between biological membranes and the cytosol, indicating that the activity of these species can respond quickly, and that regulation of glucose uptake in cancer may achieve dilution resistance through the formation of quasi-ICMs (39, 55, 80). Similar to GLUT1, it is possible to show that HK2 functions as an integral controller for the level of intracellular glucose (See Section S3 in the Supporting Material).

Tveit et al.

CONCLUSION

In this paper, we have constructed a mathematical model of glucose uptake based on the reported rewiring of glycolysis in cancer and differential gene expression of cancer and normal cells. With basis in the literature, we added control mechanisms to the model in a stepwise manner, in order to investigate the role each regulatory mechanism serve. Expectedly, we found that feedback inhibition from downstream glycolytic metabolites to glucose transporters is sufficient for homeostatic control of glycolysis in a constant volume. However, in a growing volume, we found that regulation of intermediate glycolytic enzymes is needed for homeostatic control of glycolysis. Cancer cells show a shift towards GLUT1 mediated glucose uptake and a reliance on HK2. We found that these species form regulatory mechanisms for glycolysis through their interactions with glycolytic metabolites. These regulatory mechanisms are a class of ICMs known as homeostatic controller motifs, and achieve robust homeostatic control by negative feedback with integral action (9, 62). Our simulation results show that during growth, offsets from steady state values associated with constant volume are observed. These growth associated offsets can be interpreted as set-point changes, and are dependent on the growth rate of the cell, not the total volume. In his definition of homeostasis, Cannon emphasized that homeostasis does not imply perfect adaptation to disturbances, but allows for some variability in steady state (81). Similarly, rheostasis is defined as systems that show homeostatic control at any one instant, but over the span of time show change in the regulated level (82). Living organisms are not necessarily concerned with perfect regulation, but rather with the presence of some level of regulation. Thus, it is likely that sufficient regulation can be achieved even if the growth associated offsets are fairly large. This variability in steady state can then be viewed as a relaxing condition on the control mechanisms employed (83).

Investigations into ICMs have shown that growth associated offsets becomes negligible if the rates of the controller reactions, i.e. the generation and degradation of GLUT1 and HK2, are much faster compared to the rate of dilution (9, 10, 73–75). In our model, enzymes responsible for generating and removing the controller species (E_i, $i = 1, 2, 3, 4$) are present in constant amounts only, meaning that their concentrations simply dilute with increasing volume. This is a worst-case scenario in which regulation in the presence of dilution is possible. In this scenario, we found that model C is able to compensate for dilution in a linearly increasing volume. However, most protein and mRNA concentrations are independent of cell size, and therefore it is likely that the concentrations $c_{E,i}$ ($i = 1, 2, 3, 4$) should be considered constant (7). In this case, it has been shown that regulation is possible even in the presence of dilution in an exponentially increasing cell volume (9, 10).

Taking a closer look at feedback inhibition from downstream glycolytic metabolites to GLUT1 mediated glucose uptake, we have shown how this control mechanism realizes integral action to regulate glycolysis. We have also shown how dilution affects this ICM, and related the growth associated offset in G6P to a term dependent on the growth rate of the cell. In recent years, ICMs have garnered much attention (9, 10, 62, 75, 77, 78). This paper uses glucose uptake in cancer to demonstrate a systems biology approach to the analysis of complex regulatory systems, where control mechanisms are reduced into their essential components, which can then be represented by ICMs. A benefit of this approach is simplifying the mathematical description of the complex system, while retaining the essential behavior, such that a more manageable system can be considered and an in-depth analysis of its function can be done.

AUTHOR CONTRIBUTIONS

DT, TD, KT, FF, and PR conceived and designed the research. DT and TD performed simulations. DT, TD, KT, and FF analyzed the data. DT and GF wrote the manuscript with contributions from all coauthors.

REFERENCES

1. Lang, F., G. L. Busch, M. Ritter, H. Völkl, S. Waldegger, E. Gulbins, and D. Häussinger, 1998. Functional Significance of Cell Volume Regulatory Mechanisms. *Physiological Reviews* 78:247–306.

2. Clegg, J. S., S. A. Jackson, and K. Fendl, 1990. Effects of Reduced Cell Volume and Water Content on Glycolysis in L-929 Cells. *Journal of Cellular Physiology* 142:386–391.

3. Peak, M., M. al-Habori, and L. Agius, 1992. Regulation of Glycogen Synthesis and Glycolysis by Insulin, pH and Cell Volume. Interactions between Swelling and Alkalinization in Mediating the Effects of Insulin. *Biochemical Journal* 282:797–805.

4. Häussinger, D., W. Newsome, S. vom Dahl, B. Stoll, B. Noe, R. Schreiber, M. Wettstein, and F. Lang, 1994. Control of Liver Cell Function by the Hydration State. *Biochemical Society Transactions* 22:497–502.

5. Lizana, L., B. Bauer, and O. Orwar, 2008. Controlling the Rates of Biochemical Reactions and Signaling Networks by Shape and Volume Changes. *Proceedings of the National Academy of Sciences of the United States of America* 105:4099–4104.

6. Schmoller, K. M., J. J. Turner, M. Kõivomägi, and J. M. Skotheim, 2015. Dilution of the Cell Cycle Inhibitor Whi5 Controls Budding-Yeast Cell Size. *Nature* 526:268–272.

7. Schmoller, K. M., and J. M. Skotheim, 2015. The Biosynthetic Basis of Cell Size Control. *Trends in Cell Biology* 25:793–802.

8. Saint, M., F. Bertaux, W. Tang, X.-M. Sun, L. Game, A. Köferle, J. Bähler, V. Shahrezaei, and S. Marguerat, 2019. Single-Cell Imaging and RNA Sequencing Reveal Patterns of Gene Expression Heterogeneity during Fission Yeast Growth and Adaptation. *Nature Microbiology* 4:480–491.

9. Qian, Y., and D. Del Vecchio, 2018. Realizing 'Integral Control' in Living Cells: How to Overcome Leaky Integration Due to Dilution? *Journal of the Royal Society Interface* 15:20170902.

10. Ruoff, P., O. Agafonov, D. M. Tveit, K. Thorsen, and T. Drengstig, 2019. Homeostatic Controllers Compensating for Growth and Perturbations. *PLoS ONE* 14:e0207831.

11. Vander Heiden, M. G., L. C. Cantley, and C. B. Thompson, 2009. Understanding the Warburg Effect: The Metabolic Requirements of Cell Proliferation. *Science* 324:1029–1033.

12. Gatenby, R. A., and R. J. Gillies, 2004. Why Do Cancers Have High Aerobic Glycolysis? *Nature Reviews Cancer* 4:891–899.

13. Mathupala, S. P., Y. H. Ko, and P. L. Pedersen, 2006. Hexokinase II: Cancer's Double-Edged Sword Acting as Both Facilitator and Gatekeeper of Malignancy When Bound to Mitochondria. *Oncogene* 25:4777–4786.

14. Vazquez, A., and Z. N. Oltvai, 2016. Macromolecular Crowding Explains Overflow Metabolism in Cells. *Scientific Reports* 6:31007.

15. Vazquez, A., J. Liu, Y. Zhou, and Z. N. Oltvai, 2010. Catabolic Efficiency of Aerobic Glycolysis: The Warburg Effect Revisited. *BMC Systems Biology* 4:58.

16. Guertin, D. A., and D. M. Sabatini, 2008. Chapter 12: Cell Growth. *In* The Molecular Basis of Cancer, Saunders, Philadelphia, PA, 169–175. 3 edition.

17. Furlong, T. J., and K. R. Spring, 1990. Mechanisms Underlying Volume Regulatory Decrease by Necturus Gallbladder Epithelium. *American Journal of Physiology-Cell Physiology* 258:C1016–C1024.

18. Natarajan, R., N. Gonzales, L. Xu, and J. L. Nadler, 1992. Vascular Smooth Muscle Cells Exhibit Increased Growth in Response to Elevated Glucose. *Biochemical and Biophysical Research Communications* 187:552–560.

19. Di Chiro, G., J. Hatazawa, D. A. Katz, H. V. Rizzoli, and D. J. De Michele, 1987. Glucose Utilization by Intracranial Meningiomas as an Index of Tumor Aggressivity and Probability of Recurrence: A PET Study. *Radiology* 164:521–526.

20. Sánchez-Aragó, M., M. Chamorro, and J. M. Cuezva, 2010. Selection of Cancer Cells with Repressed Mitochondria Triggers Colon Cancer Progression. *Carcinogenesis* 31:567–576.

21. Hay, N., 2016. Reprogramming Glucose Metabolism in Cancer: Can It Be Exploited for Cancer Therapy? *Nature Reviews Cancer* 16:635–649.

22. Hsu, P. P., and D. M. Sabatini, 2008. Cancer Cell Metabolism: Warburg and Beyond. *Cell* 134:703–707.

23. Hanahan, D., and R. A. Weinberg, 2011. Hallmarks of Cancer: The next Generation. *Cell* 144:646–674.

24. DeBerardinis, R. J., J. J. Lum, G. Hatzivassiliou, and C. B. Thompson, 2008. The Biology of Cancer: Metabolic Reprogramming Fuels Cell Growth and Proliferation. *Cell Metabolism* 7:11–20.

25. Carruthers, A., J. DeZutter, A. Ganguly, and S. U. Devaskar, 2009. Will the Original Glucose Transporter Isoform Please Stand Up! *American Journal of Physiology-Endocrinology and Metabolism* 297:E836–E848.

26. Joost, H.-G., G. I. Bell, J. D. Best, M. J. Birnbaum, M. J. Charron, Y. T. Chen, H. Doege, D. E. James, H. F. Lodish, K. H. Moley, J. F. Moley, M. Mueckler, S. Rogers, A. Schürmann, S. Seino, and B. Thorens, 2002. Nomenclature of the GLUT/SLC2A Family of Sugar/Polyol Transport Facilitators. *American Journal of Physiology-Endocrinology and Metabolism* 282:E974–E976.

Tveit et al.

27. Thorens, B., and M. Mueckler, 2010. Glucose Transporters in the 21st Century. *American Journal of Physiology-Endocrinology and Metabolism* 298:E141–E145.

28. Bell, G. I., T. Kayano, J. B. Buse, C. F. Burant, J. Takeda, D. Lin, H. Fukumoto, and S. Seino, 1990. Molecular Biology of Mammalian Glucose Transporters. *Diabetes Care* 13:198–208.

29. Thorens, B., 1996. Glucose Transporters in the Regulation of Intestinal, Renal, and Liver Glucose Fluxes. *American Journal of Physiology-Gastrointestinal and Liver Physiology* 270:G541–G553.

30. Ganapathy, V., M. Thangaraju, and P. D. Prasad, 2009. Nutrient Transporters in Cancer: Relevance to Warburg Hypothesis and Beyond. *Pharmacology & Therapeutics* 121:29–40.

31. Semenza, G. L., 2003. Targeting HIF-1 for Cancer Therapy. *Nature Reviews Cancer* 3:721–732.

32. Pedersen, P. L., S. Mathupala, A. Rempel, J. Geschwind, and Y. H. Ko, 2002. Mitochondrial Bound Type II Hexokinase: A Key Player in the Growth and Survival of Many Cancers and an Ideal Prospect for Therapeutic Intervention. *Biochimica et Biophysica Acta (BBA) - Bioenergetics* 1555:14–20.

33. Berg, J. M., J. L. Tymoczko, G. J. Gatto, Jr., and L. Stryer, 2015. Biochemistry. W. H. Freeman & Company, New York, NY, 8 edition.

34. Moon, J.-S., H. E. Kim, E. Koh, S. H. Park, W.-J. Jin, B.-W. Park, S. W. Park, and K.-S. Kim, 2011. Krüppel-like Factor 4 (KLF4) Activates the Transcription of the Gene for the Platelet Isoform of Phosphofructokinase (PFKP) in Breast Cancer. *Journal of Biological Chemistry* 286:23808–23816.

35. Kim, N. H., Y. H. Cha, J. Lee, S.-H. Lee, J. H. Yang, J. S. Yun, E. S. Cho, X. Zhang, M. Nam, N. Kim, Y.-S. Yuk, S. Y. Cha, Y. Lee, J. K. Ryu, S. Park, J.-H. Cheong, S. W. Kang, S.-Y. Kim, G.-S. Hwang, J. I. Yook, and H. S. Kim, 2017. Snail Reprograms Glucose Metabolism by Repressing Phosphofructokinase PFKP Allowing Cancer Cell Survival under Metabolic Stress. *Nature Communications* 8:14374.

36. Filipp, F. V., 2013. Cancer Metabolism Meets Systems Biology: Pyruvate Kinase Isoform PKM2 Is a Metabolic Master Regulator. *Journal of Carcinogenesis* 12:14.

37. Asaka, M., T. Kimura, T. Meguro, M. Kato, M. Kudo, T. Miyazaki, and E. Alpert, 1994. Alteration of Aldolase Isozymes in Serum and Tissues of Patients with Cancer and Other Diseases. *Journal of Clinical Laboratory Analysis* 8:144–148.

38. Young, C. D., E. C. Nolte, A. Lewis, N. J. Serkova, and S. M. Anderson, 2008. Activated Akt1 Accelerates MMTV-c-ErbB2 Mammary Tumourigenesis in Mice without Activation of ErbB3. *Breast Cancer Research* 10:R70.

39. Klip, A., T. Tsakiridis, A. Marette, and P. A. Ortiz, 1994. Regulation of Expression of Glucose Transporters by Glucose: A Review of Studies in Vivo and in Cell Cultures. *The FASEB Journal* 8:43–53.

40. Celenza, J. L., L. Marshall-Carlson, and M. Carlson, 1988. The Yeast SNF3 Gene Encodes a Glucose Transporter Homologous to the Mammalian Protein. *Proceedings of the National Academy of Sciences of the United States of America* 85:2130–2134.

41. Haspel, H. C., D. C. Mynarcik, P. A. Ortiz, R. A. Honkanen, and M. G. Rosenfeld, 1991. Glucose Deprivation Induces the Selective Accumulation of Hexose Transporter Protein GLUT-1 in the Plasma Membrane of Normal Rat Kidney Cells. *Molecular Endocrinology* 5:61–72.

42. Haspel, H. C., E. W. Wilk, M. J. Birnbaum, S. W. Cushman, and O. M. Rosen, 1986. Glucose Deprivation and Hexose Transporter Polypeptides of Murine Fibroblasts. *Journal of Biological Chemistry* 261:6778–6789.

43. Takakura, Y., S. L. Kuentzel, T. J. Raub, A. Davies, S. A. Baldwin, and R. T. Borchardt, 1991. Hexose Uptake in Primary Cultures of Bovine Brain Microvessel Endothelial Cells. I. Basic Characteristics and Effects of D-Glucose and Insulin. *Biochimica et Biophysica Acta (BBA) - Biomembranes* 1070:1–10.

44. Boado, R. J., and W. M. Pardridge, 1993. Glucose Deprivation Causes Posttranscriptional Enhancement of Brain Capillary Endothelial Glucose Transporter Gene Expression via GLUT1 mRNA Stabilization. *Journal of Neurochemistry* 60:2290–2296.

45. Tordjman, K. M., K. A. Leingang, and M. Mueckler, 1990. Differential Regulation of the HepG2 and Adipocyte/Muscle Glucose Transporters in 3T3L1 Adipocytes. Effect of Chronic Glucose Deprivation. *Biochemical Journal* 271:201–207.

46. John, S. A., M. Ottolia, J. N. Weiss, and B. Ribalet, 2008. Dynamic Modulation of Intracellular Glucose Imaged in Single Cells Using a FRET-Based Glucose Nanosensor. *Pflügers Archiv - European Journal of Physiology* 456:307–322.

47. Macheda, M. L., S. Rogers, and J. D. Best, 2005. Molecular and Cellular Regulation of Glucose Transporter (GLUT) Proteins in Cancer. *Journal of Cellular Physiology* 202:654–662.

48. Jeon, S.-M., 2016. Regulation and Function of AMPK in Physiology and Diseases. *Experimental & Molecular Medicine* 48:e245.

49. Davies, S. P., S. A. Hawley, A. Woods, D. Carling, T. A. J. Haystead, and D. G. Hardie, 1994. Purification of the AMP-activated Protein Kinase on ATP-γ-Sepharose and Analysis of Its Subunit Structure. *European Journal of Biochemistry* 223:351–357.

50. Ruderman, N. B., X. J. Xu, L. Nelson, J. M. Cacicedo, A. K. Saha, F. Lan, and Y. Ido, 2010. AMPK and SIRT1: A Long-Standing Partnership? *American Journal of Physiology-Endocrinology and Metabolism* 298:E751–E760.

51. Vander Heiden, M. G., and R. J. DeBerardinis, 2017. Understanding the Intersections between Metabolism and Cancer Biology. *Cell* 168:657–669.

52. Galbo, T., R. J. Perry, E. Nishimura, V. T. Samuel, B. Quistorff, and G. I. Shulman, 2013. PP2A Inhibition Results in Hepatic Insulin Resistance despite Akt2 Activation. *Aging* 5:770–781.

53. Kabashima, T., T. Kawaguchi, B. E. Wadzinski, and K. Uyeda, 2003. Xylulose 5-Phosphate Mediates Glucose-Induced Lipogenesis by Xylulose 5-Phosphate-Activated Protein Phosphatase in Rat Liver. *Proceedings of the National Academy of Sciences of the United States of America* 100:5107–5112.

54. Barnes, K., J. C. Ingram, O. H. Porras, L. F. Barros, E. R. Hudson, L. G. D. Fryer, F. Foufelle, D. Carling, D. G. Hardie, and S. A. Baldwin, 2002. Activation of GLUT1 by Metabolic and Osmotic Stress: Potential Involvement of AMP-Activated Protein Kinase (AMPK). *Journal of Cell Science* 115:2433–2442.

55. Wu, N., B. Zheng, A. Shaywitz, Y. Dagon, C. Tower, G. Bellinger, C.-H. Shen, J. Wen, J. Asara, T. E. McGraw, B. B. Kahn, and L. C. Cantley, 2013. AMPK-Dependent Degradation of TXNIP upon Energy Stress Leads to Enhanced Glucose Uptake via GLUT1. *Molecular Cell* 49:1167–1175.

56. Xi, X., J. Han, and J.-Z. Zhang, 2001. Stimulation of Glucose Transport by AMP-Activated Protein Kinase via Activation of P38 Mitogen-Activated Protein Kinase. *Journal of Biological Chemistry* 276:41029–41034.

57. ter Kuile, B. H., and M. Cook, 1994. The Kinetics of Facilitated Diffusion Followed by Enzymatic Conversion of the Substrate. *Biochimica et Biophysica Acta (BBA) - Biomembranes* 1193:235–239.

58. Stein, W. D., and W. R. Lieb, 1986. Transport and Diffusion across Cell Membranes. Academic Press, San Diego, California.

59. Lee, M. G., and P. L. Pedersen, 2003. Glucose Metabolism in Cancer: Importance of Transcription Factor-DNA Interactions within a Short Segment of the Proximal Region Og the Type II Hexokinase Promoter. *Journal of Biological Chemistry* 278:41047–41058.

60. Mathupala, S. P., A. Rempel, and P. L. Pedersen, 1995. Glucose Catabolism in Cancer Cells. Isolation, Sequence, and Activity of the Promoter for Type II Hexokinase. *Journal of Biological Chemistry* 270:16918–16925.

61. Rempel, A., S. P. Mathupala, and P. L. Pedersen, 1996. Glucose Catabolism in Cancer Cells: Regulation of the Type II Hexokinase Promoter by Glucose and Cyclic AMP. *FEBS Letters* 385:233–237.

62. Drengstig, T., I. Jolma, X. Ni, K. Thorsen, X. Xu, and P. Ruoff, 2012. A Basic Set of Homeostatic Controller Motifs. *Biophysical Journal* 103:2000–2010.

63. Bustamante, E., and P. L. Pedersen, 1977. High Aerobic Glycolysis of Rat Hepatoma Cells in Culture: Role of Mitochondrial Hexokinase. *Proceedings of the National Academy of Sciences of the United States of America* 74:3735–3739.

Tveit et al.

64. Nakashima, R. A., M. G. Paggi, L. J. Scott, and P. L. Pedersen, 1988. Purification and Characterization of a Bindable Form of Mitochondrial Bound Hexokinase from the Highly Glycolytic AS-30D Rat Hepatoma Cell Line. *Cancer Research* 48:913–919.

65. Marín-Hernández, A., S. Rodríguez-Enríquez, P. A. Vital-González, F. L. Flores-Rodríguez, M. Macías-Silva, M. Sosa-Garrocho, and R. Moreno-Sánchez, 2006. Determining and Understanding the Control of Glycolysis in Fast-Growth Tumor Cells. Flux Control by an over-Expressed but Strongly Product-Inhibited Hexokinase. *The FEBS Journal* 273:1975–1988.

66. Petryszak, R., M. Keays, Y. A. Tang, N. A. Fonseca, E. Barrera, T. Burdett, A. Füllgrabe, A. M.-P. Fuentes, S. Jupp, S. Koskinen, O. Mannion, L. Huerta, K. Megy, C. Snow, E. Williams, M. Barzine, E. Hastings, H. Weisser, J. Wright, P. Jaiswal, W. Huber, J. Choudhary, H. E. Parkinson, and A. Brazma, 2016. Expression Atlas Update—an Integrated Database of Gene and Protein Expression in Humans, Animals and Plants. *Nucleic Acids Research* 44:D746–D752.

67. Shampine, L. F., and M. W. Reichelt, 1997. The MATLAB ODE Suite. *SIAM Journal on Scientific Computing* 18:1–22.

68. Wyatt, E., R. Wu, W. Rabeh, H.-W. Park, M. Ghanefar, and H. Ardehali, 2010. Regulation and Cytoprotective Role of Hexokinase III. *PLoS ONE* 5:e13823.

69. Cornish-Bowden, A., 2012. Fundamentals of Enzyme Kinetics. Wiley-Blackwell, Weinheim, Germany, 4 edition.

70. Keener, J., and J. Sneyd, 2009. Mathematical Physiology I: Cellular Physiology, volume 8/1 of *Interdisciplinary Applied Mathematics*. Springer, New York, NY, 2 edition.

71. Stadtman, E. R., 1963. Symptosium on Multiple Forms of Enzymes and Control Mechanisms. II. Enzyme Multiplicity and Function in the Regulation of Divergent Metabolic Pathways. *Bacteriological Reviews* 27:170–181.

72. Cohen, G. N., 1965. Regulation of Enzyme Activity in Microorganisms. *Annual Review of Microbiology* 19:105–126.

73. Ang, J., and D. R. McMillen, 2013. Physical Constraints on Biological Integral Control Design for Homeostasis and Sensory Adaptation. *Biophysical Journal* 104:505–515.

74. Ang, J., S. Bagh, B. P. Ingalls, and D. R. McMillen, 2010. Considerations for Using Integral Feedback Control to Construct a Perfectly Adapting Synthetic Gene Network. *Journal of Theoretical Biology* 266:723–738.

75. Aoki, S. K., G. Lillacci, A. Gupta, A. Baumschlager, D. Schweingruber, and M. Khammash, 2019. A Universal Biomolecular Integral Feedback Controller for Robust Perfect Adaptation. *Nature* 570:533–537.

76. Khalil, H. K., 2002. Nonlinear Systems. Prentice Hall, Upper Saddle River, New Jersey, 3 edition.

77. Briat, C., A. Gupta, and M. Khammash, 2016. Antithetic Integral Feedback Ensures Robust Perfect Adaptation in Noisy Biomolecular Networks. *Cell Systems* 2:15–26.

78. Drengstig, T., X. Y. Ni, K. Thorsen, I. W. Jolma, and P. Ruoff, 2012. Robust Adaptation and Homeostasis by Autocatalysis. *The Journal of Physical Chemistry B* 116:5355–5363.

79. Tveit, D. M., and K. Thorsen, 2017. Passivity-Based Analysis of Biochemical Networks Displaying Homeostasis. *In* Proceedings of the 58th Conference on Simulation and Modelling (SIMS 58) Reykjavik, Iceland, September 25th – 27th, 2017. Linköping University Electronic Press, Linköpings universitet, Reykjavik, Iceland, Linköping Electronic Conference Proceedings, 108–113.

80. John, S., J. N. Weiss, and B. Ribalet, 2011. Subcellular Localization of Hexokinases I and II Directs the Metabolic Fate of Glucose. *PLoS ONE* 6:e17674.

81. Cannon, W. B., 1929. Organization for Physiological Homeostasis. *Physiological Reviews* 9:399–431.

82. Mrosovsky, N., 1990. Rheostasis: The Physiology of Change. Oxford University Press, New York.

83. Risvoll, G. B., K. Thorsen, P. Ruoff, and T. Drengstig, 2017. Variable Setpoint as a Relaxing Component in Physiological Control. *Physiological Reports* 5:e13408.

Paper 3:
Using UK5099 and galloflavin to examine glutamine metabolism through sequential inhibition in a real time setting

Using UK5099 and galloflavin to examine glutamine metabolism through sequential inhibition in a real time setting

Gunhild Fjeld[a], Oddmund Nordgård[b,a], Kristian Thorsen[c]

[a]Dep. of Chemistry, Bioscience and Environmental Engineering, University of Stavanger, Stavanger, Norway
[b]Dep. of Hematology and Oncology, Stavanger University Hospital
[c]Dep. of Electrical Engineering and Computer Science, University of Stavanger, Stavanger, Norway

Abstract

Background

The metabolism of cancer cells is typically arranged to maximize growth. Although glucose is often considered the main energy and carbon source, there is an increasing interest for understanding how cancer cells utilize glutamine as an alternative fuel and why some cancer cells even seem to be addicted to glutamine in order to proliferate. Glutaminolysis branches into three possible paths at the tricarboxylic acid (TCA) cycle intermediate malate, and the different branches have different implications for the cell in relation to redox balance, oxygen consumption, energy (ATP) production, extracellular acidification, and availability of growth precursors. The aim of this study was to evaluate our two new protocols by investigating how two cancer cell lines that differ in growth and metabolism, utilize these three paths.

Methods

In this study we used real time measurements of oxygen consumption and extracellular acidification by a Seahorse XFp analyzer to investigate the metabolic flux in the different branches of glutaminolysis. We used inhibitors, that targets specific enzymes or transporters, in a sequential order. In our protocols we used UK5099 and galloflavin as novel inhibitors, together with inhibitors that were already common in Seahorse XFp studies. The new protocols were evaluated in the two colon cancer cell lines Caco2 and HCT116.

Results

The new inhibitors UK5099 and galloflavin were shown to extend the information obtained from Seahorse experiments with regard to glutamine metabolism in cancer cell lines. Caco2 used less glucose and glutamine overall and metabolized glutamine via the cytosolic malic enzyme (ME1) branch to eventually produce lactate. HCT116 on the other hand, used glutamine primarily through the full TCA cycle via the mitochondrial malic enzyme (ME2) branch.

Conclusions

This study shows how UK5099 and galloflavin can be used as sequential inhibitors to decipher how glutamine is metabolized through real time measurements of oxygen consumption and extracellular acidification using a Seahorse XFp analyzer. Glutamine is metabolized differently in the two cell lines we tested, and a differentiation between the use of ME1 and ME2 was found.

Keywords: cancer glutamine metabolism UK5099 Galloflavin Caco2 HCT116 Seahorse XFp ME1 ME2

Introduction

Metabolic flexibility and adaptability vary between cell types, but generally, cancer cells seem to be more flexible than normal cells and adapt better to changing environ-
5 ments Herst and Berridge (2013); Lanning et al. (2017). Although glucose is the main cellular energy and carbon source, there is an increasing interest in the way cancer cells utilize glutamine as an alternative fuel. Glutamine has the advantage of also being a nitrogen source, and is

10 thus a highly flexible metabolite. Some cancer cells also seem to be addicted to glutamine in order to proliferate Wise and Thompson (2010).

Glutamine is the most abundant free amino acid in muscles and plasma, and it is one of the most flexible ones,
15 serving many different functions Driskell (2007). Glutamine is also a normal media component, in addition to glucose, as it is known to ensure normal growth for most cells, especially cancer cells Yang and Xiong (2012); Zhang et al. (2017). Metabolism of glutamine starts with glu-

tamine being transported in to the cell. Glutamine can then enter the mitochondria, where it in the inner membrane is converted to glutamate by glutaminase Scalise et al. (2017); Matés et al. (2019), see fig. 2. Glutamate in turn, can be converted to the TCA cycle intermediate α-ketoglutarate (α-KG) by glutamate dehydrogenase (GDH). The latter step can also be fulfilled by a transaminase; either the glutamate pyruvate transaminases (GPTs, that is, alanine aminotransferases) or the glutamate oxaloacetate transaminases (GOTs, that is, aspartate aminotransferase) Vroon and Israili (1990). The difference here is whether or not there is pyruvate or oxaloacetate in surplus in the mitochondria to also produce the amino acids alanine and aspartate, respectively.

Figure 1: Anaplerosis by glutamine. Glutamine catabolism by glutaminase (Gase) to produce glutamate and ammonium. The subsequent deamination of glutamate by glutamate dehydrogenase (GDH) releases a second ammonium to yield the TCA cycle intermediate α-ketoglutarate. The process also generates one NADH. The reactions are reversible, with GDH and Glutamine Synthetase (GS) working in the opposite direction, consuming one NADH, two ammoniums and one ATP.

α-KG can either be converted to citrate, or continue along the cycle through conversion to succinate and fumerate to produce malate, see fig. 2. From malate there are three possible paths, each with a different outcome, either:

- continuation along the TCA cycle (path 6 in fig. 2)

- conversion of malate into cytosolic pyruvate by cytosolic malic enzyme (ME1) (path 7a in fig. 2)

- conversion of malate into mitochondrial pyruvate by the mitochondrial malic enzyme (ME2) (path 7b in fig. 2)

In addition to ME1 and ME2, there also exists a third malic enzyme that converts malate to pyruvate called ME3. ME3 is also mitochondrial, and is thought to have a redundant role supporting ME2 if ME2 is blocked or nonfunctional Dey et al. (2017).

These three different metabolic pathways have different implications for the cell. Path 6 is used to anaplerotically supply the TCA cycle with a carbon source. Cytosolic pyruvate from path 7a can be used in the mitochondria if it re-enters via the mitochondrial pyruvate carrier (MPC), or it can be fermented to lactate by lactate dehydrogenase (LDH). The latter is more common in cancer cells Wehrle et al. (2000); Murai et al. (2017). Mitochondrial pyruvate from path 7b can be brought back into the

TCA cycle through intramitochondrial recycling, making 7b a pathway that generates acetyl-CoA from glutamine-derived pyruvate. This again makes it possible for a cell to keep the TCA cycle going without the need for glycolytic pyruvate. The two different malic enzyme paths leading from the TCA cycle intermediate malate (7a and 7b) have not been extensively compared, despite indicating differences in metabolic requirements. Path 7a, using ME1, leads to the formation of NAD(P)H in the cytosol, which is important for redox balance and lipid synthesis, as well as the PPP, in the cytosol Nakashima et al. (2018). Path 7b, using ME2, leads to the formation of NAD(P)H in the mitochondria, which affects the mitochondrial redox balance and enables more production of ATP Ren et al. (2014); Sarfraz et al. (2018). The ME2 pathway also helps removing reactive oxygen species in the mitochondria Chang et al. (2015).

Figure 2: Glutamine metabolism. Glutamine is catabolized by glutaminase (1) into glutamate which again is turned into α-ketoglutarate, an intermediate of the TCA cycle, by glutamate dehydrogenase (2). Glutamine-derived α-ketoglutarate can either follow the whole TCA cycle (3-6), or break off from malate to be turned into pyruvate. The conversion of malate to pyruvate can happen either through transport of malate to the cytosol and conversion to cytosolic pyruvate by the cytosolic malic enzyme (ME1), through path 7a; or through the mitochondrial malic enzyme (ME2) to produce mitochondrial pyruvate, through path 7b.

In this work we present a method to examine how different cancer cells divert their glutamine metabolism through these pathways by using real time measurements of oxygen consumption and extracellular acidification from a Seahorse XFp metabolic flux analyzer (Agilent Technologies, USA). The Seahorse XFp metabolic flux analyzer is an instrument that has recently become popular in laboratories studying cancer metabolism, as well as others studying metabolism in relation to neurodegenerative diseases Teves et al. (2018); Zhang et al. (2015) or diabetes Hartman et al. (2014); Andersen et al. (2017). It mea-
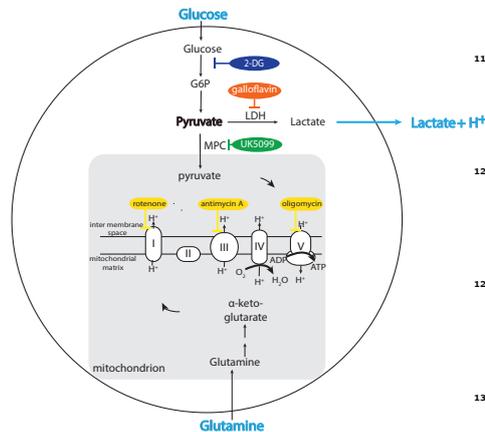
2

Figure 3: Simplified structure of glycolysis and TCA cycle with the metabolic inhibitors used in the Seahorse-experiments. 2-Deoxy Glucose (2-DG) in blue inhibiting the first step of glycolysis, Galloflavin in orange inhibiting lactate dehydrogenase (LDH), UK5099 in green inhibiting the monocarboxylate carrier (MPC) of pyruvate into the mitochondrion, Oligomycin, Rotenone, Antimycin A all in yellow, inhibiting complexes in the electron transport chain given at their respectful sites of action. Key extracellular metabolites given in blue (glucose, glutamine and lactate).

sures the extracellular acidification rate (ECAR) caused by lactate secretion, as one proton is secreted along with one lactate molecule. At the same time, it also measures the oxygen consumption rate (OCR) as the mitochondria uses oxygen to complete the TCA cycle. Thus, ECAR is a proxy for lactate secretion, and OCR a proxy for TCA cycle activity.

By utilizing the inhibitor of the first step of glycolysis, 2-DeoxyGlucose (2-DG), in combination with the LDH-inhibitor galloflavin (GF), we are able to determine glutamine's contribution to lactate production, following path 7a (fig. 2). This is because when we first block pyruvate originating from glucose with 2-DG, the lactate that is now secreted originates from either background acidification or glutamine acidification. By subsequently blocking LDH by galloflavin, one can subtract the measurement after adding galloflavin from the measurement prior to the addition, leaving the ECAR measure as the lactate secretion rate caused by glutamine alone.

When glutamine is added to a glutamine free media, we study the basic utilization to find out how much extracellular glutamine is used to increase OCR and ECAR (path 6 + path 7b).

Next we look at path 7b (fig 2) by using the MPC inhibitor UK5099. When the blockage of MPC by UK5099 is directly followed by a mixture of electron transport chain (ETC) inhibitors (rotenone, antimycin A, and oligomycin),

the difference in OCR after the UK5099 addition and ETC inhibitors is a measure for the activity of path 7b. The assumption here is that when no glycolytic pyruvate can enter the mitochondria after UK5099 has blocked MPC, the TCA cycle is kept going by acetyl-CoA from glutamine derived pyruvate via path 7b. The sites of action of the inhibitors are shown in fig. 3.

Galloflavin and UK5099 have not been used in these types of real time experiments before. Their function however, is known. Galloflavin inhibits both isoforms of LDH Manerba et al. (2012), effectively blocking lactate from being produced. Galloflavin, as far as we know, has never been used in a Seahorse XFp setting. UK5099 inhibits MPC by specifically modifying a thiol group on the carrier Hildyard et al. (2005). UK5099 has only been tested once as an acute injectant before in Agilent's own mito fuel flex kit Agilent (2019). In this kit however, UK5099 was only used in combination with etomoxir, thus, not allowing to see the effect of UK5099 by itself.

The goal of this study is to take advantage of the flexible system of the Seahorse XFp analyzer to study glutaminolytic fluxes. A Seahorse XFp analyzer allows for real-time OCR and ECAR measurements during sequential additions of metabolites and drugs to cells. By sequentially adding drugs or metabolites, one can eliminate specific pathways within the cells, and calculate the flux through isolated pathways.

Methods

Seahorse protocols for determination of glutaminolytic fluxes

To look at the different glutamine fluxes contribution to the Seahorse measurements of extracellular acidification rate (ECAR) and oxygen consumption rate (OCR), we have made two protocols that we have called *Basic inhibition protocol* and *Extended inhibition protocol*. The concentrations of the new inhibitors, galloflavin and UK5099 were titrated, to find concentrations that produce the expected effect without giving off-target effects (see fig 8 and fig 9 in the SI).

Basic inhibition protocol

The basic inhibition protocol was set up to examine the cell's natural metabolism of glutamine and glucose. This was done by having the cells start off in a media without glutamine or glucose. Then, sequential additions of glutamine, glucose, 2-DeoxyGlucose (2-DG) and galloflavin at concentrations and timepoints as shown in table 1 were performed.

ECAR assessment of the basic inhibition protocol

The measured ECAR before any additions is the non-glycolytic non-glutaminolytic acidification rate, which can be divided into acidification due to lactate from non-glycolytic and non-glutaminolytic sources (orange color in fig. 4A)

3

and background acidification not related to lactate secretion (light blue color in fig. 4A). The first addition is glutamine and the following increase in ECAR corresponded to lactate production from glutamine (dark blue color in fig. 4A). The second addition is glucose and the cells now have both glutamine and glucose available. ECAR measured after this addition corresponds to lactate production from glucose and glutamine (grey color in fig. 4A), plus the non-glycolytic non-glutaminolytic acidification rate that was measured at the start before any additions. 2-DG blocks glycolysis and is the third addition in this protocol. The measured ECAR will now again come from lactate production from glutamine, in addition to the non-glycolytic non-glutaminolytic acidification rate. Note that ideally, the ECAR measured after this third step should be approximately equal to the ECAR measured after the first step since it is the same sources that contribute. However, there may be metabolic effects that hinders the cells to switch from one nutrient source to another and back again, i.e., they may not end up in the same metabolic state as before after temporary exposure to a new nutrient source. The final addition is galloflavin which blocks LDH and thus also blocks any remaining production of lactate. After this addition we can identify the background (non-lactic) acidification as the remaining measured ECAR (light blue color in fig. 4A).

OCR assessment of the basic inhibition protocol

How the measured OCR during the same experiment is related to contributions from different metabolic sources is illustrated in fig. 4B and explained in the following. The measured OCR at the start before any additions is the basal oxidative metabolism (light blue color in fig. 4B). The increase in OCR after the first addition, of glutamine, is caused by oxidation of glutamine (green color in fig. 4B). Glucose is the second addition and the measured OCR after this addition is the basal oxidation plus oxidation of glucose and glutamine (grey color in fig. 4B). Note that the measured oxidation of glucose and glutamine may be less than the measured oxidation of glutamine alone in the previous step. This may seem counter intuitive but can be explained when the corresponding change in ECAR is taken into account. The addition of glucose enables the cells to produce ATP anaerobically from glycolysis, reducing the need for oxidative metabolism. The third addition is 2-DG that blocks glycolysis. The measured OCR is then again caused only by the oxidation of glutamine and the basal oxidation. As mentioned in the explanation of the ECAR measurements there may be a discrepancy between the OCR measured before the cell has been exposed to glucose and the OCR measured after glucose absorption has been blocked. The final addition of galloflavin blocks LDH and stops the production of lactate; it should not have a direct effect on the OCR. Nevertheless, some effects may be observed in the OCR measurements and these may be attributed to metabolic rebalancing or off-target effects of galloflavin. This is further considered in the Results and

Discussion sections. The contribution of glutamine to path 6 + 7b can be estimated as the difference given in equation 1 below,

$$\text{Total Gln ox.} = OCR_{+Gln} - OCR_{start} \qquad (1)$$

where OCR_{+Gln} is the measured OCR after the addition of glutamine and OCR_{start} is the measured OCR prior to the addition of glutamine.

Extended inhibition protocol

The extended inhibition protocol was made to assess the use of glutamine through path 7a or 7b. In this protocol, the cells start out in a media containing both glutamine and glucose. The protocol was set up with sequential addition 2-DG, galloflavin, UK5099, and a mixture of rotenone, antimycin A and oligomycin at concentrations and timepoints as shown in table 2.

ECAR assessment of the extended inhibition protocol

How the different metabolic sources contribute to ECAR during the experiment is explained in the following and illustrated in fig. 5A. The measured ECAR before any additions is the total acidification rate. This is the combination of acidification from glucose and glutamine derived lactate (grey color in fig. 5A), and lactate acidification stemming from non-glycolytic non-glutaminolytic sources (orange color in fig. 5A); and it corresponds to the ECAR after the second addition in the metabolic availability protocol. The first addition is 2-DG that blocks glycolysis. The measured ECAR after this addition is the sum from lactate production from glutamine (dark blue color in fig. 5A), lactate production from non-glycolytic non-glutaminolytic sources, and the background (non-lactic) acidification. The second addition is galloflavin which blocks LDH and thus also blocks all production of lactate. It is after this addition that we can identify the background (non-lactic) acidification as the remaining measured ECAR. The ECAR measurements after the third addition of UK5099 is not used for estimation of metabolic fluxes. The fourth and final addition of the rotenone, antimycin A and oligomycin mixture does also not have any interpretation related to the measured ECAR. The contribution of glutamine to path 7a can be estimated as the difference given in the equation 2 below,

$$\text{ME1 Gln ferm.} = ECAR_{+2DG} - ECAR_{+GF} \qquad (2)$$

where $ECAR_{+2DG}$ is the measured ECAR after the addition of 2-DG and $ECAR_{+GF}$ is the measured ECAR after the addition of galloflavin.

OCR assessment of the extended inhibition protocol

How the measured OCR during the same experiment is related to contributions from different metabolic sources is illustrated in fig. 5B and explained in the following. The

4

Step	Compound	[Port]	[Well]	Vol well
0. t=0 min	-	-	-	180 μL
1. t=24 min	Glutamine	0, 16.4, 32.8 mM	0, 2, 4 mM	205 μL
2. t=42 min	Glucose	80 mM	10 mM	230 μL
3. t=66 min	2-DG	1 M	100 mM	255 μL
4. t=84 min	Galloflavin	1.1 mM	100 μM	280 μL

Table 1: Basic inhibition protocol using the LDH inhibitor galloflavin to assess glutamine's contribution to ECAR and OCR using different concentrations of glutamine (0, 2 or 4 mM Gln). The cells start out in a media without glutamine and glucose in the experiment, but have been pregrown in high glucose (HG, 25 mM) and 2 mM glutamine. Each step marks the addition of a metabolite or inhibitor at the given timepoint. All ports are filled with 25 μL, and each new addition increases the well volume respectively.
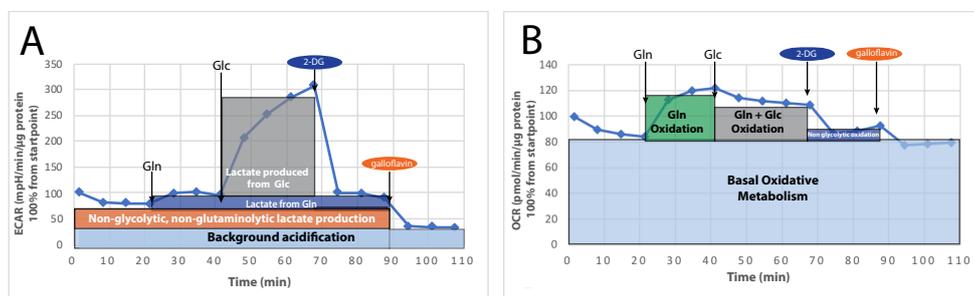
Figure 4: Example experiment using the basic inhibition protocol. **A** ECAR (mpH/min in % from basal), and **B** OCR (pmol/min in % from basal). Time of injections of metabolites and inhibitors indicated on top, and each matching contribution given in colored boxes. This contribution will vary from HCT116 and Caco2, and between the 0, 2 or 4 mM Gln wells. Calculations between the difference of each step is calculated using the two last measurement points. Note that the heights of the bars are based on an example set of measurement data. Actual height may vary depending on cell type. Some cell types may show a different type of response after the addition of a nutrient/inhibitor than what is shown here.

measured OCR at the start before any additions is the total TCA cycle and electron transport chain (ETC) related oxidative metabolism, plus oxygen consumption not related with TCA-ETC (light blue color in fig. 5B). The first addition is 2-DG that blocks glycolysis. The change in OCR after this addition depends on how much the cells rely on glucose to fuel the TCA cycle, and on how able they are to adapt by using other nutrients to drive the TCA cycle. The OCR measured after this addition will consist of a non-glycolytic TCA-ETC oxidation rate (dark blue color in fig. 5B) in addition to the non-TCA-ETC related oxidation rate. The addition of galloflavin as the second inhibitor should not have any direct effect on the OCR as it only blocks lactate production (LDH). However, there may be indirect effects that results in a change in OCR. The third addition of UK5099 blocks mitochondrial pyruvate carrier and shuts off the supply of pyruvate from the cytosol. The fourth addition of rotenone, antimycin A, and oligomycin inhibits the electron transport chain and the mitochondrial ATP production, leaving only the non-TCA-ETC oxidation (light blue color in fig. 5B) left in the OCR measurements. The use of UK5099 together with the consecutive addition of electron transport chain

blockers makes it possible to estimate the contribution of glutamine to the TCA cycle through path 7a and 7b from fig. 2. The difference between the OCR measured after the addition of UK5099 and the OCR measured after the addition of the electron transport chain inhibitors is an estimate of the intramitochondrial contribution of glutamine to the TCA cycle through path 7b and can be estimated as the difference given in equation 3 below,

$$\text{ME2 Gln ox.} = OCR_{+UK5099} - OCR_{+Rot,Ant,Oli} \quad (3)$$

where $OCR_{+UK5099}$ is the measured OCR after the addition of UK5099 and $OCR_{+Rot,Ant,Oli}$ is the measured OCR after the addition of the rotenone, antimycin A and oligmycin mixture. In addition the difference between the OCR after the addition of 2-DG and after the addition of UK5099 can be an estimate of glutamine's contribution to the TCA cycle via cytosolic pyruvate and path 7a.

Cell line culturing

Caco2 and HCT116 cells were grown in DMEM without glutamine or glucose (Corning), with addition of 10% FBS (Biowest) and 5% PenStrep (Biowest). Glucose and

Step	Compound	[Port]	[Well]	Vol well
0. t=0 min	-	-	-	180 μL
1. t=18 min	2-DG	1 M	100 mM	205 μL
2. t=48 min	Galloflavin	1 mM	100 μM	230 μL
3. t=66 min	UK5099	2 mM	200 μM	255 μL
4. t=84 min	Rotenone	10 μM	1 μM	280 μL
	Antimycin A	10 μM	1 μM	
	Oligomycin	30 μM	3 μM	

Table 2: Extended inhibition protocol using the MPC inhibitor UK5099 and the LDH inhibitor galloflavin to assess glutamine's contribution to ECAR and OCR. Cells are pregrown in low glucose (LG, 5 mM) or high glucose (HG, 25 mM), and the starting media in the experiments contains the same concentration of glucose as the cells have been pregrown in. Each step marks the addition of a metabolite or inhibitor, at the given timepoint. All ports are filled with 25 μL, and each new addition increases the well volume respectively.
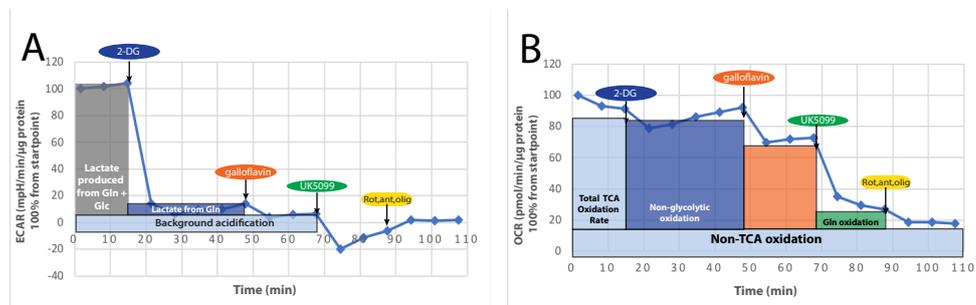

Figure 5: Example experiment using the extended inhibition protocol. **A** ECAR (mpH/min in % from basal), and **B** OCR (pmol/min in % from basal). Time of injections of inhibitors indicated on top, and each matching contribution given in colored boxes. This contribution will vary from HCT116 and Caco2, and possibly low glucose (LG) and high glucose (HG) as well. Calculations between the difference of each step is calculated using the two last measurement points. Note that the heights of the bars are based on an example set of measurement data. Actual height may vary depending on cell type. Some cell types may show a different type of response after the addition of a nutrient/inhibitor than what is shown here.

glutamine were added fresh, with 25 mM glucose and 2 mM L-glutamine used for the normal growth media. Once 70% confluent, cells were split and seeded for experiments.

Preperations of cells for Seahorse experiments

Cells were seeded in Seahorse 8 well cartridges to be used in the Seahorse XFp Metabolic Flux Analyzer (Agilent Technologies, USA). Caco2 cells were seeded at 15 000 cells per well in 80 μL of media and HCT116 cells were seeded at 10 000 cells per well in 80 μL media. The difference in seeding density was to ensure that the measurements were within the linear range of the device in OCR readings, and to ensure a sufficient confluency for the monolayer that was measured. The wells were coated with collagen 24 hours prior to seeding, to assure better attachment. The cells were typically grown in low glucose (LG, 5 mM) media or high glucose (HG, 25 mM) media with 2 mM Gln in the cartridge wells for 24 hours prior to experiments. The medium was exchanged 1 hour before the experiment to 180 μL of a serum-free Seahorse base medium. Glutamine and glucose were added to the Sea-

horse base medium according to the protocols, and the pH was adjusted to 7.4 using NaOH.

Determination of protein content

The cells in the Seahorse well-plates were abruptly frozen in a -80°C freezer. The plates were subsequently exposed to one more freeze-thaw cycle to ensure lysis. Protein content was measured using the Pierce BCA Protein Assay Kit (ThermoFisher, USA) in a microplate setting, directly into the Seahorse-well plates. A Spectromax plate reader was used to read this colorimetric assay at A562nm, using two set of standards for each run.

Units and normalization of ECAR and OCR measurements

The protein measurements from each well was used to normalize ECAR and OCR values. Then, the first datapoint from each measurement series was set to 100 % to ease the comparison between the cell lines, and percentage wise contribution of each inhibitor. The two last datapoints in each measure were used to calculate the effect of the inhibitors in percentage, working in duplets for

the basic inhibition protocol (two 0 mM Gln wells, two 2 mM Gln wells and two 4 mM Gln wells), and triplicates for the extended inhibition protocol (three LG wells and three HG wells).

Statistics

Statistical tests were performed using IBM SPSS statistical software (version 25); an unpaired sample t-test was used to assess the statistical significance of differences between the two cell lines, whereas a paired sample t-test was performed to test the significance of the effect of each inhibitor or metabolite within each run under each condition. The two last data points after each addition was used, resulting in n = 4 for the basic inhibition protocol, and n = 6 for the extended inhibition protocol. All parameters were tested for normality using normality plots and Kolmogorov-Smirnov tests with p > 0.05. Significance was reported when p < 0.05.

Results

Basic inhibition protocol gives the total use of glutamine in the TCA cycle (path 6 + 7b)

The glutamine addition only increased the ECAR for the 2 mM Gln wells of HCT116 (fig. 6A), and actually decreased the ECAR for the 2 mM and 4 mM Gln wells for Caco2 (fig. 6C). Glutamine increased the OCR for HCT116 (fig. 6B), and the effect is clearly different compared to the cells that got no glutamine added (0 mM) which had a continued decline in OCR for both HCT116 and Caco2 cells (fig. 6B and fig. 6D). It does however not seem to be a difference between 2 or 4 mM Gln wells.

For Caco2 cells there seemed to be only a slight (but significant) increase in OCR when glutamine was added to Caco2 (fig. 6D). The increase in OCR after addition of glutamine is significantly different between the two cell lines, indicating that Caco2 does not oxidize as much glutamine in the mitochondria as HCT116.

This *Gln oxidation* is the oxidation of glutamine via both path 6 and 7b in the mitochondria. Calculations of the total glutamine oxidation is calculated using equation 1 and the results are given in table 3.

The glucose addition yielded close to a 3-fold increase in ECAR for all wells for HCT116 (fig. 6A), whereas Caco2 had a much higher increase for the 0mM Gln wells than the 2 mM or 4 mM wells (fig. 6C). The dynamics were also different, as HCT116 had a much more rapid response in ECAR for the 0 mM Gln well (fig. 6A) compared to the 2 mM Gln and 4 mM wells. The rise in ECAR for Caco2, however, seemed to follow a more similar dynamics for all concentrations of glutamine, but with 0 mM giving the highest ECAR reading, followed by 2 mM Gln, and finally 4 mM Gln (fig. 6C). The glucose addition made OCR drop for all wells, though not significantly for the 4 mM Gln of HCT116 (fig. 6B and fig. 6D). This drop coincided with a compensatory increase in ECAR.

Once the glucose-induced ECAR was blocked by 2-DG, we were left with acidification from non-glycolytic sources and background acidification. This inhibition by 2-DG efficiently decreased ECAR for HCT116 (fig. 6A), and had a slower, but similar response in ECAR for Caco2 (fig. 6C). The inhibition also decreased OCR for the 2 and 4 mM Gln wells in both HCT116 and Caco2 (fig. 6B and fig. 6D), as it also blocked the glucose supply to the TCA cycle (dark blue in fig. 4B). 2-DG did not lower the OCR for the 0 mM Gln wells of HCT116, but slightly lowered the OCR for the 0 mM Gln wells of Caco2.

By subsequently adding galloflavin after 2-DG inhibition, we can isolate the background acidification. After the blockage of LDH by galloflavin, ECAR dropped to around 30% for HCT116 and around 18% for Caco2. The reduction in ECAR from the 2-DG addition to the galloflavin addition resulted in an ECAR reading lower than the first measure from before the additions of glutamine. Finally, the addition of galloflavin lowered all the wells' OCR (fig. 6B and fig. 6D).

Extended inhibition protocol reveals the difference in path 7a and 7b

2-DG lowered the ECAR of HCT116 to an average of 10 % (fig 7A), which is a significantly larger reduction than an average of 32 % for Caco2 (fig 7C). The basal starting ECAR is however much higher for HCT116 (3.85 pmol/min/μg protein) than for Caco2 (2.52 pmol/min/μg protein), see Supplementary Information. This leaves a relatively higher acidification rate for Caco2 than HCT116. 2-DG also lowered the OCR (fig 7B and 7D) to around 80% for Caco2 and 90% for HCT116, meaning that the glycolysis that was blocked upstream, also affected the pyruvate availability downstream for oxidative phosphorylation. The decrease in OCR was significant for all measurement series, except for the HG HCT116 wells.

Galloflavin was added after 2-DG using the same rational as before. Glutamine's contribution to ECAR should be similar to the inhibition of glucose's contribution to ECAR is found from the difference in ECAR measured before and after the inhibition of LDH by galloflavin (path 7a in figure 2). The contribution of amino acids to ECAR, with glutamine being the most predominant as it has the highest concentration, is path 7a. Our results show that Caco2 (fig 7C) is more affected than HCT116 (fig 7A) by the addition of galloflavin. Calculations on ME1's glutamine fermentation through path 7a is calculated using equation 2 and the results are given in table 4.

Next, UK5099 was added, so that no cytosolic pyruvate can enter the mitochondria through the MPC. Most importantly, UK5099 is added after 2-DG so that acetyl-CoA now needs to come from glutamine through path 7b alone. The OCR for HCT116 and Caco2 was significantly blocked by UK5099 (fig 7B and fig 7D, respectively). Also, ECAR dropped significantly in fig 7A and 7C after the UK5099 addition.
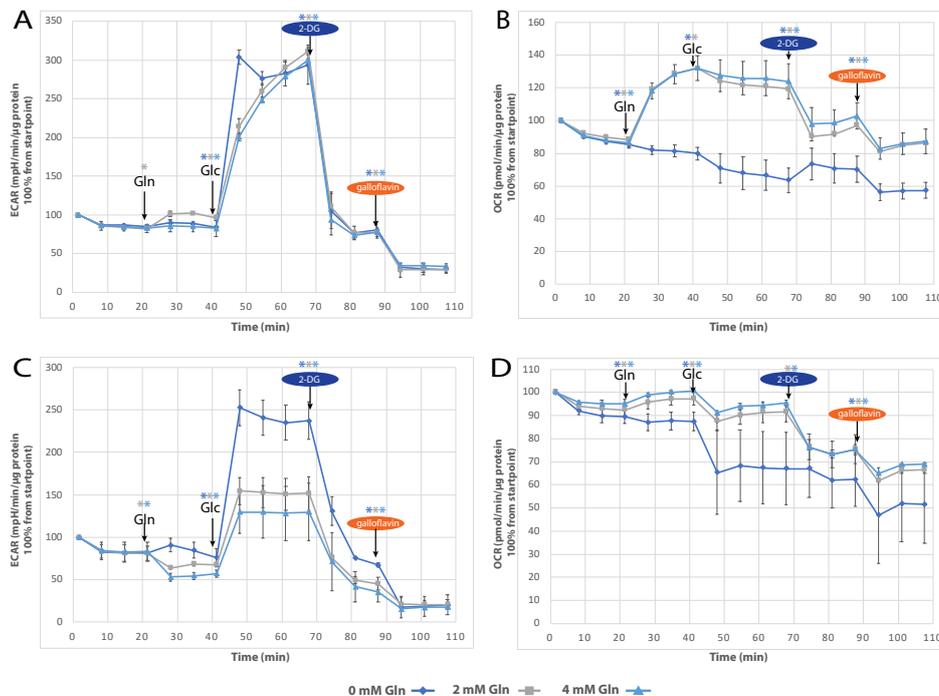
7

Figure 6: **A** ECAR HCT116 (mpH/min/μg protein in % from startpoint), **B** OCR HCT116(pmol/min/μg protein in % from startpoint), **C** ECAR Caco2 (mpH/min/μg protein in % from startpoint), **D** OCR Caco2 (pmol/min/μg protein in % from startpoint). Measurements from 10 000 HCT116 cells per well and 15 000 Caco2 cells per well, using the basic inhibition protocol, in duplicates. Additions are 0, 2 or 4 mM glutamine (Gln) (t = 24 min) as indicated by each group, followed by 10 mM glucose (Glc) (t = 42 min), 2-deoxyglucose (2-DG) (t = 66 min) and the LDH inhibitor galloflavin (t = 84 min). Significant changes between the two last datapoints from before and after each addition are marked by * of the respectful color between the 0 mM Gln, 2 mM Gln and 4 mM Gln wells.

Finally, by adding the electron transport chain inhibitors Rotenone, Antimycin A and Oligomycin (see fig 3 for target sites), we can infer glutamine's contribution to just path 7b in figure 2. This is because UK5099 already blocked MPC, making glutamine the sole contributor to the TCA cycle's carbon fuel (green color in fig 5B). Again, the calculations were done on the last two data points after the injection of UK5099 (t = 84 min) minus Rot, Ant, Oligo's two last data points (t = 108 min). Calculations on ME2's glutamine oxidation through path 7b is calculated using equation 3 and the results are given in table 5.

Discussion

In this study, we have developed two new protocols to assess glutamine's metabolism through three different pathways. For this, we have used the mitochondrial pyruvate carrier (MPC) inhibitor UK5099, and the LDH inhibitor galloflavin as acute injectants in Seahorse XFp metabolic flux analyzer to assess glutamine's and glucose's contributions to OCR and ECAR. Using the new inhibitors in this setting, we found that the more aggressive cancer cell line, HCT116 Zhuang et al. (2016), primarily metabolized glutamine to fuel the TCA cycle through path 6 and 7b, whereas the more differentiated cell line, Caco2 Zhuang et al. (2016), primarily secreted excess glutamine as lactate through path 7a.

UK5099 has been used in previous studies, but with other concentrations and experimental setting than those used in this study. We found that UK5099 had a large and significant impact on OCR for both HCT116 and Caco2. The relative decrease in OCR were similar for the two cell lines. Although previous use of UK5099 has been with

8

Condition	OCR$_{+Gln}$ %	OCR$_{start}$ %	Tot Gln ox. %	Tot Gln ox/OCR$_{start}$	Tot Gln ox/OCR$_{+Gln}$
HCT116, 2 mM Gln	130.22 ± 10.82	89.20 ± 4.93	41.03 ± 6.38	46.0 ± 10.3	31.5 ± 8.2
HCT116, 4 mM Gln	130.25 ± 5.92	87.17 ± 1.85	43.08 ± 4.88	49.4 ± 6.8	33.1 ± 5.5
Caco2, 2 mM Gln	97.19 ± 2.29	92.63 ± 2.40	4.56 ± 0.37	4.9 ± 0.6	4.7 ± 0.5
Caco2, 4 mM Gln	100.39 ± 0.70	94.93 ± 1.49	5.46 ± 1.10	5.8 ± 1.3	5.4 ± 1.2

Table 3: Total glutamine oxidation (4th column), calculated by equation 1 based on the addition of either 2, or 4 mM Gln to the media without glutamine and glucose for each of the cell lines. Measurements of OCR before (3rd column) and after (2nd column) the addition of glutamine are together with the calculated results (4th column) given as means, with standard deviations (SD). The percentage wise contribution to the total OCR (5th column) and relative increase in OCR following the glutamine addition (6th column) is calculated based on the previous columns. The difference in this step is significantly different between the two cell lines, with p = 0.014 < 0.05 for 2 mM Gln and p = 0.000005 < 0.05 for 4 mM Gln.

Condition	ECAR$_{+2DG}$ %	ECAR$_{+GF}$ %	ME1 Gln ferm. %	ECAR$_{start}$ %	ME1 Gln ferm./ECAR$_{start}$
HCT116, LG	7.88 ± 2.37	3.38 ± 1.08	4.50 ± 1.62	97.50 ± 6.12	4.6 ± 2.1
HCT116, HG	12.89 ± 3.94	6.53 ± 1.78	6.36 ± 2.39	100.53 ± 3.04	6.3 ± 2.7
Caco2, LG	30.09 ± 1.78	10.48 ± 4.22	19.61 ± 4.10	91.87 ± 3.57	21.3 ± 5.6
Caco2, HG	35.19 ± 3.61	19.94 ± 7.07	15.26 ± 4.84	101.12 ± 6.33	15.1 ± 6.1

Table 4: ME1 fermentation rate caused by amino acids, primarily glutamine (4th column). Calculated as the difference between the measured ECAR after the addition of 2-DG (2nd column) and measured ECAR after the addition of GF (3rd column). Results shown for HCT116 and Caco2 cells in media with low glucose (LG) or high glucose (HG) concentrations (4th column). The starting ECAR values (5th column) are followed by percentage of ME1 Gln fermentation from the starting ECAR (6th column). Calculations are given by means, with standard deviations (SD). The difference in this step is significantly different between the two cell lines, with p = 0.00001 < 0.05 for LG and p = 0.0045 < 0.05 for HG.

concentrations as low as 2 μM Agilent (2019), this study uses 200 μM, as this was the highest concentration that yielded a response with no seemingly off-target effects (for titration, see fig 9 in the Supporting Information). Zhong et al reports that the higher concentrations of UK5099 (100 μM) resulted in a decreased growth rate, and therefore, they opted for a concentration of 10 μM Zhong et al. (2015). Since we do not consider continued growth, as it is clear that this would be inhibited by a blocked TCA cycle, we stuck to our 200 μM concentration of UK5099. As an alternative to study glutamine oxidation, the glutaminase inhibitor BPTES can be used. Glutaminase converts glutamine to glutamate, so BPTES would effectively limit the use of glutamine in OCR, as only glutamate can be utilized by the mitochondria. Lu et al 2017 Lu et al. (2017) used BPTES in a Seahorse experiment, and Agilent also have a mito-fuel flex protocol that uses both BPTES and UK5099 to check the dependencies of OCR on glutamine or glucose. It was however not considered for this study as it would be similar to not having glutamine in the media or not, and not the branching points of the pathways. Inhibition of glutaminase could effectively stop the uptake of glutamine, and no delineation can be performed on which of the intracellular paths glutamine takes.

Galloflavin has also been used in previous studies, in different types of experiments, and is among a group of other LDH inhibitors. Galloflavin inhibits both isoforms of LDH Manerba et al. (2012), effectively blocking lactate from being produced. One off-target effect here is that galloflavin decreases OCR as well as ECAR, which is evident in all the experiments, and even more prevalent for a 200 μM addition of galloflavin, seen in the titration of galloflavin for determining its concentration in fig 8. This effect could be because of the generation of L-2 hydroxyglutarate (L-2HG). When the pH is lowered, LDH can produce L-2HG from α-ketoglutarate in the cytosol, which inhibits the use of α-ketoglutarate in the TCA cycle. This could cause the lowering of OCR in the acidic environment Oldham et al. (2015). The addition of galloflavin in the basic inhibition protocol in fig 6, decreased the ECAR for both HCT116 and Caco2. The reading after the galloflavin addition is even lower than the initial readings, prior to the additions of glutamine and glucose. This allows us to get a reading for the background acidification. It also underlines what can be seen following the glutamine addition, which is that there is mainly an increase in OCR, not ECAR. In fact, ECAR drops for Caco2 following the 2 mM addition and 4 mM addition of glutamine. Thus, 2-DG is successful in bringing the ECAR reading back to where it was prior to the glucose addition, as glutamine did not affect this ECAR reading. This could be because of the glutamine following path 7a was free to re-enter the mitochondria, and then contribute to OCR rather than ECAR.

An alternative to galloflavin could be to use another LDH inhibitor, like oxamate. It does however have some problems with influencing fatty acid synthesis, and also low solubility. That being said, it has been used to pretreat cells for Seahorse experiments, and have shown an effective decrease in glycolysis Valvona and Fillmore (2018), and it has also been used as an acute injectant Delgado et al. (2010).
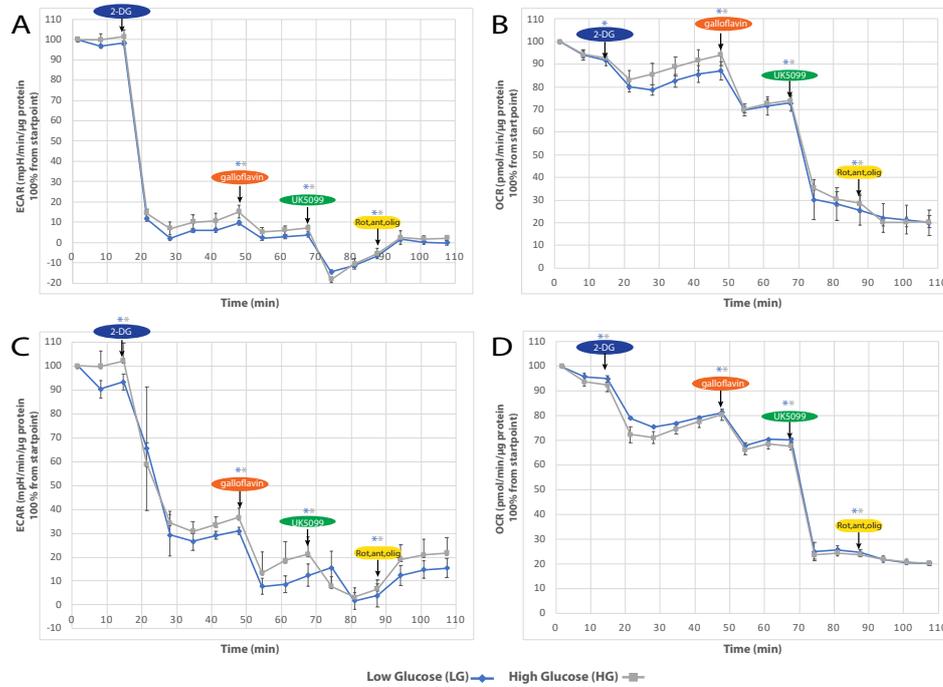
We found that glutamine's metabolism through ME1

Figure 7: **A** ECAR HCT116 (mpH/min/μg protein in % from startpoint), **B** OCR HCT116 (pmol/min/μg protein in % from startpoint), **C** ECAR Caco2 (mpH/min/μg protein in % from startpoint), **D** OCR Caco2 (pmol/min/μg protein in % from startpoint). Measurements from 10 000 HCT116 cells per well and 15 000 Caco2 cells per well, using the extended inhibition protocol. Cells were pregrown in their respective groups, low glucose (LG, 5 mM) and high glucose (HG, 25 mM) and also ran in LG and HG accordingly. Additions were 2-deoxyglucose (2-DG) (t = 18 min) followed the LDH inhibitor galloflavin (t = 48 min), the MPC inhibitor UK5099 (t = 66 min) and finally the electron transport chain inhibitors rotenone, antimycin and oligomycin (Rot,Ant,Olig) (t = 84 min). Significant changes between the two last datapoints from before and after each addition are marked by * of the respectful color between LG and HG.

and ME2 is different between the two cell lines. Both Caco2 and HCT116 have been shown to proliferate faster in the presence of glutamine Yamauchi et al. (2002); Song et al. (2017). However, our results indicate that they must exploit glutamine in different ways. We found that whereas Caco2 utilizes more glutamine through path 7a, using ME1 and secreting it as lactate, HCT116 has a higher consumption of glutamine and utilizes it more through either path 7b using ME2, directly as an anaplerotic metabolite to support the TCA cycle. This in turn, can be linked to other properties of the cells. Whereas ME1 is used to make cytosolic acetyl-CoA and eventually palmatate to support lipid synthesis in the cytosol, as well as NAD(P)H redox balance, ME2 is used to ensure that ATP production persists in the TCA cycle with the recycling of acetyl-CoA, and fighting reactive oxygen species in the mitochon-

dria. In fact, ME2 is more highly expressed in HCT116 than ME1 Jiang et al. (2013), another study on melanoma also show that while the tumor progresses, ME1 expression goes down as ME2 expression goes up Chang et al. (2015). With the use of UK5099 and GF, we were able to make this fine delineation, with a result comporting with other studies on ME1 and ME2, as well as on glutamine metabolism in cancer cells.

Our results show that HCT116 is more glutamine dependent and that Caco2 is less (see table 3). Yang et al found in a trace study that glutamine's contribution to the TCA cycle varied between 15 and 40 % of the total TCA cycle intermediate pool in different ovarian cancer cells Yang et al. (2014). Here, we report around 5% for Caco2 (fig 6D) and 42-46% for HCT116 (fig 6B). Yang et al also showed that glutamine addition increases the OCR

10

Condition	OCR$_{+UK5099}$ %	OCR$_{+Rot,Ant,Oli}$ %	ME2 Gln ox. %	OCR$_{start}$ %	ME2 Gln ox/OCR$_{start}$
HCT116, LG	26.88 ± 6.34	20.75 ± 5.36	6.13 ± 1.39	92.93 ± 2.38	6.6 ± 1.7
HCT116, HG	29.49 ± 3.43	20.41 ± 2.19	9.09 ± 4.71 •	93.64 ± 1.69	9.7 ± 5.3
Caco2, LG	25.20 ± 1.45	20.42 ± 0.71	4.78 ± 1.09	95.39 ± 1.29	5.0 ± 1.2
Caco2, HG	24.19 ± 1.01	20.52 ± 0.91	3.68 ± 0.46 •	93.05 ± 2.13	4.0 ± 0.6

Table 5: ME2 glutamine oxidation (4th column), given as the oxygen consumption rate limited to path 7b. Calculated as the difference between the measured OCR after the addition of UK5099 (2nd column) and the measured OCR after the final addition of rotenone, antimycin and oligomycin (3rd column), see eq 3. Results shown for HCT116 and Caco2 cells in media with low glucose (LG) or high glucose (HG) concentrations (4th column). The starting OCR values (5th column) are followed by percentage wise contribution to the starting OCR (6th column). Calculations are given by means, with standard deviations (SD).The difference in this step is significantly different for HG between the two cell lines with p = 0.037 < 0.05 for HG. Statistical significance is marked by •.

in high-invasive cell lines, such that OCR by glutamine is also linked to invasiveness. This is interesting, since HCT116 is a much more and invasive cell line than Caco2 Zhuang et al. (2016).

The strength of our approach to use real time measurements of OCR and ECAR to examine glutamine metabolism, is its flexibility and clear effect. Once an inhibitor is added, you immediately can read off the effect. It leaves room for many different conditions, and most cells that can grow in a confluent monolayer can be studied. This study offers similar benefits of more advanced systems, like NMR or MS, but with additional dynamics and compensatory measures in real time. The information on dynamics can help fine-tune drugs to limit the growth of cancer cells. It is also arguably much cheaper and easier to use than NMR and MS. The limitations are the nutrients, like the additional amino acids already in the base media, that cannot be controlled easily, as they are essential to ensure normal growth conditions. Also, if pyruvate had been added to the media, you would most likely get different dynamics, as pyruvate is not solely dependent on stemming from glucolysis nor glutaminolysis anymore.

There is also a problem of lactate buildup on other reactions in the cell, as the media is no longer the pH it was before. In addition, you do not know how effective or how specific an inhibitor is. This is however also a problem for Agilent, and seeing how they have developed these various kits, this study arguably has the same strengths and limitations already held by Agilent. It is a comparable, relative study, that gives dynamics and reveals differences in central carbon metabolism.

Although the rationale behind the consecutive addition of inhibitors stands, metabolites that have not been blocked by especially 2-DG include serine, glycine, cysteine, alanine and tyrosine, which can all be converted to pyruvate. All of these are components in the Seahorse base media, and should therefore be mentioned. However, their effects are arguable, as their concentrations are so much lower than that of glutamine or glucose. We have also not addressed glutamine's conversion to citrate. Glutamine can be converted to citrate through a backwards progression in the TCA cycle, or in the cytosol. Whether or not some of the glutamine has been converted to citrate

in this study, is not accounted for.

Conclusions

This study showed how UK5099 and galloflavin can be used as sequential inhibitors to decipher how glutamine was metabolized. This was achieved through real time measurements of oxygen consumption and extracellular acidification using a Seahorse XFp analyzer. Glutamine was metabolized differently in the two cell lines, and a differentiation between the use of ME1 and ME2 was found.

References

Agilent, 2019. Seahorse xf cell mito fuel flex kit - user manual.

Andersen, J.V., Nissen, J.D., Christensen, S.K., Markussen, K.H., Waagepetersen, H.S., 2017. Impaired hippocampal glutamate and glutamine metabolism in the db/db mouse model of type 2 diabetes mellitus. Neural plasticity 2017.

Chang, Y.L., Gao, H.W., Chiang, C.P., Wang, W.M., Huang, S.M., Ku, C.F., Liu, G.Y., Hung, H.C., 2015. Human mitochondrial nad (p)+–dependent malic enzyme participates in cutaneous melanoma progression and invasion. Journal of Investigative Dermatology 135, 807–815.

Delgado, T., Carroll, P.A., Punjabi, A.S., Margineantu, D., Hockenbery, D.M., Lagunoff, M., 2010. Induction of the warburg effect by kaposi's sarcoma herpesvirus is required for the maintenance of latently infected endothelial cells. Proceedings of the National Academy of Sciences 107, 10696–10701.

Dey, P., Baddour, J., Muller, F., Wu, C.C., Wang, H., Liao, W.T., Lan, Z., Chen, A., Gutschner, T., Kang, Y., et al., 2017. Genomic deletion of malic enzyme 2 confers collateral lethality in pancreatic cancer. Nature 542, 119.

Driskell, J.A., 2007. Sports nutrition: fats and proteins. CRC Press.

Hartman, M.L., Shirihai, O.S., Holbrook, M., Xu, G., Kocherla, M., Shah, A., Fetterman, J.L., Kluge, M.A., Frame, A.A., Hamburg, N.M., et al., 2014. Relation of mitochondrial oxygen consumption in peripheral blood mononuclear cells to vascular function in type 2 diabetes mellitus. Vascular medicine 19, 67–74.

Herst, P., Berridge, M., 2013. Cell hierarchy, metabolic flexibility and systems approaches to cancer treatment. Current pharmaceutical biotechnology 14, 289–299.

Hildyard, J.C., Ämmälä, C., Dukes, I.D., Thomson, S.A., Halestrap, A.P., 2005. Identification and characterisation of a new class of highly specific and potent inhibitors of the mitochondrial pyruvate carrier. Biochimica et Biophysica Acta (BBA)-Bioenergetics 1707, 221–230.

Jiang, P., Du, W., Mancuso, A., Wellen, K.E., Yang, X., 2013. Reciprocal regulation of p53 and malic enzymes modulates metabolism and senescence. Nature 493, 689.

Lanning, N.J., Castle, J.P., Singh, S.J., Leon, A.N., Tovar, E.A., Sanghera, A., MacKeigan, J.P., Filipp, F.V., Graveel, C.R., 2017. Metabolic profiling of triple-negative breast cancer cells reveals metabolic vulnerabilities. Cancer & metabolism 5, 6.

Lu, J., K. Montgomery, B., P. Chatain, G., Bugarini, A., Zhang, Q., Wang, X., A. Edwards, N., Ray-Chaudhury, A., J. Merrill, M., Lonser, R., Chittiboina, P., 2017. Corticotropin releasing hormone can selectively stimulate glucose uptake in corticotropinoma via glucose transporter 1. Molecular and Cellular Endocrinology 470.

Manerba, M., Vettraino, M., Fiume, L., Di Stefano, G., Sartini, A., Giacomini, E., Buonfiglio, R., Roberti, M., Recanatini, M., 2012. Galloflavin (cas 568-80-9): a novel inhibitor of lactate dehydrogenase. ChemMedChem 7, 311–317.

Matés, J.M., Di Paola, F.J., Campos-Sandoval, J.A., Mazurek, S., Márquez, J., 2019. Therapeutic targeting of glutaminolysis as an essential strategy to combat cancer, in: Seminars in cell & developmental biology, Elsevier.

Murai, S., Ando, A., Ebara, S., Hirayama, M., Satomi, Y., Hara, T., 2017. Inhibition of malic enzyme 1 disrupts cellular metabolism and leads to vulnerability in cancer cells in glucose-restricted conditions. Oncogenesis 6, e329–e329.

Nakashima, C., Yamamoto, K., Fujiwara-Tani, R., Luo, Y., Matsushima, S., Fujii, K., Ohmori, H., Sasahira, T., Sasaki, T., Kitadai, Y., et al., 2018. Expression of cytosolic malic enzyme (me 1) is associated with disease progression in human oral squamous cell carcinoma. Cancer science 109, 2036–2045.

Oldham, W.M., Clish, C.B., Yang, Y., Loscalzo, J., 2015. Hypoxia-mediated increases in l-2-hydroxyglutarate coordinate the metabolic response to reductive stress. Cell metabolism 22, 291–303.

Ren, J.G., Seth, P., Clish, C.B., Lorkiewicz, P.K., Higashi, R.M., Lane, A.N., Fan, T.W.M., Sukhatme, V.P., 2014. Knockdown of malic enzyme 2 suppresses lung tumor growth, induces differentiation and impacts PI3K/AKT signaling. Scientific reports 4, 5414.

Sarfraz, I., Rasul, A., Hussain, G., Hussain, S.M., Ahmad, M., Nageen, B., Jabeen, F., Selamoglu, Z., Ali, M., 2018. Malic enzyme 2 as a potential therapeutic drug target for cancer. IUBMB life 70, 1076–1083.

Scalise, M., Pochini, L., Galluccio, M., Console, L., Indiveri, C., 2017. Glutamine transport and mitochondrial metabolism in cancer cell growth. Frontiers in oncology 7, 306.

Song, Z., Wei, B., Lu, C., Li, P., Chen, L., 2017. Glutaminase sustains cell survival via the regulation of glycolysis and glutaminolysis in colorectal cancer. Oncology letters 14, 3117–3123.

Teves, J.M., Bhargava, V., Kirwan, K.R., Corenblum, M.J., Justiniano, R., Wondrak, G.T., Anandhan, A., Flores, A.J., Schipper, D.A., Khalpey, Z., et al., 2018. Parkinson's disease skin fibroblasts display signature alterations in growth, redox homeostasis, mitochondrial function, and autophagy. Frontiers in neuroscience 11, 737.

Valvona, C., Fillmore, H., 2018. Oxamate, but not selective targeting of ldh-a, inhibits medulloblastoma cell glycolysis, growth and motility. Brain sciences 8, 56.

Vroon, D., Israili, Z., 1990. Aminotransferases. Boston, Butterworths.

Wehrle, J.P., Ng, C.E., McGovern, K.A., Aiken, N.R., Shungu, D.C., Chance, E.M., Glickson, J.D., 2000. Metabolism of alternative substrates and the bioenergetic status of emt6 tumor cell spheroids. NMR in Biomedicine: An International Journal Devoted to the Development and Application of Magnetic Resonance In Vivo 13, 349–360.

Wise, D.R., Thompson, C.B., 2010. Glutamine addiction: a new therapeutic target in cancer. Trends in biochemical sciences 35, 427–433.

Yamauchi, K., Komatsu, T., Kulkarni, A.D., Ohmori, Y., Minami, H., Ushiyama, Y., Nakayama, M., Yamamoto, S., 2002. Glutamine and arginine affect caco-2 cell proliferation by promotion of nucleotide synthesis. Nutrition 18, 329–333.

Yang, L., Moss, T., Mangala, L.S., Marini, J., Zhao, H., Wahlig, S., Armaiz-Pena, G., Jiang, D., Achreja, A., Win, J., et al., 2014. Metabolic shifts toward glutamine regulate tumor growth, invasion and bioenergetics in ovarian cancer. Molecular systems biology 10.

Yang, Z., Xiong, H.R., 2012. Culture conditions and types of growth media for mammalian cells. Biomedical Tissue Culture 1, 3–18.

Zhang, J., Pavlova, N.N., Thompson, C.B., 2017. Cancer cell metabolism: the essential role of the nonessential amino acid, glutamine. The EMBO journal 36, 1302–1315.

Zhang, L., Zhang, S., Maezawa, I., Trushin, S., Minhas, P., Pinto, M., Jin, L.W., Prasain, K., Nguyen, T.D., Yamazaki, Y., et al., 2015. Modulation of mitochondrial complex i activity averts cognitive decline in multiple animal models of familial alzheimer's disease. EBioMedicine 2, 294–305.

Zhong, Y., Li, X., Yu, D., Li, X., Li, Y., Long, Y., Yuan, Y., Ji, Z., Zhang, M., Wen, J.G., et al., 2015. Application of mitochondrial pyruvate carrier blocker uk5099 creates metabolic reprogram and greater stem-like properties in lncap prostate cancer cells in vitro. Oncotarget 6, 37758.

Zhuang, K., Zhang, J., Xiong, M., Wang, X., Luo, X., Han, L., Meng, Y., Zhang, Y., Liao, W., Liu, S., 2016. Cdk5 functions as a tumor promoter in human colorectal cancer via modulating the erk5–ap-1 axis. Cell death & disease 7, e2415.

1. Supplementary Information

1.1. Seahorse titrations

Both galloflavin and UK5099 were titrated using three different concentrations with increments of 2x. The concentrations were 50 μM, 100 μM and 200 μM for the galloflavin titrations, and 100 μM, 200 μM and 400 μM for the UK5099 titrations. UK5099 was also first tested with much lower concentrations (0.5 μM, 1 μM and 2 μM), but showed little effect and no difference between the concentrations. Both the titrations resulted in the middle concentration value, as the lowest concentrations yielded little effect, and the highest concentrations yielded unwanted effects, seen as a major dip in OCR for both galloflavin in fig 8 and UK5099 in fig 9.

The attached excel files show the protein amount in μg protein for each well, as well as their original raw data, and the normalized data.
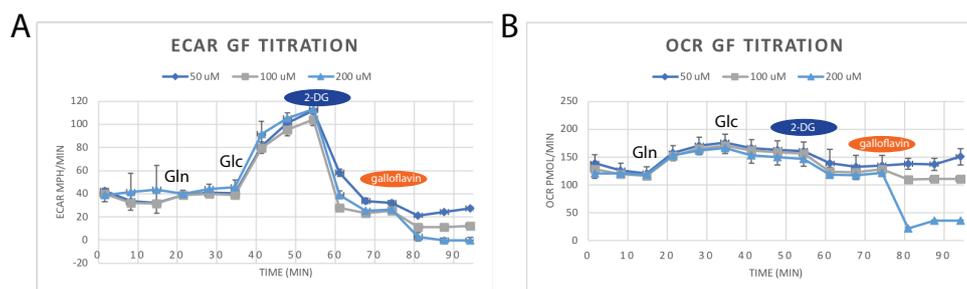
Figure 8: Titration of galloflavin on 12 000 HCT116 cells. 50 μM, 100 μM and 200 μM was run to conclude a final concentration of 100 μM GF. This is because 50 μM showed little or no effect on ECAR, whereas 200 μM affected OCR to a large degree without showing that much more effect than 100 μM on ECAR.

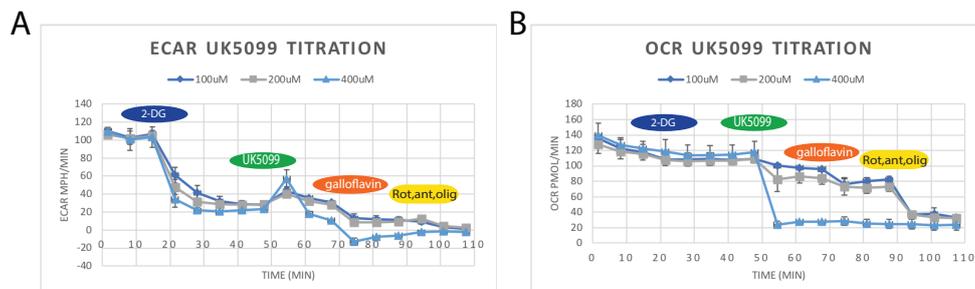Figure 9: Titration of UK5099 on 10 000 HCT116 cells. 100 μM, 200 μM and 400 μM was run to conclude a final concentration of 200 μM UK5099. This is because 100 μM showed little effect on OCR, whereas 400 μM showed an even greater effect on OCR than even the Rot, ant, olig mixture in the last addition. This suggests that 400 μM may induce apoptosis in the cells.